# The representation of multimodal tactile sensations in the human somatosensory system

Thesis by

Isabelle A. Rosenthal

In Partial Fulfillment of the Requirements for the

Degree of

Doctor of Philosophy


CALIFORNIA INSTITUTE OF TECHNOLOGY

Pasadena, California

2023

(Defended April 26, 2023)

Isabelle A. Rosenthal
ORCID: 0000-0002-9791-3820

# ACKNOWLEDGEMENTS

I have been enormously fortunate to be able to write this thesis, and owe many people a debt of gratitude. Firstly, I would like to thank my advisor, Richard Andersen, for giving me the opportunity to work on some of the most interesting neuroscience research I can imagine, and the independence to design my own experiments. It is a credit to Richard that his lab is composed of some of the most supportive and welcoming people I have met in science. I also want to thank Luke Bashford, my postdoc mentor, whose constant faith in my abilities, patience with my tendency to stress myself out about small problems, and cheerful demeanor was invaluable to me throughout my PhD. I owe thanks to David Bjånes and Spencer Kellis for all the guidance over the years, especially on experimental design and implementation, and Sumner Norman, who always went out of his way to help me, even on projects to which he had no affiliation or obligation.

I am grateful to have shared the lab with some phenomenal graduate students–Sarah Wandelt, Whitney Griggs, Kelly Kadlec, Charles Guan, and HyeongChan Jo–whose friendship and intellectual insights I feel very fortunate to have enjoyed. I want to give a special thanks to Sarah, who worked most closely with me. Over the years, Sarah and I have had countless conversations (some more productive than others) about my research, and her kindness and infallible support have meant so much to me. As my desk neighbor, Whitney also graciously allowed me to pester him with questions about whatever problem was plaguing me at the moment, and gave good answers for far too many of them.

I am incredibly thankful to FG, the participant who so generously donated his time and effort to my experiments, and without whom, none of the work presented here would have been possible. I am very grateful for his patience with my complicated experimental setups, and it has been my pleasure to get to know him over the years.

I also want to thank the other lab members who helped make my work possible, and who built such a supportive and intellectually stimulating environment: Kelsie Pejsa, Liang She, Jorge Gamez, Xinyun Zou, Thierri Callier, Tyson Aflalo, Sri Chivukula, Vasileios Christopoulos, Mac Thurston, Jennifer Yu, and Sherri McKinney. Additionally, I want to thank my thesis committee, Ralph Adolphs, Ueli Rutishauser, and Frederick Eberhardt, for considering my work thoughtfully and offering useful and constructive feedback. I want to extend particular thanks to Ralph, in whose lab I worked as an undergrad almost a decade ago. Since that time, Ralph has always been an academic mentor who makes my ideas feel valued and who I can trust to give sincere, well-reasoned advice.

Outside of the lab, I want to thank H Perry Hatchfield for being the most supportive partner I could ever ask for. Perry's love and unwavering confidence in me has meant more to me than I could ever express, and I dedicate this thesis to him. I also count myself incredibly lucky to have wonderful friends, from high school to the present day, who I have used as role models on how to be kind, thoughtful, and successful. These friends include: Natalie Solomon, Kaitlyn Brady, Allie Mathews, Joanna Tung, Kyle Spindelman, Kellan Moorse, Gabe Salmon, Christian Leefmans, Konrad Pilch, Jieyu Zheng, Kevin Mei, Aashrita Mangu, Tiffany Chen, Diana Huang, Morgan Palma, Lorena Huang Liu, Michelle Ozaki, and Christian Seitz.

I also want to thank my parents, Paula Scott and Jean-Laurent Rosenthal, and my sister, Juliette Rosenthal. They have always made me feel that I could accomplish anything I set my mind to, and encouraged me to pursue my passions to the fullest. Their love and support mean the world to me.

Finally, I would be remiss if I did not thank my cat, Faye, for encouraging me throughout my PhD by simply being the best cat possible.

# ABSTRACT

The sense of touch is critical to executing basic motor tasks and generating a feeling of embodiment. To construct touch percepts, the brain integrates information from tactile mechanoreceptors with inputs from other senses and top-down variables such as attention and task context. In this thesis, we investigate how these factors influence neural activity within the somatosensory system at different stages of tactile processing, using electrophysiological and behavioral data from a human tetraplegic participant implanted with microelectrode arrays. First, we find that neural responses to imagined touches of different types are decodable in the primary somatosensory cortex, ventral premotor cortex, and the supra-marginal gyrus, and these responses remain stable over many months. Following this analysis, the primary somatosensory cortex is explored in greater depth to better characterize early-stage cortical tactile processing. Touches to the arm and finger are examined during a passive task, in a variety of conditions including visually observed physical touches, physical touches without vision, and visual touches without physical contact. Analysis of the two touch locations suggests that touch encoding in primary somatosensory cortex may be less rigid than in the classical topographic view. Additionally, this experiment uncovers a modulatory effect of vision in the primary somatosensory cortex when it is paired with a physical touch, but no effect of vision alone. Finally, we investigate how visual information impacts artificial tactile sensations, which can be elicited using intra-cortical microstimulation to the primary somatosensory cortex. The ability to elicit reliable, naturalistic artificial touch sensations is vital to the implementation of a tactile brain-machine interface, which would benefit patients with spinal cord injury and others with somatosensory impairments. We find that visual information biases the qualitative percept of artificial stimulation towards an interpretation that is visually plausible. The temporal binding window between

vision and stimulation is found to be larger when visual information is biologically relevant, suggesting that the brain's ability to causally relate artificial stimulation to visual cues depends on visual context. Additionally, recordings from the primary somatosensory cortex indicate that visual information relevant to artificial stimulation is represented across contexts, during an active task. The effect of task on the responsiveness of the primary somatosensory cortex to visual information points to a role of attention in mediating early cortical tactile processing. In combination, the findings presented in this thesis provide insight into the basic neuroscience of how tactile experiences are constructed by the brain, suggesting that early tactile processing is influenced by multisensory, contextual factors. These findings also have clinical applications to developing a brain-machine interface capable of providing naturalistic sensations within a complex real world environment.

# PUBLISHED CONTENT AND CONTRIBUTIONS

Bashford, L., Rosenthal, I., Kellis, S., Pejsa, K., Kramer, D., Lee, B., Liu, C., Andersen, R.A., 2021. The neurophysiological representation of imagined somatosensory percepts in human cortex. J. Neurosci. 41, 2177–2185. https://doi.org/10.1523/JNEUROSCI.2460-20.2021

I.A.R. participated in data curation, formal analysis, investigation, methods development, software development and programming, validation and visualization of the data, and writing and editing of the manuscript.

Rosenthal, I.A., Bashford, L., Kellis, S., Pejsa, K., Lee, B., Liu, C., Andersen, R.A., 2023. S1 represents multisensory contexts and somatotopic locations within and outside the bounds of the cortical homunculus. Cell Reports 42, 112312. https://doi.org/10.1016/j.celrep.2023.112312

I.A.R. participated in conceptualization, data curation, formal analysis, investigation, methods development, software development and programming, validation and visualization of the data, and writing and editing of the manuscript.

# TABLE OF CONTENTS

**Acknowledgements** ..... iii

**Abstract** ..... v

**Published Content and Contributions** ..... vii

**Table of Contents** ..... viii

**List of Illustrations and Tables** ..... x

**Nomenclature** ..... xii

**Chapter 1: Introduction** ..... 1

**Chapter 2: Background** ..... 4

**1.1 The importance of tactile sensations** ..... 4
**1.1.1** Somatosensation in everyday life ..... 4
**1.1.2** Tactile experiences and the sense of embodiment ..... 6

**1.2 The sensorimotor loop** ..... 8
**1.2.1** Primary somatosensory cortex (S1) ..... 9
**1.2.2** Motor and premotor cortex ..... 15
**1.2.3** Posterior parietal cortex (PPC) ..... 16
**1.2.4** Sensory remapping in the brain ..... 18

**1.3 Brain-Machine Interfaces (BMIs)** ..... 19
**1.3.1** Methodology ..... 21
**1.3.2** Intra-cortical microstimulation (ICMS) ..... 21
**1.3.3** Benefits of a BMI with sensory capabilities ..... 24
**1.3.4** Multisensory integration of ICMS ..... 25
**1.3.5** Current challenges ..... 26

**Chapter 3: Imagined somatosensory percepts in human cortex** ..... 29

**3.1 Introduction** ..... 29

**3.2 Methods** ..... 32
**3.2.1** Participant ..... 32
**3.2.2** Task ..... 33
**3.2.3** Experiment design and data collection ..... 33
**3.2.4** Statistics and analysis methods ..... 34

**3.3 Results** ..... 36
**3.3.1** Classifying sensations ..... 36
**3.3.2** Longitudinal representational of sensations ..... 40

**3.4 Discussion** ..... 43

**Chapter 4: The role of visual information and the cortical homunculus in S1 ..... 49**
**4.1 Introduction ..... 49**
**4.2 Methods ..... 52**
**4.2.1** Participant and implant details ..... 52
**4.2.2** Experimental paradigm ..... 54
**4.2.3** Data collection ..... 55
**4.2.4** Quantification and statistical analysis ..... 57
**4.3 Results ..... 61**
**4.3.1** Condition identity decoding ..... 62
**4.3.2** Representational Similarity Analysis (RSA) ..... 63
**4.3.3** Location and touch type generalization decoding ..... 65
**4.3.4** Individual channel tuning analysis ..... 66
**4.4 Discussion ..... 69**
**4.4.1** Neural activity is specialized for arm touches and represents finger touches more generally ..... 70
**4.4.2** Visual information modulates neural activity if accompanied by a physical stimulus ..... 73
**4.4.3** Conclusion ..... 77
**4.4.4** Limitations of the study ..... 78
**4.5 Supplemental video legends ..... 80**

**Chapter 5: The integration of ICMS and visual context ..... 81**
**5.1 Introduction ..... 81**
**5.2 Methods ..... 83**
**5.2.1** Participant ..... 83
**5.2.2** Experimental paradigm ..... 85
**5.2.3** Data collection ..... 86
**5.2.4** Quantification and statistical analysis ..... 87
**5.3 Results ..... 90**
**5.3.1** ICMS-elicited tactile sensations ..... 92
**5.3.2** The temporal binding window between vision and ICMS ..... 93
**5.3.3** S1 neural responses to visual stimuli ..... 97
**5.4 Discussion ..... 98**
**5.4.1** ICMS-elicited sensations are affected by visual information and ICMS current amplitude ..... 98
**5.4.2** The biological relevance of visual stimuli influences the temporal binding window ..... 100
**5.4.3** S1 represents ICMS-relevant visual content in a context-independent fashion ..... 101
**5.4.4** Conclusion ..... 104
**5.4.5** Limitations of the study ..... 105
**5.5 Supplemental figure ..... 106**
**5.6 Supplemental video legends ..... 107**

**Chapter 6: Conclusion ..... 108**

**Bibliography ..... 113**

# LIST OF ILLUSTRATIONS AND TABLES

**Figure 3.1 Implant locations and task design** ..... **31**

**Table 3.1 Classification accuracies** ..... **37**

**Figure 3.2 Sensation classification** ..... **39**

**Figure 3.3 Sample firing rates and mean power** ..... **41**

**Figure 3.4 Longitudinal decoding** ..... **43**

**Table 4.1 Experimental task conditions** ..... **52**

**Figure 4.1 Experimental methods and paradigm** ..... **53**

**Figure 4.2 Pairwise decoding and RSA** ..... **58**

**Figure 4.3 Generalization decoding results** ..... **65**

**Figure 4.4 Tuning analysis** ..... **67**

**Figure 4.5 Neural dynamics of tuned channels** ..... **69**

**Supplemental Video 4.1 Sample stimulus from the VrFPa condition** ..... **80**

**Supplemental Video 4.2 Pairwise identity decoding at 0.1s resolution** ..... **80**

**Supplemental Video 4.3 Generalization decoding of effector across all pairs of touch types at 0.1s resolution** ..... **80**

**Supplemental Video 4.4 Generalization decoding of touch type, training on Finger trials and testing on Arm trials at 0.1s resolution** ..... **80**

**Supplemental Video 4.5 Generalization decoding of effector, training on Arm trials and testing on Finger trials, at 0.1s resolution** ..... **80**

**Figure 5.1 Experimental methods and paradigm** ..... **84**

**Figure 5.2 ICMS-elicited tactile percepts** ..... **91**

**Figure 5.3 The temporal binding window between vision and ICMS** ..... **94**

**Figure 5.4 Neural activity during catch trials** ..... **96**

**Supplemental Figure 5.1 Behavioral accuracy by ICMS current ..... 106**

**Supplemental Video 5.1 Sample abstract visual stimulus ..... 107**

**Supplemental Video 5.2 Sample realistic visual stimulus ..... 107**

# NOMENCLATURE

**Brodmann areas:** cortical regions originally anatomically delineated by Korbinian Brodmann according to histological structure.

**BMI:** brain-machine interface; any system capable of decoding neural information to affect the environment and/or directly stimulating the brain to provide relevant information to the user.

**Cutaneous sensations:** tactile sensations including texture, vibration, and pressure.

**ECoG:** electrocorticography; a type of electrophysiology in which electrodes are typically configured in a grid and placed on the cortex during a craniotomy to record LFPs.

**EEG:** electroencephalography; a non-invasive method of recording electrical activity in the brain through scalp electrodes.

**Electrophysiology:** the measurement of voltage changes in the brain to detect neural activity.

**Embodiment:** the physical intuition of one's one body and the sense that its components belong to oneself as a whole**.**

**Firing rate:** the number of action potentials generated per second by a neuron or group of neurons.

**MRI:** magnetic resonance imaging; a method of neuroimaging that measures blood-oxygen levels in the brain as a correlate of neural activity.

**Homunculus:** a representation of the human body that is proportioned to reflect the amount of cortex dedicated to each body part in sensorimotor areas such as S1 (e.g., large hands and small feet).

**ICMS:** intra-cortical microstimulation; the electrical stimulation of cortex using microelectrodes.

**JND:** just-noticeable difference; the amount of change in a stimulus necessary for it to be detected a significant fraction of the time.

**LFP:** local field potential; the voltage generated by the combined neural activity of a population of neurons.

**PPC:** posterior parietal cortex; a brain region known for multisensory integration and representing motor intentions.

**PMv:** ventral premotor cortex; a brain region involved in motor planning and action selection.

**Proprioception:** the tactile sense of where one's limbs are relative to the environment and oneself.

**M1:** primary motor cortex; a brain region known for executing motor actions.

**MEG:** magnetoencephalography; a method of neuroimaging that measures the magnetic fields generated by neural activity.

**Neural prosthetic:** a BMI which uses implanted electrodes to record and/or stimulate the brain.

**Qualia:** the perceptual conscious nature of experiences.

**Rubber hand illusion:** a classic illusion in which a fake, realistic hand is touched or moved at the same time as one's real hand is touched or moved, resulting in the illusory embodiment of the fake hand.

**S1:** primary somatosensory cortex; a brain region known to represent tactile sensations with a topographic organization.

**SCI:** spinal cord injury.

**SMG:** supra-marginal gyrus, a sub-region of PPC involved in grasping, tool use, and language.

**Somatosensation:** the sense of touch, including cutaneous and proprioceptive information.

**Temporal binding window:** the window of time in which two stimuli from different sensory modalities are percieved to occur simultaneously.

**TMS:** transcranial magnetic stimulation; a non-invasive method of stimulating the brain by using a magnetic coil on the scalp to affect the electrical activity of neurons.

**Tetraplegia:** paralysis of all four limbs and the torso, typically caused by a high-level SCI.

**Topographic organization:** a schema in which body parts that are anatomically adjacent to one another are represented by neural populations that are close to one another along the cortical surface.

**Tuning:** when a neuron exhibits different activity in a condition compared to baseline or another condition.

**VET:** visual enhancement of touch; a phenomenon in which tactile acuity is enhanced when observing the touched limb even when the visual information is non-informative.

# *Chapter 1*

# INTRODUCTION

We depend on our senses to understand our environments and how best to interact with them. The sense of touch is particularly important because in addition to supplying highly useful information about the world, like the texture, shape, and size of objects in an environment, it also contributes to the natural physical intuition of what it feels like to inhabit our own bodies. When the sense of touch is lost, motor abilities are drastically impaired, as is the ability to keep track of where the body is in the environment (Miall et al., 2019; Robles-De-La-Torre, 2006; Sobinov and Bensmaia, 2021). Touch experiences are generated as part of the sensorimotor loop, which is the cycle of performing actions, collecting and interpreting the sensory feedback from those actions, and using this information to decide on new actions. It is known that touch experiences are affected by multisensory stimuli, such as visual information (Kennett et al., 2001; Tipper et al., 2001), but our understanding of how–and where–tactile and visual information are integrated together in the brain continues to evolve as more studies are conducted and recording technologies become more advanced.

Individuals with spinal cord injury (SCI) lose somatosensory and motor abilities below the level of their injury. Over 50% of cases of SCI in the United States are tetraplegic, meaning that the patient is impaired to some degree in all four limbs (National SCI Statistical Center, 2022). Brain-machine interfaces (BMIs) are a potential method of restoring some motor ability and providing artificial tactile sensations to tetraplegic patients. Motor BMIs have made impressive strides in recent years (Dekleva et al., 2021; Keshtkaran et al., 2022; Willsey et al., 2022). While intra-cortical microstimulation (ICMS) is a known method to elicit artificial tactile sensations, a generalizable,

robust somatosensory BMI remains in the proof-of-concept stage (Flesher et al., 2021). In order to create a viable somatosensory BMI, the neural underpinnings of tactile experiences, how they are influenced by multisensory factors, and how ICMS is integrated into the somatosensory processing hierarchy, must be better understood.

To better understand this issue, an overview of the importance of somatosensation, the neuroanatomy of touch, and the implementation of brain-machine interfaces (BMIs) is given in **Chapter 2**. This background will provide a foundation for **Chapters Chapter 3**,**Chapter 4**, and**Chapter 5**, which focus on current research on tactile experiences and their neural encoding.

In **Chapter 3**, the brain's representation of tactile imagery is investigated. Specifically, the primary somatosensory cortex (S1), the supramarginal gyrus (SMG), and ventral premotor cortex (PMv) are examined as they represent a diverse set of cortical locations within the sensorimotor loop. S1 is an early-stage tactile processing area, SMG is a higher order location involved in multisensory integration and action intentions, and PMv is a region which represents motor planning.

**Chapter 4** explores how S1 represents touches that occur in different body locations, and how vision is integrated into these representations. This work adds nuance to the conventional representation of S1 as an area with a highly segregated topographic organization (Ejaz et al., 2015; Penfield and Boldrey, 1937), and also presents a hypothesis involving task design as to why prior studies have found conflicting results concerning S1's responses to visual information (Blakemore et al., 2005; Keysers et al., 2004).

**Chapter 5** departs from the study of real touches in order to better understand how ICMS is processed and experienced. In particular, we examine how ICMS is combined with visual information to evoke tactile percepts, and how visual context affects the perceived timing of these percepts. The results suggest that vision can bias ICMS percepts towards qualia that are plausible in a multisensory

environment, and also supports the hypothesis advanced in **Chapter 4** regarding the effect of task design on S1 representations of visual information.

Finally, **Chapter 6** summarizes these findings and contextualizes them within the current literature. In particular, we consider possible experiments to address the questions raised by these investigations, and how to use our findings to better understand the requirements of a viable somatosensory BMI.

# *Chapter 2*

# BACKGROUND

## 1.1 The importance of tactile sensations

Like all the senses, tactile experiences are formed by the brain through a constructive process. This process relies on mechanoreceptors embedded throughout the body, as well as information from other sensory inputs and the brain's priors about the environment which are used to interpret the incoming information cohesively. Cutaneous sensors in the skin are used to form a detailed understanding of the environment around us, like the texture, shape, and size of objects. While tactile acuity varies across the body, the human somatosensory system can detect changes in texture down to 10 nanometers in amplitude on the pad of the index finger (Skedung et al., 2013). Additionally, proprioceptive sensors in muscles and tendons convey information about the posture and movement of one's body with respect to itself and to the environment (Sobinov and Bensmaia, 2021). Both cutaneous and proprioceptive signals are carried through thousands of nerve fibers through the spinal cord to the brain (Johansson and Vallbo, 1979). These signals are integrated by the brain to yield embodied experiences of existing in, and interacting with, the environment. In other words, the somatosensory system provides us with the sensation of what it feels like to exist in our bodies and in the world at large.

### *1.1.1 Somatosensation in everyday life*

Accomplishing basic motor coordination tasks, like picking up a pen, may appear trivial, but without a sense of touch, the ability to perform such manual dexterity tasks becomes highly impaired even when the motor system remains intact (Miall et al., 2019; Sobinov and Bensmaia, 2021). In studies

of healthy participants where local anesthetic was applied to abolish touch sensations, reaching to towards objects became slower and less accurate, and the participants were unable to generate grasps with correctly graded force (Augurelle et al., 2003; Gentilucci et al., 1997). More drastically, patients who selectively lose their sense of touch due to nerve damage find themselves having to relearn foundational motor skills, like how to chew food, walk, or speak. In one patient, relearning how to stand upright took over a year to accomplish, and required constant, conscious control of his limbs, heavily supported by visual information (Robles-De-La-Torre, 2006). In another study, patients with sensory neuropathy attempted to draw straight lines from one target to another (Ghez et al., 1995). Due to their lack of proprioception, the patients were unable to draw lines of the right length or direction without using vision to guide them. Even when they were able to see both targets, the lines they drew were wobbly and imprecise.

While such studies provide strong evidence for the brain's reliance on tactile information to execute and adapt motor plans, it is relatively rare to find clinical cases where the sense of touch is lost and motor pathways remain intact. Cases with combined tactile and motor impairment are much more common, such as patients with spinal cord injury (SCI). According to the National SCI Statistical Center in 2022, in the United States, there are approximately 300,000 people living with SCI, with an estimated 18,000 new cases every year. In these cases, damage to the spinal cord severs the connection between the brain and the peripheral nervous system everywhere below the level of the injury, resulting in an inability to move or sense in these locations. If the SCI is not complete, this loss of ability may be only partial, allowing some motion and sensation below the level of the injury to remain or be recovered over time. Surveying patients with SCI, regaining motor and sensory abilities in the arm and hand is listed as a top priority for improving quality of life (Anderson, 2004).

### *1.1.2 Tactile experiences and the sense of embodiment*

Embodiment is the physical intuition of one's own body, and the sense that its component parts belong to the whole (Longo et al., 2008). The sense of embodiment typically applies solely to one's true body, but can become distorted in cases of brain damage or mental illness (Blakemore et al., 2003; Daprati et al., 1997; Feinberg et al., 2010). In healthy people, the sense of embodiment usually remains relatively stable, due to top-down processes retaining a consistent concept of what constitutes the body, but this concept is also highly dependent on bottom-up information from the somatosensory, motor, vestibular, and visual systems (Giummarra et al., 2008).

This dependency on sensory information can be exploited by illusions that trigger altered states of embodiment–for instance, the sense of embodying a virtual reality avatar (Banakou et al., 2013; Lenggenhager et al., 2007; Petkova and Ehrsson, 2008; Slater et al., 2010). In these experiments, typically the participant is shown a first person perspective of a surrogate body which either moves synchronously with the participant (Banakou et al., 2013; Kilteni et al., 2012b), or is depicted being touched at the same time as the participant is being touched (Petkova and Ehrsson, 2008), or both (Slater et al., 2010). Many studies of embodiment do not examine the entire body, but instead focus on just one hand. The illusion in which a fake, lifelike hand is embodied by viewing touches or motion on that hand at the same time as touches or motion occur on one's own hidden hand (the "rubber hand illusion") has been extensively studied (Botvinick and Cohen, 1998; Dummer et al., 2009; Kilteni and Ehrsson, 2017; Tsakiris and Haggard, 2005).

Whether focused on the entire body or just the hand, the mechanism of the illusion remains the same: it arises from visuotactile and/or visuomotor temporal synchrony linking the actual body with a virtual one (Maselli et al., 2016), and disappears if the stimuli have too large of a temporal offset between them (Bekrater-Bodmann et al., 2014). Specifically, a 500ms offset is sufficient to dispel the rubber

hand illusion (Shimada et al., 2014), and at 300ms the effect occurs more weakly (Bekrater-Bodmann et al., 2014), with the just-noticeable difference (JND) occurring approximately at 150ms, although these numbers vary substantially across individuals (Costantini et al., 2016). This effect proves that tactile experiences are capable of having a modulatory effect on how embodiment is generated in the brain.

In addition to tactile experiences influencing embodiment, the opposite is also true–embodiment can influence how tactile information is interpreted. When visual input meshes with the known body image and can be easily embodied, touches are perceived differently than with non-embodied visual input. For instance, when participants viewed either two sticks or two hands from a first person perspective and were asked to detect the temporal order of a visual cue relative to a touch on one of the sticks or hands, the JND was larger in the hands condition (Maselli et al., 2016). In other words, the participants were less able to detect a difference in timing between a tactile stimulus and a visual stimulus when the visual stimulus was biologically plausible and more easily embodied. However, not all studies have replicated this effect (Smit et al., 2019), leaving open the question of how the temporal binding window is affect by embodiment.

In patients with missing limbs or SCI, embodiment of virtual, mirrored, or artificial limbs can help alleviate phantom limb pain (Chan et al., 2019; Pozeg et al., 2017; Ramachandran and Rogers-Ramachandran, 1996). Embodiment of a fake hand has also been used to elicit illusory tactile sensations in SCI patients (Lenggenhager et al., 2013).

Proprioceptive inputs have also been found to have an effect on the process of attributing actions to oneself, which contributes to the sense of embodiment (Kilteni et al., 2012a). In a study of a chronically deafferented patient, the patient was significantly impaired at identifying which cursor movements were controlled by him, and which were controlled by the computer (Balslev et al., 2007).

Given the strong link between tactile sensations and embodiment, restoring the sense of touch to patients who have lost it represents not just another sensory modality with which to navigate their environment but also a means by which these patients can more easily feel embodied in their limbs or prosthetics (Maimon-Mor and Makin, 2020; Marasco et al., 2011). In addition to feeling more natural, an embodied prosthetic can have other benefits: for example, in one participant missing a lower leg, it was found that they perceived their prosthetic to be lighter when the prosthetic was equipped with intraneural sensory feedback (Preatoni et al., 2021).

### 1.2 The sensorimotor loop

Traditionally, the computations encompassing the process of making an action plan, executing the action, and interpreting the sensory consequences of the action, are known as the sensorimotor loop. In this loop, planning areas in the brain, such as the premotor cortex, send action plans to the motor cortex, which transmits motor commands down the spinal cord to the muscles. Mechanoreceptors in the skin and muscles send cutaneous and proprioceptive information during the action back up the spinal cord to the primary somatosensory cortex, and this tactile feedback is integrated with other sensory information in higher order sensory areas and the posterior parietal cortex to decide on the next action. In reality, this process is much less linear, and the somatosensory and motor processing pathways are highly intertwined, containing many lateral and recurrent connections (de Haan and Dijkerman, 2020).

In this work, we will primarily focus on the primary somatosensory cortex (S1), which is classically known as an early-stage tactile processing area (Delhaye et al., 2018), but we will also consider the ventral premotor cortex (PMv) which is involved in motor planning, and the supramarginal gyrus (SMG), which represents higher-order multisensory integration and action planning.

### *1.2.1 Primary somatosensory cortex (S1)*

S1 is one of the first cortical areas to receive incoming tactile information, passed from mechanoreceptors in the skin, muscles, and tendons, up the spinal cord, and through the cuneate nucleus in the medulla and the ventroposterior complex of the thalamus (Delhaye et al., 2018; Sobinov and Bensmaia, 2021). S1 is located immediately caudal to the central gyrus and forms the rostral edge of the parietal lobe, and is typically characterized as representing tactile stimuli characteristics rather than the perceptual experiences they elicit (de Lafuente and Romo, 2006, 2005; Hernandez et al., 2000; Long et al., 2022). Motor planning also modulates S1, which may be due to representations of anticipated tactile information from the upcoming movement (Gale et al., 2021).

S1 encompasses Brodmann areas 1, 2, 3a, and 3b: Area 3b receives thalamic inputs, and is thus considered the base level of hierarchical processing within S1 (Kaas, 1983; Keysers et al., 2010), while areas 1 and 2 are thought to be more integrative, with neurons exhibiting more complex response properties than areas 3b or 3a (Felleman and Van Essen, 1991; Iwamura, 1998; Keysers et al., 2010). However, all four areas are interconnected with one another and have outputs to either S2, posterior parietal cortex, or both (Delhaye et al., 2018). Generally speaking, areas 3b and 1 respond to cutaneous stimuli, area 3a responds primarily to proprioceptive stimuli, and area 2 responds to both cutaneous and proprioceptive stimuli (Goodman et al., 2019; Iwamura et al., 1993; Kaas, 1983; Krubitzer et al., 2004; Long et al., 2022). While there are four distinct types of mechanoreceptors that respond to cutaneous stimuli, area 3b and area 1 of S1 appear respond to an amalgamation of the responses from these receptors, rather than segregating these inputs (Pei et al., 2009; Saal et al., 2015).

Given area 1's location at the top of the postcentral gyrus, it is more easily surgically accessed than area 3b (Pandarinath and Bensmaia, 2022). It is therefore a prime target for human electrophysiological studies that embed microelectrode arrays in the cortical surface of S1 (Armenta

Salas et al., 2018; Flesher et al., 2016). This work will primarily examine electrophysiological data from area 1 for this reason.

*1.2.1.1 The cortical homunculus*

S1 is known for having a distinct topographic organization in which body parts that are adjacent to one another anatomically are represented in cortical locations that are close to each other (Ejaz et al., 2015; Penfield and Boldrey, 1937; Sanders et al., 2019). This layout of the body along the surface of cortex is not to scale – instead, body parts with higher tactile acuity have substantially more cortical area devoted to them (Kolasinski et al., 2016). The representation of the body that reflects the amount of cortex assigned to each body part is known as the homunculus, which has very large hands, especially the thumbs, as well as an oversized face, while the torso and legs are much smaller (Kaas, 1983; Qi and Kaas, 2004; Sobinov and Bensmaia, 2021). Originally it was thought S1 formed one topographic map as a whole (Marshall et al., 1937) but it has since been found that area 3a, 3b, 1, and 2 each have their own distinct maps which run parallel to one another along the post-central gyrus (Kaas et al., 1979).

Although the S1 cortical homunculus was discovered in the early days of human cortical stimulation (Marshall et al., 1937; Penfield and Boldrey, 1937) and has been verified in many experiments since (Ejaz et al., 2015; Kaas et al., 2019, 1979; Kolasinski et al., 2016; Sanchez-Panchuelo et al., 2010; Sanders et al., 2019), recent work has suggested that tactile encoding in S1 may be more complex than previously assumed (Arbuckle et al., 2022; Muret et al., 2022; Thakur et al., 2012; Wesselink et al., 2022). For instance, Arbuckle et al. (2021) used 7T MRI to find nonlinear interactions in S1 areas 3b, 1, and 2 when stimulating multiple digits at the same time, suggesting touches in different locations result in a neural representation that is more than the sum of its parts. This work is supported by similar findings in area 3b of S1 in non-human primates (Qi et al., 2016; Thakur et al., 2012).

Most recently, fMRI in humans has shown that information about body parts is represented (albeit more weakly) outside of their traditionally defined areas in S1 (Muret et al., 2022), and that selectively anesthetizing a digit results in changes to the neural representations of other digits (Wesselink et al., 2022). In combination, these results indicate that S1 is not a purely linear readout of tactile input, but has multiple encoding schemes beyond the cortical homunculus.

*1.2.1.2 Multisensory modulation of S1*

Tactile experiences are constructed primarily from information relayed by cutaneous and proprioceptive mechanoreceptors, but are also affected by other types of stimuli such as visual information (Popovich and Staines, 2014; Staines et al., 2014). For example, the sight of a body part is known to improve tactile acuity and decrease reaction times to tactile stimuli, even when the visual input provides no information about the touch itself; this phenomenon is known as the visual enhancement of touch (VET) (Cardini et al., 2012; Colino et al., 2017; Haggard et al., 2007; Heller, 1982; Kennett et al., 2001; Press et al., 2004). VET has been shown to occur on a variety of body parts including the arm, the hand, the back of the neck, and the face (Colino et al., 2017; Kennett et al., 2001; Press et al., 2004; Tipper et al., 2001). Furthermore, detecting touches on a body part becomes more difficult when viewing a different body part (Tipper et al., 2001), although the limitations on what counts as the "same" body part are still being investigated–the fingertips and the back of the hand for instance may be distinct enough to fail to trigger VET (French et al., 2022).

Clearly, visual input affects how tactile stimuli are perceived. If touch experiences are constructed in a hierarchical manner, then the question is raised: at what stage of this processing is visual information integrated with tactile representations? S1 is the primary cortical site to receive mechanoreceptor-based tactile information from the thalamus before passing it to higher order processing regions, so visual information could be integrated in S1 to affect early processing or it could be integrated at a

later, more integrative stage of the tactile processing stream. Work in EEG has shown an effect of VET on the P50 and P80 somatosensory evoked potentials, which are thought to arise from S1 activity (Cardini et al., 2012, 2011; Deschrijver et al., 2016; Dionne et al., 2013; Taylor-Clarke et al., 2002). Using MEG, it has been shown that the topographic mapping of S1 shifts based on the relative timing of tactile stimuli relative to viewed touches of an embodied fake hand (Schaefer et al., 2006), or based on the level of magnification of the fake hand during touches (Schaefer et al., 2008). The application of transcranial direct stimulation (TMS) over S1 leads to impaired detection and discrimination of tactile stimuli, if viewing a human hand simultaneously, but not if viewing a neutral object like a wooden block (Fiorio and Haggard, 2005). Interestingly, this effect holds even if the stimuli are simply observed touches, not felt touches, suggesting that S1 has a role in processing touches that are purely observed (Bolognini et al., 2011; Rossetti et al., 2012).

A large body of literature spanning the last 20 years has examined the role of observed touch in S1, but the extent to which visual stimuli depicting touches are represented in S1 remains unclear. Many studies have found that S1 does respond to observation of touch in others or in first-person perspective (Blakemore et al., 2005; Ebisch et al., 2008; Kuehn et al., 2018, 2013; Longo et al., 2011; Meyer et al., 2011; Pihko et al., 2010; Schaefer et al., 2009). For example, in one EEG study, it was shown that S1 responses correlated with the intensity but not the unpleasantness of touch stimuli delivered to others (Bufalari et al., 2007). S1 also exhibited activity to a variety of observed touches including those that are accidental or intentional and those delivered by animate or inanimate objects (Ebisch et al., 2008). Notably, activity in S1 is much stronger to physical touches than observed touches (Pihko et al., 2010).

However, other studies in both humans and non-human primates have failed to find any substantial effect of observed touches on S1 at all (Chan and Baker, 2015; Keysers et al., 2004; Morrison et al.,

2004; Sharma et al., 2018). Using MRI, Keysers et al. (2004) found an effect of visual touches in S2 but not S1, and Morrison et al. (2004) found that S1 responded to painful, cutaneous sensations but not visual observation of these sensations being delivered to others. In another study of 40 participants, posterior parietal cortex adjacent to S1 was found to be modulated by observed touch, but S1 itself was not modulated (Chan and Baker, 2015). In combination, these studies indicate that S1's encoding of observed touches is nuanced and yet to be fully untangled.

In the real world, visual information is often paired with, and highly relevant to deciphering tactile stimuli. S1 has been shown to have an increased response to visuotactile stimuli in comparison to tactile stimuli alone (Dionne et al., 2013; Staines et al., 2014). Similarly, it was found that some neurons in S1 in non-human primates respond to visual cues when they had established associations with tactile stimuli (Zhou and Fuster, 2000). In fact, visual cues that are predictive of tactile events have bene shown to modulate S1 approximately 300ms before the tactile event (Kimura, 2021).

Considering the literature as a whole, it seems apparent that S1 is not a mono-sensory area. While it is primarily concerned with the processing of tactile information, there are clearly cases where it is modulated by vision (Blakemore et al., 2005; Bolognini et al., 2011; Dionne et al., 2013; Kuehn et al., 2013; Taylor-Clarke et al., 2002). It is likely that these effects are not due to direct connections between the primary visual cortex and S1; rather, it is probable that S1 has recurrent connections with multimodal integrative areas which receive information from other sensory sources and allow S1 to be modulated by relevant stimuli (Schaefer et al., 2008).

*1.2.1.3 Higher order cognitive factors*

If S1 is modulated by higher order integrative brain areas to represent multisensory information, it follows that the same pathways could allow it to be affected by other context-dependent factors relevant to touch.

One of the most ubiquitous context-dependent factors is attention. In non-human primates, it has been found that some S1 neurons increase their firing rates during tactile stimuli when the primates' attention was directed towards the tactile stimuli (Chapman and Meftah, 2005; Meftah et al., 2002). In humans, EEG was used to show an analogous finding: S1 activity was modulated by the task-relevance of tactile stimuli (Dionne et al., 2013).

S1 also appears to reflect more nuanced social contexts of touch. For instance, early onset S1 activity was shown to be modulated by whether the visual stimulus paired with a physical touch was a human hand or a wooden hand, as well as whether the touched finger on the observed hand matched the touched finger of the hand feeling the physical stimulus (Deschrijver et al., 2016). In addition to this effect which the authors ascribed to "animacy" of the hand, S1 also is capable of being modulated by self/other dynamics: tactile responses are larger when the touch comes from an outside source than when it is self-generated (Blakemore et al., 1998). This attenuation of self-touches may be due to a forward model generated by the brain which predicts the sensory outcomes of planned movements, such that S1 responds more to unpredicted tactile inputs (Blakemore et al., 1999). S1 has also been implicated in affective processing; in a study where heterosexual men experienced caresses with the belief that the caresses came from either a man or a woman, S1 was modulated by the perceived gender of the caresser (Gazzola et al., 2012). These studies all support the idea that complex environmental contexts can affect tactile processing even at early stages.

S1 is also recruited during tactile imagery, when no physical or visual stimulus is presented at all, and the S1 sub-areas activated by tactile imagery overlap with those which respond to real tactile stimuli (Yoo et al., 2003), suggesting a degree of commonality between imagined and real tactile representations.

In addition to representing a wide variety of touch types in different contexts, the neural encoding patterns of S1 can also be altered based on experience (Miller et al., 2019; Schaefer et al., 2004; Schettler et al., 2019). Schaefer et al. (2004) showed that the topography of S1 changed when participants manipulated an object with their hands in comparison to using a pair of tongs – widening the distance between the thumb and pinky representations. Following up on this finding, it was shown that S1 encodes touch locations on a hand-held stick immediately once it is in hand (Miller et al., 2019), corresponding with the idea that the brain is able to refer touches to tools directly instead of the hand in which the tool is held (Yamamoto et al., 2005; Yamamoto and Kitazawa, 2001). Thus S1 plays a role in allowing the brain to treat tools as natural extensions of the body (Miller et al., 2019, 2018).

### *1.2.2 Motor and premotor cortex*

Just as the primary somatosensory cortex is one of the first cortical areas to receive tactile information, the primary motor cortex (M1) is one of the final cortical areas which sends motor commands down the spinal cord to the muscles, and this region contains a similarly-scaled topographic map which represents desired direction of movements (Georgopoulos et al., 1982; Sobinov and Bensmaia, 2021; Woolsey et al., 1979). The map is not as highly segregated at S1 and contains overlapping representations of body parts (Graziano and Aflalo, 2007; Sanes et al., 1995). The close relationship between M1 and the movements produced by the body is causally established: electrically stimulating M1 elicits movements (Baldwin et al., 2018), and lesions in M1 result in pronounced motor impairments, especially with respect to motion requiring dexterity or individuated finger movements (Lang and Schieber, 2003; Murata et al., 2008; Rouiller et al., 1998).

Before motor commands can be sent out of motor cortex, actions and motor plans must be decided upon and refined in higher-order areas (Gallivan et al., 2018). Premotor cortex, which lies

immediately frontal to motor cortex, has inputs from posterior parietal cortex (see Section 1.2.3) and is highly involved in refining motor plans (Kaufman et al., 2014; Schaffelhofer and Scherberger, 2016; Umilta et al., 2007). Neurons in premotor cortex have been found to be tuned to a variety of sensorimotor variables, including 3D object shape, as well as planned grasps (Schaffelhofer et al., 2015; Theys et al., 2013; Wandelt et al., 2022), and visual, tactile, and proprioceptive information (Fogassi et al., 1996; Graziano, 1999; Graziano et al., 1997). Stimulating the premotor cortex directly during awake brain surgery has been shown to disrupt conscious awareness of whether movements are successfully performed (Fornia et al., 2020). Using fMRI, premotor cortex has been shown to be affected by embodiment illusions, and is capable of representing embodied fake limbs (Alchalabi et al., 2019; Ehrsson et al., 2004; Gentile et al., 2015), with a preference for stimuli that appear visually and proprioceptively congruent (Limanowski and Blankenburg, 2016; Petkova et al., 2011).

Given its role in representing desired movements, premotor cortex is a viable target for electrophysiological studies seeking to decode sensorimotor variables in the context of neural prosthetics (Armenta Salas et al., 2018; Willett et al., 2020).

### *1.2.3 Posterior parietal cortex (PPC)*

PPC represents a large swath of the brain located dorsal to the central sulcus, with S1 forming its frontal border. As a whole, PPC is thought of as a higher level, integrative brain area, where information from different sensory inputs meet and are combined with contextual variables to better inform action plans (Chivukula et al., 2019; de Haan and Dijkerman, 2020). PPC is composed of many sub-regions, each of which appear to be concerned with a subset of sensory, contextual, and motor factors (Hadjidimitrakis et al., 2019). For instance, in non-human primates, the anterior intraparietal area (AIP) is known to be selective for object characteristics like shape, size, and orientation, during grasping tasks or even during simple fixation (Murata et al., 2000; Schaffelhofer

and Scherberger, 2016). In humans, PPC neurons have been shown to exhibit tuning to both real touches and imagined ones (Chivukula et al., 2021), as well as touches on hand-held tools (Miller et al., 2019). PPC also appears to play a role in maintaining representations of bodily posture within the external environment (Azañón et al., 2010; Bolognini and Maravita, 2007), and fMRI studies have shown PPC responds to embodiment illusions (Petkova et al, 2011; Ehrsson et al, 2004).

In addition to sensory characteristics, PPC neurons represent movement intentions before the movement is initiated (Snyder et al., 1997). Electrical stimulation of PPC with long-train stimulation in non-human primates has elicited complex, biologically relevant movements like hand grasps (Baldwin et al., 2018). Human electrophysiology work has demonstrated that PPC representations include imagined movements, trajectories, and goals (Aflalo et al., 2015). Because of its high level encoding of task variables and motor intentions, PPC has been identified as a target site for neural prosthetics seeking to restore motor function (Andersen and Buneo, 2002; Chivukula et al., 2019). Recordings from PPC are sufficient to decode the 2D movement of a computer cursor, and can be dynamically modulated through the use of different cognitive strategies (Sakellaridi et al., 2019).

Due to the diverse and multifaceted nature of representations in PPC, there are many sub-regions that would be viable, interesting targets for human electrophysiology studies (Chivukula et al., 2019). This work will principally focus on the supramarginal gyrus (SMG), one sub-region of PPC with potential use to neural prosthetics, with the understanding that the findings there may not generalize to other sub-regions, and that further work will be needed to characterize PPC as a whole.

SMG is a region on the ventral side of PPC, located just dorsal of the Sylvian fissure. It is near Weirnicke's area, which is instrumental for the understanding of speech (Bogen and Bogen, 1976; Harpaz et al., 2009), as well as the temporo-parietal junction which is implicated in theory of mind, morality judgements and maintaining the sense of embodiment (Saxe and Kanwisher, 2003; Tsakiris

et al., 2008; Young et al., 2007). The precise functionality of SMG itself remains under investigation, but it is thought to be part of association cortex, with well-documented responses to language processes (Sliwinska et al., 2012; Wandelt et al., 2022) and sensorimotor stimuli, like tool use (McDowell et al., 2018; Orban and Caruana, 2014; Peeters et al., 2009) and grasps (Sakata et al., 1995; Wandelt et al., 2022). Thus SMG is a brain region in which variables of interest could potentially be decoded to restore function to patients with sensorimotor impairments along multiple axes, such as speech, somatosensory responses, and movement planning.

### *1.2.4 Sensory remapping in the brain*

When the body's sensorimotor abilities are altered, how does the somatosensory brain map change? Initial evidence seemed to point to a strong remapping effect. In cases of impaired arm and hand somatosensation, it has been found that touching the face activates the traditional "hand area" of S1 (Pons et al., 1991; Ramachandran et al., 1992). However, the extent of remapping varies depending on the source of limb loss: those born with one hand (congenital one-handers) exhibit significant remapping of facial sensations whereas amputees show much less remapping (Root et al., 2022). This result suggests that remapping may not occur if the hand is lost later in life, due to neural pathways being more fully developed. In cases of SCI, evidence from the rubber hand illusion seems to suggest remapping does occur: tetraplegic patients are able to sense the illusion while observing the hand and feeling strokes to the face (Scandola et al., 2014; Tidoni et al., 2014).

However, if S1 contains multiple layers of encoding (Muret et al., 2022) rather than just a simple topography, then referral of facial sensations to the hand area could occur without meaning that the original primary pathways are removed (Makin and Bensmaia, 2017). Recent work in fMRI has shown that individuals with tetraplegia exhibit hand somatotopy that is highly similar to healthy controls, even years after injury (Kikkert et al., 2021). Similarly, representations of attempted hand

movements in PPC in a tetraplegic patient retained strong correspondences to the representations of hand movements in healthy humans (Guan et al., 2022).

It is also possible that somatosensory topography in the brain is highly plastic, able to adapt to current tactile demands while preserving prior pathways. For instance, just 5 days of wearing an artificial "third thumb" on one hand was sufficient for healthy humans to exhibit an altered neural representation of the fingers in that hand (Kieliba et al., 2021). Thus, it is perhaps unsurprising that when the sensory system faces a massive change such as SCI or limb loss, the dominant topography of sensory encoding changes, but this fact does not necessarily mean the original topography has been entirely overwritten.

### 1.3 Brain-Machine Interfaces (BMIs)

The term "brain-machine interface," also commonly referred to as a "brain-computer interface," is a broad one, which can refer to any system which reads neural information and uses it to affect the environment, or additionally any system which provides information to the brain bypassing the peripheral nervous system. Here, we will consider the subtype of BMIs known as neural prosthetics, which typically directly record from the brain using implanted electrodes in order to decode motor intentions, such as desired movement of a robotic limb (Collinger et al., 2013; Fagg et al., 2007) or articulating a spoken phrase (Metzger et al., 2022; Moses et al., 2021; Stavisky et al., 2019). In an open-loop BMI, the implanted patient usually relies on visual cues in order to decide what motor actions to perform with the BMI, but has no tactile feedback (Collinger et al., 2013; Dekleva et al., 2021). In a closed-loop BMI, artificial tactile sensations carrying task-relevant information are also provided by electrically stimulating the brain (Armenta Salas et al., 2018; Flesher et al., 2021, 2016). In general, neural prosthetics have the twin goals of collecting data to understand the science of how

the sensorimotor loop is implemented, and using this understanding to develop viable technology for people with motor and sensory impairments to regain lost functionality.

Historically, the field of neural prosthetics has focused more on decoding motor intentions than on restoring sensation, possibly because recording information from motor areas is more simply implemented and contains fewer safety concerns that using electrical current to stimulate sensory areas. Additionally, speed and accuracy in motor tasks can be easily measured as a tractable external metric of BMI performance (Collinger et al., 2013; Dekleva et al., 2021), while understanding artificial qualia and how they impact quality of life is a more nuanced task often relying on subjective internal reports (Armenta Salas et al., 2018; Flesher et al., 2016).

Motor BMIs have seen a good deal of performance improvement over the last 15 years and can be used to decode arm and finger movements (Collinger et al., 2013; Willsey et al., 2022) as well as cursor clicks and movements on a computer screen (Dekleva et al., 2021; Santhanam et al., 2006) with high fidelity. Up to seven dimensions of arm movement can successfully be decoded from motor cortex (Collinger et al., 2013), and there have even been recent efforts to make a fully at-home BMI that is operable through the patient's smartphone or tablet with only minimal assistance from caregivers (Davis et al., 2022; Simeral et al., 2021). There has also been substantial computational work to make BMIs more robust over time by mapping neural activity to lower dimensional spaces so less recalibration data is needed day-to-day (Keshtkaran et al., 2022; Pandarinath et al., 2018).

While motor BMIs continue to improve, a viable, widely-applicable somatosensory BMI has yet to be developed, although it has been demonstrated that percepts elicited through artificial stimulation are distinguishable (O'Doherty et al., 2019, 2011), and that they can lead to performance improvements to motor tasks (Bensmaia and Miller, 2014; Flesher et al., 2021; Klaes et al., 2014).

Current work, including this thesis, aims to better understand how to elicit reliable, replicable sensations across individuals using electrical stimulation.

### *1.3.1 Methodology*

Typically, patients enrolled in neural prosthetics clinical trials undergo neurosurgery in order to have microelectrode arrays (Blackrock Neurotech, Salt Lake City, Utah) implanted in motor and/or sensory locations in the surface of the cortex. Arrays are usually 4.2mm square grids of 96 electrodes, each 1.5mm long. Given this length, it is likely that the bulk of electrodes are recording in layers 3 or 4 of cortex, although the curved nature of the cortical surface combined with the flat array may result in some electrodes being embedded in different layers.

Typical locations for implants include M1, premotor cortex, PPC, and S1 (Armenta Salas et al., 2018; Collinger et al., 2013; Flesher et al., 2016; Sakellaridi et al., 2019; Willett et al., 2020). Once implanted, the arrays can be used to record electrophysiological data–and in some cases, stimulate the cortex electrically–for many years, although there is some degradation of the recording quality as the electrodes age (Hughes et al., 2021b; Woeppel et al., 2021). Neural data is recorded at a very high temporal resolution (30,000 Hz) as well as a high spatial resolution within the microelectrode array locations, but this spatial resolution is limited to the relatively small surface area covered by the arrays. Given that currently no more than 6 arrays have been implanted in any one participant, the arrays' limited recording area renders their accurate placement in the brain critical.

### *1.3.2 Intra-cortical microstimulation (ICMS)*

Electrical stimulation of the human brain has been used for nearly 100 years to better understand the purpose of different regions by eliciting qualia relevant to their function–for example, tactile sensations are evoked by stimulating S1 (Penfield and Boldrey, 1937; Sagar et al., 2019; Woolsey et al., 1979). Intra-cortical microstimulation (ICMS) refers specifically to electrical stimulation within

the cortex, passed through microelectrodes. Foundational work in macaques demonstrated that the frequency of ICMS through electrodes in S1 can be discriminated qualitatively (London et al., 2008; Romo et al., 1998), and that performance in a tactile detection or discrimination task with ICMS can equal to that with real tactile stimuli (Berg et al., 2013; Tabot et al., 2015). Further work in macaques, and later in humans, proved that virtual objects explored only using ICMS feedback could be discriminated from each other (Klaes et al., 2014; O'Doherty et al., 2011; Osborn et al., 2021).

While it is now well-established that ICMS is capable of conveying tactile information to some degree, it remains under investigation how well the properties of ICMS match up to the properties of real tactile sensation. In one study where macaques explored ridged gratings to discriminate textures with ICMS, their discrimination accuracy conformed to Weber's law (O'Doherty et al., 2019), which states that the JND of a sensory percept should increase proportionally to the change in the stimulus– in this case, the distance between the grating ridges (Ekman, 1959). Another study found that JNDs do not increase proportionally to the stimulation current amplitude, although only two amplitudes were assessed (Kim et al., 2015b). In contrast, it was shown that in rats, JNDs do follow Weber's law with respect to ICMS current amplitude and pulse-width (Bjånes and Moritz, 2019). More investigation is needed to determine in what aspects ICMS does obey Weber's law, if there are some properties which reliably violate it, and if there are meaningful differences across species.

While the neural activation patterns during ICMS remain poorly understood, one study used calcium imaging of mice during 30s ICMS trains to demonstrate that low frequencies of ICMS result in neurons remaining active throughout stimulation while high frequencies cause neurons to become inactive by the end of stimulation (Michelson et al., 2019). Computational modeling work has also shown that with increased ICMS current amplitude, the density of activated neurons at the stimulation

site increases, but the volume occupied by activated neurons remains relatively stable (Kumaravelu et al., 2022).

One major benefit of working with human participants over non-human animal models is that humans can report qualia elicited by ICMS. This has allowed for an exploration of what type of parameters elicit what type of sensations, but has also highlighted how little is understood about of these methods–experiences of ICMS appear to vary widely between participants, and the same parameters even within one participant do not always elicit the same sensation at the same location (Armenta Salas et al., 2018; Flesher et al., 2016). However, a few rule-of-thumb guidelines have emerged. Continuous high-frequency stimulation leads to extinguishing of sensations while low-frequency stimulation leads to longer percepts, but this effect can be alleviated with intermittent stimulation (Hughes et al., 2022). Increasing the ICMS current amplitude or stimulation duration leads to more intense sensations overall (Armenta Salas et al., 2018; Flesher et al., 2016; Hughes et al., 2021a). Location of percepts tend to follow the topographic organization of S1 (Armenta Salas et al., 2018; Flesher et al., 2021).

When it comes to designing ICMS inputs, one approach is to create arbitrary stimuli and rely on the user to learn how these stimuli encode real-world variables de novo. However, it is generally agreed that a biomimetic approach, where ICMS is designed to best replicate real sensory inputs, would be best if it is viable because it would be the most intuitive for a user to adopt (Tabot et al., 2015). In this framework, ICMS should aim to create sensations that are close to what would be experienced with an intact nervous system. One attempt at biomimicry in peripheral nerve stimulation of trans-radial amputees has been to modulate pulse frequency and current amplitude to be more similar to natural nerve responses to the onset and offset of touch (Saal and Bensmaia, 2015). This approach has

resulted in increased sensation naturalness and tactile sensitivity (Valle et al., 2018), but it remains to be seen if this result replicates with ICMS.

### *1.3.3 Benefits of a BMI with sensory capabilities*

The tight link between somatosensation and motor abilities has been well-established (Miall et al., 2019; Robles-De-La-Torre, 2006; Sainburg et al., 1995), as has the link between somatosensation and embodiment (Balslev et al., 2007; Giummarra et al., 2008; Kilteni et al., 2012a). Additionally, amputees equipped with artificial sensory feedback pertaining to a prosthetic hand via intraneural stimulation have shown improved manual dexterity, enhanced prosthetic embodiment, and perceive the prosthesis to be lighter (Page et al., 2018; Preatoni et al., 2021; Valle et al., 2018). It is highly likely that an advanced BMI could provide comparable benefits, which would be critical for it to be able to deliver meaningful improvements in patient quality of life.

In a recent study, a tetraplegic patient used a motor BMI recording from their motor cortex to perform a task involving reaching to an object with a robotic limb, picking the object up, and transporting it to a target destination (Flesher et al., 2021). When equipped with ICMS sensory feedback from the robotic limb, the patient performed the task twice as fast, primarily saving time during object grasping. This finding clearly shows that ICMS can supplement visual information to improve motor dexterity improvements. However, it is important to note that the ICMS feedback provided was quite crude: electrodes mapped to the finger topography of S1 delivered stimulation varying in current amplitude based on torque measurements from the robotic fingers. The substantial potential, yet unrealized, to improve the sensitivity and dimensionality of ICMS feedback means that assessing the full extent of performance improvements, or the effects on the sense of embodiment, is not yet possible (Beckerle et al., 2018).

### *1.3.4 Multisensory integration of ICMS*

Studies of the effects of ICMS often consider it alone, without any outside context (Armenta Salas et al., 2018; Flesher et al., 2016; Hughes et al., 2022, 2021a). However, just like the natural sense of touch, ICMS feedback should exist as part of a rich multisensory environment (Risso and Valle, 2022). When the qualia elicited by ICMS are unreliable, even over repetitions of the same parameters (Armenta Salas et al., 2018; Flesher et al., 2016), it is possible that the addition of context, particularly in the form of visual information, will allow for stabilization of these percepts.

While it might seem intuitive that the relative time between onset of an artificial tactile stimulus and its evoked sensation would be as fast or faster than a physical tactile stimulus given the immediacy of the injected input to S1, ICMS is perceived approximately 50ms more slowly than an intensity-matched physical vibrotactile stimuli (Christie et al., 2022). This discrepancy suggests that the brain may have difficulty synchronizing visual and ICMS input if it assumes the same processing speed for ICMS and real physical touches. Other studies have corroborated this finding, showing that reaction times to single-channel ICMS cues are slower than visual or tactile cues (Godlove et al., 2014), and that electrocorticographic (ECoG) stimulation is also perceived more slowly slower than tactile stimuli (Caldwell et al., 2019). Similarly, it was shown using peripheral intraneural stimulation in amputees that stimulation felt synchronous with visual stimuli at different offsets depending on whether the lower or upper limb was stimulated (Christie et al., 2019b). This study also tested the temporal binding window for peripheral stimulation and vision–in other words, the maximum length of time between the two stimuli in which they still felt synchronous–which was approximately 100ms. Understanding the temporal binding window of ICMS and vision will be critical because it will provide a sense of what latencies are permissible in a functional sensory BMI.

ICMS paired with visual information can improve motor task performance better than either sensory modality alone (Dadarlat et al., 2015; Flesher et al., 2021), but it is unclear how this multisensory integration occurs in the brain. It will be important to understand the weight that the brain assigns to incoming tactile information based on the sensory modality it comes from, and how it reconciles sensory information that conflicts with ICMS (Risso et al., 2019). For instance, trans-tibial amputees who experienced intraneural stimulation localized to their missing foot while watching touches being applied to a prosthetic foot attached to them were biased to interpret the location of the touch based on visual information (Christie et al., 2019a).

Ideally, visual information could provide a lens through which ICMS is interpreted, which could contribute to the stabilization of unpredictable qualia. Encouragingly, the rubber hand illusion has been successfully elicited in epilepsy patients using a combination of vision and stimulation of ECoG channels (Collins et al., 2017). This indicates that the interpretation of artificial tactile stimulation can be biased by vision in how it contributes to the sense of embodiment, just as vision biases the interpretation of real physical touches in the classic version of the illusion.

### *1.3.5 Current challenges*

Every year, new research pushes forward our understanding of the somatosensory system and how to better interface with it to create restorative devices for patients with impaired sensorimotor abilities. However, major obstacles exist that must be reckoned with before a BMI capable of truly providing an artificial sense of touch can be created.Firstly, because of the highly specialized and technical nature of this research, patients who enroll in BMI clinical trials are rare. In order to establish a potential BMI as useful to a broad patient population, it will be necessary to conduct studies with sample sizes large enough to be sure that individual differences are not confounding the results, and

protocols must be established to map neural responses to motor output, and sensory stimuli to ICMS, in a generalizable fashion.

Another massive challenge is that the relationship between ICMS and the qualia of evoked sensations remains to be elucidated. While it is encouraging that microelectrode arrays remain usable for years after implantation, the properties of the electrodes change and degrade over time, making it difficult to establish a map of sensation in even one individual (Hughes et al., 2021b). Even across weeks, stimulating with a given set of parameters multiple times frequently generates results that differ in intensity, location, and qualitative aspects (Armenta Salas et al., 2018; Flesher et al., 2016), and the relationships between parameters and percepts seem to change between electrodes on the same microelectrode array (Callier et al., 2020). Without a better understanding of how to elicit a specific sensation at the appropriate location on the body on demand, it will be very difficult to create a BMI that approximates the experience of real touch.

A persistent difficulty in establishing this better understanding is that the parameter space of possible ICMS frequencies, amplitudes, pulse widths, and durations is massive, even before considering stimulating on multiple electrodes simultaneously or in one of a near-infinite number of patterns. It is simply not possible to test all permutations in a single participant, let alone in a significant sample size of people. However, studies are beginning to break this problem down into manageable pieces by selectively examining subsections of this parameter space (Armenta Salas et al., 2018; Callier et al., 2020; Flesher et al., 2016; Hughes et al., 2022, 2021a), including differences between single channel and multiple channel ICMS (Kim et al., 2015b; Sombeck and Miller, 2020). One promising result is that stimulating with multiple channels appears to lower reaction times to ICMS, potentially minimizing the lag between ICMS and other sensory modalities (Sombeck and Miller, 2020).

Hopefully, moving forward, other findings of this type will contribute to a better understanding of how to improve ICMS experiences and make them more naturalistic.

# *Chapter 3*

# IMAGINED SOMATOSENSORY PERCEPTS IN HUMAN CORTEX

The following chapter's contents are taken and adapted from Bashford et al. (2021) with modifications done to fit the dissertation format.

Bashford, L., Rosenthal, I., Kellis, S., Pejsa, K., Kramer, D., Lee, B., Liu, C., Andersen, R.A., 2021. The neurophysiological representation of imagined somatosensory percepts in human cortex. J. Neurosci. 41, 2177–2185. https://doi.org/10.1523/JNEUROSCI.2460-20.2021

## 3.1 Introduction

In recent studies, intra-cortical microstimulation (ICMS) in the primary somatosensory cortex (S1) has been successfully used to elicit somatosensory sensations in tetraplegic humans below the level of spinal cord lesion (Armenta Salas et al., 2018; Flesher et al., 2016). Many parameters of the electrical stimulus, such as amplitude, frequency, duration, and electrode location, have been found to manipulate the qualitative experience of elicited sensory responses in both non-human primates and humans (Armenta Salas et al., 2018; Callier et al., 2020; Flesher et al., 2016; Kim et al., 2015a, 2015b; Sombeck and Miller, 2020). It is therefore important to develop our understanding of the correspondence between stimulation parameters and the sensations they elicit if we are to further understand the mode of action of ICMS and elicit specific sensations more reliably via ICMS. To begin, we seek to uncover the neurophysiology underlying those sensations previously elicited by ICMS.

In previous work (Armenta Salas et al., 2018), we found the top five most elicited somatic sensations

with ICMS in S1 of a human participant. These were naturalistic sensations which the subject had not experienced in deafferented locations since being injured. We seek to examine for the first time the intra-cortical electrophysiological behavior of human sensorimotor circuits while experiencing these same sensations. Since it is not possible to use normal touch to elicit a sensation below the level of paralysis in a tetraplegic individual, we performed our experiment using "somatosensory imagery," the vivid recollection of a somatosensory experience, to evoke activity in these circuits specific to the same sensations experienced during electrical stimulation. We chose to use sensations that were previously elicited by ICMS, rather than any sensation the subject was able to imagine, because these sensations were elicited with known stimulation parameters in the same cortical area we record from during somatosensory imagery.

Somatosensory imagery has previously been shown in functional magnetic resonance imaging (fMRI) studies to activate the somatosensory system (Fitzgibbon et al., 2012; Hodge et al., 1996). Both primary and secondary somatosensory areas are activated by tactile imagery (Yoo et al., 2003) in areas that respond to actual touch. Imagined movements after amputation of the fingers have also been shown to produce neural activation in somatosensory cortex (Rosén et al., 2001). We record intra-cortically from three areas of human cortex (**Figure 3.1a**), S1, ventral premotor cortex (PMv), and the supramarginal gyrus (SMG). Each of these areas is involved in somatosensory processing. Neurons in S1 respond to cutaneous and proprioceptive stimuli (Hyvärinen and Poranen, 1978; Iwamura et al., 1993; Seelke et al., 2012; Taoka et al., 2000) and electrical stimulation in this area produces naturalistic somatosensory percepts (Armenta Salas et al., 2018; Flesher et al., 2016). The SMG array, on the SMG near the anterior end of the intraparietal sulcus (**Figure 3.1a**), is in a region of cortex often studied in the context of grasp for both human (Binkofski et al., 1998; Culham et al., 2003) and non-human primate (Baumann et al., 2009; Dong et al., 1994) studies. There is not yet

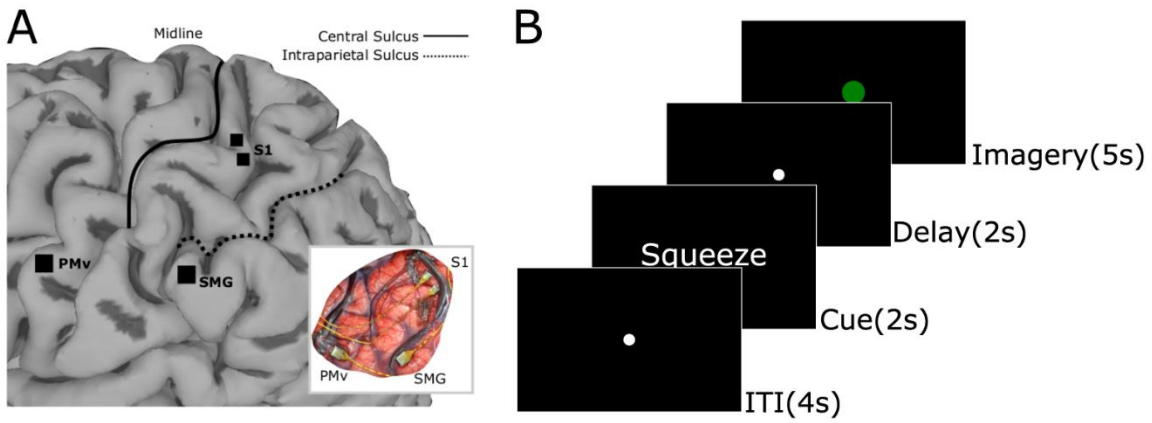


**Figure 3.1 Implant locations and task design**
**a)** Array implant locations. **b)** Task paradigm: (1) ITI, 4 s; (2) cue phase displaying the sensation to be imagined, 2 s; (3) delay phase, 2 s; (4) imagery phase during which time the participant recalls as vividly as possible the sensation presented during the cue, 5 s.

enough evidence in this literature and our study to make exact homological assignments between the two species. Similarly, this same region of cortex responds to somatosensory stimuli in both species (Dong et al., 1994; Leinonen et al., 1979) and has reciprocal connections to other sensorimotor regions such as BA1, BA2, BA5, S2 (Neal et al., 1990), and premotor cortex (Gregoriou et al., 2006). Broadly, posterior parietal cortex is a higher order area in sensorimotor and somatosensory processing (Aflalo et al., 2015; Romo et al., 1998; Romo and de Lafuente, 2013). PMv neurons respond to tactile and proprioceptive somatosensory stimuli (Fogassi et al., 1996; Graziano, 1999; Graziano et al., 1997). Given the role of these areas in somatosensory processing, we expect to observe neurophysiological modulation because of somatosensory imagery.

In this work we investigated the neural correlates of imagined sensations and how this representation is distributed across different sensorimotor cortical areas. We used the sensations previously experienced by our participant during ICMS (Armenta Salas et al., 2018) and sought to demonstrate a discriminable representation of the sensations in the brain. We examined neurophysiological responses to somatosensory imagery from intra-cortical human recordings across three brain areas, each implanted with recording microelectrode arrays (Utah Array, Blackrock Neurotech): S1, SMG,

and PMv. We found a highly significant classification accuracy between sensations was attainable using both threshold crossing spiking activity and spectral power of various common frequency bands in the continuous brain signal.

Our results demonstrate that unique sensory experiences can be classified from human neural signals during somatosensory imagery and explore how the encoding of different aspects of sensation are distributed across different brain areas. The correspondence between the neural signal during somatosensory imagery and the stimulation parameters that elicit the same sensations may inform the choice of stimulation parameters for eliciting novel and robust sensations via ICMS in future work.

## 3.2 Methods

### *3.2.1 Participant*

We recruited and consented a male participant with C5-level incomplete spinal cord injury (34 years old, three years and six months post-injury, and one year and eight months post-implant, at the time of the first experiment) to participate in a clinical trial of a brain-machine interface (BMI) system with intra-cortical recording and stimulation. All data were recorded through electrode arrays that were implanted in three locations of the left hemisphere (**Figure 3.1a**): SMG, PMv, and S1. One 96-channel, platinum tipped Neuroport microelectrode recording array (Blackrock Neurotech, Salt Lake City, UT) was implanted in each of SMG and PMv. Two 48-channel SIROF-tipped (sputtered iridium oxide film) microelectrode arrays were implanted in S1. Further information regarding specific surgical planning and implantation details are described in (Armenta Salas et al., 2018). All procedures were approved by the Institutional Review Boards (IRB) of the California Institute of Technology, University of Southern California, and Rancho Los Amigos National Rehabilitation Hospital.

### *3.2.2 Task*

Based on the outcome of S1-only stimulation mapping we identified the five most commonly elicited sensations with ICMS: “squeeze,” “tap,” “rightward movement,” “vibration,” and “blowing.” These sensations represented 24.9%, 17.3%, 9.7%, 8.1%, and 6.6%, respectively, of 381 total ICMS elicited sensations (for full details of ICMS mapping see, Salas et al., 2018). These sensations were experienced in the same body locations of the contralateral forearm and upper arm. In our somatosensory imagery experiment, each trial consisted of an intertrial interval (ITI), a cue, a delay, and an imagery phase. During the ITI, a black screen with a gray circle (1-cm diameter) in the middle was shown for 4 s during which time the participant was instructed to rest and fixate gaze on the circle, although gaze was not measured. In the cue phase, one of the sensations listed above was presented as a written word for 2 s, then in the 2-s delay phase, only a black screen with the fixation circle was shown. In the final 5-s imagery phase of the task, the fixation circle changed to green and the participant began somatosensory imagery. The instruction for the imagery phase given at the beginning of each experiment was to “imagine the sensation as you experienced it during electrical stimulation as vividly as possible” (**Figure 3.1b**). The participant confirmed to us that the sensations were all imagined in the same location at the forearm, thus controlling for the inadvertent classification of location rather than sensation. In each run of the task, each individual sensation was imagined 10 times (total 50 trials per run), pseudo-randomly shuffled. The full dataset consists of 400 trials with N =80 repetitions of each imagined sensation.

### *3.2.3 Experiment design and data collection*

Data were collected from each array site using a 128-channel Neural Signal Processor (Blackrock Neurotech). Broadband signals were recorded at 30,000 samples/s. Spectral power was computed for each phase of each trial using MATLAB’s pspectrum function (MathWorks Inc. MA). Unsorted

threshold crossings (Christie et al., 2015; Dai et al., 2019; Oby et al., 2016) extracted from the broadband signal using a threshold of -3.5 times the noise RMS of the continuous signal voltage, were used as spike activity. The first full data set (herein referred to as experiment 1) was collected across 10 d. The second full data set was collected 11 months later, across 24 d (herein referred to as experiment 2). This time delay allowed us to explore the stability of the representations initially observed. ICMS sensory mapping (Armenta Salas et al., 2018) that produced the percepts used for imagery in this study were collected 16 months before experiment 1 began.

### *3.2.4 Statistics and analysis methods*

Classification was performed independently for each array and each phase of the somatosensory-imagery task using linear discriminant analysis (LDA) with the fitcdiscr function in MATLAB. For analysis using spike firing rates, the average threshold crossing rates from each channel, calculated from the entirety of each phase in 50-ms time bins, were passed as features to the classifier. For analysis of the spectral power data, power in the 4–8 ($\theta$), 8–12 ($\alpha$), 12–30 ($\beta$), 30–70, 70–150, and 150–300 Hz ($\gamma$) bands, computed for each channel, were used as features. Classification was performed separately for each frequency band. We note that in these very high-frequency bands the signal is likely to reflect the spiking activity of local neurons.

For both threshold crossings and spectral power, LDA was performed over 1000 repetitions. In each repetition, all 400 trials were randomly divided in a 50/50 cross-validation training and testing paradigm. Following 1000 repetitions, mean classification accuracy and 95% confidence intervals were computed. This procedure was repeated in a null condition where class labels were randomly shuffled during each repetition to generate a chance-level distribution of classification accuracies. Significance for classification performance was calculated by comparison of the overlapping percentile values of the actual and null data set. The full results are available in **Table 3.1**.

In order to test the ability of our datasets to generalize to one another, a decoder was trained on all of experiment 1 data and tested on all of experiment 2 data (another decoder was trained using the opposite train/test regime). This analysis yielded only one accuracy for each phase and electrode array as opposed to a distribution over 1000 iterations, because of the nature of testing which used one specific split of the data. However, the null condition was calculated as before, by shuffling the trial labels of both train and test datasets randomly over 1000 iterations. For this reason, in the generalization analysis, for each phase and electrode array, a single accuracy value was compared with the percentiles of the null distribution. For instance, we report $p > 0.05$ if the accuracy was greater than the value at the 97.5th percentile of the null distribution. Initially we performed LDA without preprocessing (e.g., without performing dimensionality reduction) as this allows for a direct analysis of the relationship between the neural activity recorded on each channel and imagined sensations. However, since the absence of preprocessing results in a small trade-off in classification accuracy, we separately repeated the classification using singular value decomposition (SVD) feature selection before model fitting. For threshold-crossing features, SVD was computed on mean-centered firing rates averaged within each task phase (svd function in MATLAB). Average firing rate data were projected onto the top $N$ features that represent the dimensions of greatest variance in the data. $N$ was determined by examining accuracy scores across phases and electrode arrays in experiment 1. $N$ was calculated separately for spike decoding and for each frequency band in spectral power decoding. $N$ was initially set to 5 features, and then increased in increments of 5. Each run yielded a mean accuracy across phases (cue, delay, imagery) and arrays (SMG, PMv, S1) over 1000 iterations. For each of these accuracies, the current run was compared with the previous run with $N$–5 features. In all cases, accuracies as $N$ increased followed a curve with a single peak or plateau at some $N > 0$ and smaller than the original number of features. The run with the greater number of superior

accuracies was chosen as the "better" run. In the case of a tie, the lower number of features was chosen. The number of features *N* is given in **Table 3.1**, dimensions. The number of features determined to be best for experiment 1 data were also used to decode experiment 2 data, and to perform the cross-experiment decoding (i.e., training on experiment 1 and testing on experiment 2 and vice versa). The best number of features was recomputed with the combined data from experiment 1 and experiment 2 following the same procedure. For spectral-power classification, the same approach was used to determine the optimal number of features for each frequency band individually. As appropriate, *p* values were corrected for multiple comparisons using the Bonferroni–Holm method.

## 3.3 Results

In this study, a human tetraplegic participant with intra-cortical microelectrode arrays in the SMG, PMv, and S1 performed somatosensory imagery, the vivid recollection of sensory experiences, of five sensations. These sensations were the most common ones that the same participant experienced in a previously published sensory mapping of S1 by ICMS (Armenta Salas et al., 2018). We investigated the hypothesis that somatosensory imagery would generate unique representations for each sensation, which could be classified from the neural signal.

### *3.3.1 Classifying sensations*

Using unsorted threshold crossings recorded during experiment 1 (see Methods), we trained an LDA classifier to identify the five sensations we tested. We trained the classifier on half of the trials (see **Methods**) at a single phase of the task and on data from a single array, using the average firing rate during the phase at each channel as features. We tested the classification on the other half of the trials in the same phase and array. We found a significant classification accuracy for the cue, delay and imagery phases of the task in SMG and in the imagery phase in S1 (**Figure 3.2a**; **Table 3.1**). To

| | | SMG | | | PMv | | | S1 | | | |
|---|---|---|---|---|---|---|---|---|---|---|---|
| | | Cue | Delay | Imagery | Cue | Delay | Imagery | Cue | Delay | Imagery | Dimensions |
| Experiment 1 | Spikes | 78%, *** | 69%, *** | 82%, *** | 24%, n/s | 30%, n/s | 37%, ** | 18%, n/s | 23%, n/s | 38%, *** | 35 |
| | 4-8Hz | 33%, * | 22%, n/s | 24%, n/s | 23%, n/s | 21%, n/s | 24%, n/s | 19%, n/s | 19%, n/s | 20%, n/s | 45 |
| | 8-12Hz | 32%, n/s | 21%, n/s | 34%, ** | 20%, n/s | 22%, n/s | 33%, * | 19%, n/s | 22%, n/s | 20%, n/s | 20 |
| | 12-30Hz | 31%, * | 21%, n/s | 28%, n/s | 17%, n/s | 16%, n/s | 27%, n/s | 17%, n/s | 20%, n/s | 23%, n/s | 15 |
| | 30-70Hz | 35%, ** | 27%, n/s | 60%, *** | 18%, n/s | 19%, n/s | 24%, n/s | 16%, n/s | 17%, n/s | 27%, n/s | 30 |
| | 70-150Hz | 57%, *** | 44%, *** | 75%, *** | 20%, n/s | 22%, n/s | 28%, n/s | 19%, n/s | 22%, n/s | 28%, n/s | 40 |
| | 150-300Hz | 63%, *** | 46%, *** | 77%, *** | 22%, n/s | 21%, n/s | 32%, * | 19%, n/s | 20%, n/s | 34%, * | 45 |
| Experiment 2 | Spikes | 92%, *** | 62%, *** | 75%, *** | 27%, n/s | 35%, ** | 54%, *** | 21%, n/s | 20%, n/s | 31%, n/s | 35 |
| | 4-8Hz | 34%, * | 24%, n/s | 25%, n/s | 21%, n/s | 20%, n/s | 25%, n/s | 18%, n/s | 18%, n/s | 21%, n/s | 45 |
| | 8-12Hz | 37%, ** | 23%, n/s | 27%, n/s | 20%, n/s | 22%, n/s | 32%, * | 18%, n/s | 19%, n/s | 20%, n/s | 20 |
| | 12-30Hz | 31%, * | 20%, n/s | 30%, n/s | 20%, n/s | 18%, n/s | 25%, n/s | 18%, n/s | 17%, n/s | 21%, n/s | 15 |
| | 30-70Hz | 36%, ** | 28%, n/s | 53%, *** | 24%, n/s | 26%, n/s | 38%, ** | 17%, n/s | 16%, ** | 20%, n/s | 30 |
| | 70-150Hz | 62%, *** | 39%, *** | 71%, *** | 35%, * | 30%, n/s | 51%, *** | 19%, n/s | 19%, n/s | 25%, n/s | 40 |
| | 150-300Hz | 64%, *** | 43%, *** | 69%, *** | 31%, n/s | 28%, n/s | 52%, *** | 21%, n/s | 20%, n/s | 25%, n/s | 45 |
| Combined 1 & 2 | Spikes | 75%, *** | 59%, *** | 73%, *** | 23%, n/s | 27%, n/s | 31%, ** | 19%, n/s | 21%, n/s | 33%, *** | 60 |
| | 4-8Hz | 31%, ** | 22%, n/s | 24%, n/s | 19%, n/s | 20%, n/s | 27%, n/s | 19%, n/s | 18%, n/s | 19%, n/s | 10 |
| | 8-12Hz | 31%, ** | 21%, n/s | 32%, *** | 20%, n/s | 21%, n/s | 31%, ** | 18%, n/s | 21%, n/s | 20%, n/s | 25 |
| | 12-30Hz | 30%, * | 20%, n/s | 29%, * | 19%, n/s | 18%, n/s | 26%, n/s | 17%, n/s | 19%, n/s | 21%, n/s | 25 |
| | 30-70Hz | 35%, *** | 28%, n/s | 52%, *** | 21%, n/s | 21%, n/s | 30%, * | 17%, n/s | 17%, n/s | 22%, n/s | 75 |
| | 70-150Hz | 53%, *** | 37%, *** | 68%, *** | 24%, n/s | 23%, n/s | 36%, *** | 20%, n/s | 20%, n/s | 27%, n/s | 75 |
| | 150-300Hz | 57%, *** | 37%, *** | 67%, *** | 23%, n/s | 22%, n/s | 37%, *** | 19%, n/s | 19%, n/s | 29%, * | 60 |
| 2 trained on 1 | Spikes | 21%, n/s | 23%, n/s | 30%, *** | 19%, n/s | 23%, n/s | 16%, n/s | 20%, n/s | 17%, n/s | 21%, n/s | 35 |
| | 4-8Hz | 24%, n/s | 20%, n/s | 20%, n/s | 23%, n/s | 18%, n/s | 18%, n/s | 21%, n/s | 19%, n/s | 22%, n/s | 45 |
| | 8-12Hz | 27%, *** | 21%, n/s | 29%, *** | 22%, n/s | 23%, n/s | 26%, *** | 21%, n/s | 22%, n/s | 25%, * | 20 |
| | 12-30Hz | 32%, *** | 20%, n/s | 26%, *** | 17%, n/s | 20%, n/s | 22%, n/s | 21%, n/s | 23%, n/s | 22%, n/s | 15 |
| | 30-70Hz | 27%, *** | 22%, n/s | 24%, * | 24%, ** | 19%, n/s | 24%, *** | 20%, n/s | 19%, n/s | 21%, n/s | 30 |
| | 70-150Hz | 24%, * | 30%, *** | 20%, n/s | 20%, n/s | 23%, n/s | 21%, n/s | 18%, n/s | 20%, n/s | 21%, n/s | 40 |
| | 150-300Hz | 27%, *** | 22%, n/s | 22%, n/s | 21%, n/s | 21%, n/s | 20%, n/s | 19%, n/s | 19%, n/s | 20%, n/s | 45 |
| 1 trained on 2 | Spikes | 29%, *** | 33%, *** | 35%, *** | 19%, n/s | 23%, n/s | 23%, n/s | 18%, n/s | 18%, n/s | 21%, n/s | 35 |
| | 4-8Hz | 26%, ** | 20%, n/s | 21%, n/s | 22%, n/s | 23%, n/s | 26%, ** | 22%, n/s | 20%, n/s | 24%, * | 45 |
| | 8-12Hz | 27%, *** | 22%, n/s | 31%, *** | 22%, n/s | 23%, n/s | 29%, *** | 18%, n/s | 22%, n/s | 22%, n/s | 20 |
| | 12-30Hz | 23%, n/s | 21%, n/s | 23%, n/s | 21%, n/s | 21%, n/s | 23%, n/s | 19%, n/s | 21%, n/s | 21%, n/s | 15 |
| | 30-70Hz | 26%, ** | 26%, ** | 25%, ** | 23%, n/s | 19%, n/s | 22%, n/s | 20%, n/s | 21%, n/s | 19%, n/s | 30 |
| | 70-150Hz | 20%, n/s | 23%, n/s | 20%, n/s | 22%, n/s | 23%, ** | 20%, n/s | 19%, n/s | 18%, n/s | 18%, n/s | 40 |
| | 150-300Hz | 24%, * | 21%, n/s | 29%, *** | 20%, n/s | 22%, n/s | 19%, n/s | 23%, n/s | 19%, n/s | 21%, n/s | 45 |

**Table 3.1 Classification accuracies**
Table showing the classification accuracy as a percentage and significance (n/s = not significant, *p < 0.05, **p < 0.01, ***p < 0.001) from each of the experiments in which the five sensations tested were classified with LDA and SVD. Classification was performed separately for each data type (spike or spectral power band), each trial phase (cue, delay, and imagery), and for each brain area (SMG, PMv, and S1). The number of features used for each classification is listed in the dimensions column (see **Methods**).

improve the classification accuracy, we applied SVD feature preprocessing before the LDA was trained (see **Methods**). We found significant classification for the cue, delay and imagery phases of

the task in SMG and in the imagery phase in both S1 and PMv (**Figure 3.2b**, experiment 1; **Table 3.1**). In all cases, classification accuracy was compared with that of a null distribution (**Figure 3.2b**, null), where the classification was performed identically but the trial labels were randomly shuffled. LDA analysis determines discriminability across the population activity of the whole array; however, we also observed individual channel firing activity capable of significantly discriminating between two or more sensations (exemplary channels shown in **Figure 3.3a**). The total percentage of channels, 96 in each brain area, whose activity significantly discriminated between two or more sensations in the imagery phase only ($p < 0.05$) was 49% in SMG, 22% in PMv, and 20% in S1. This metric was calculated per channel, pooling across all trials, using a Kruskal–Wallis test with the averaged firing rate in the imagery phase of the task. Data were corrected for multiple comparisons with the Bonferroni-Holm method. To compare the correspondence between results from both stimulation (in previous work) and imagery for all individual channel-sensation pairs (96 channels x 5 sensations, $N = 480$), we identified tuning of the channel to the sensation by looking for a significant difference in firing rate across all trials of a pair between the ITI and imagery phase of the task, using a Wilcoxon signed rank test ($p < 0.05$). We identified responses to ICMS for each channel-sensation pair by looking for at least one instance of the pair during ICMS mapping in the previous study (Salas et al., 2018). We found 89 (18.5%) pairs (38/96 unique channels, 5/5 unique sensations) which had both neurophysiological tuning and a response to ICMS. We also used the same method as above to perform a classification using the spectral power in various frequency bands of the raw neural signal as features (see **Methods**; **Figure 3.2**; **Table 3.1**). In SMG, we found significant classification accuracy in the cue phase across several frequency bands. We also found significant classification accuracy in the delay phase in higher frequency bands only. In the imagery phase we saw significant classification accuracy across several frequency bands. In PMv, we found significant classification

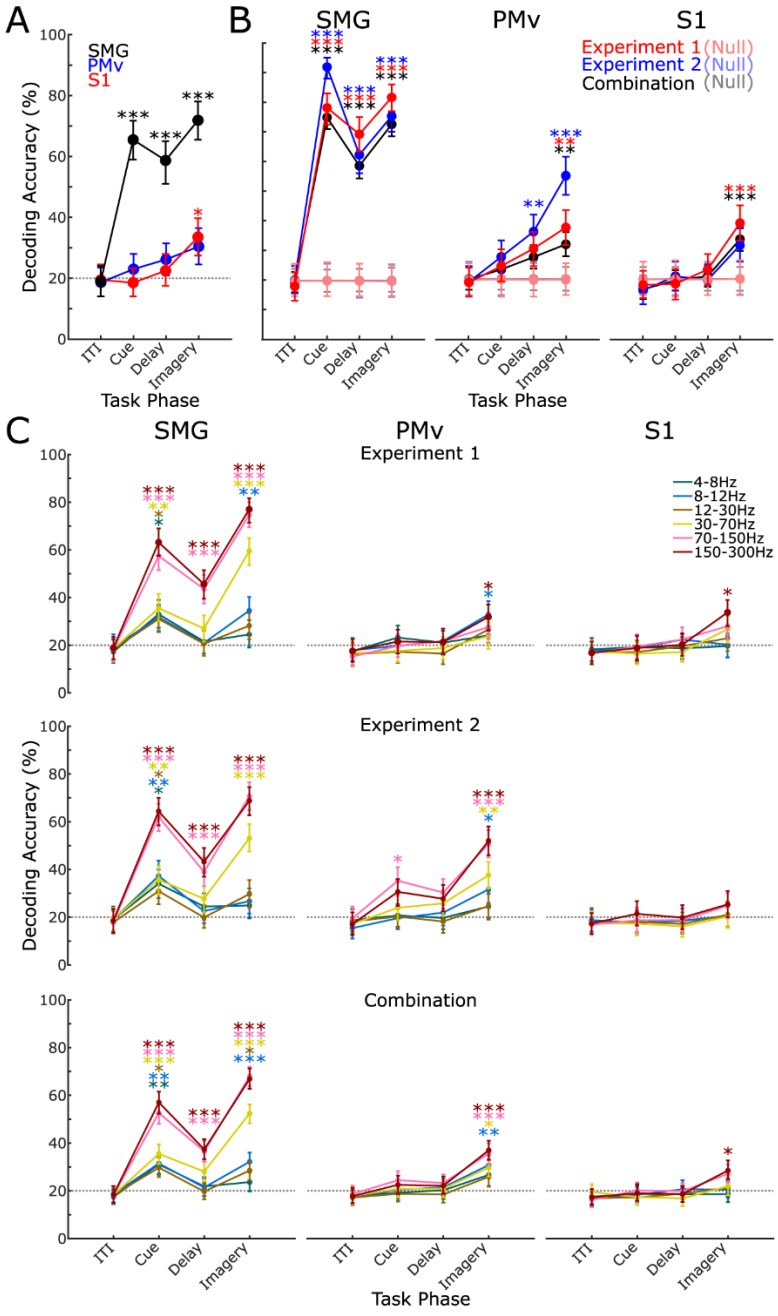


**Figure 3.2 Sensation classification**
**a)** Classification accuracy of sensations with LDA using the spike activity on all channels as features from experiment 1. **b)** Improved classification accuracy when classifying the sensations using LDA with the spike activity and SVD feature selection from experiment 1 (red), experiment 2 (blue), and the combined experiments 1 and 2 data (black). Each with their own null distribution. **C)** Classification using spectral power in different frequency bands for experiment 1 (top row), experiment 2 (middle row), and combined experiments 1 and 2 (bottom row). In all subplots, error bars show 95% confidence interval, asterisks denote classification significantly above null distribution. Gray dotted line shows the classification chance level.

accuracy only in the imagery phase at high and low frequencies. Likewise, in S1, we found significant classification accuracy only in the imagery phase and only in the highest frequency band (150–300 Hz).

During the ITI phase of the trial, while the subject was at rest, we never achieved classification performance different to chance level with any method or neural signal used. This confirms that the discriminable activity in other task phases is related specifically to the somatosensory imagery task.

### *3.3.2 Longitudinal representational of sensations*

We have demonstrated above that different sensations can be uniquely represented in distributed cortical areas. However, to what extent are the representations stable over time? Recordings of the human neural signal can be unstable over time (Aflalo et al., 2015), so to assess longitudinal stability, the participant performed experiment 2, repeating the imagery task ~11 months after the initial experiment 1. We found that sensations could be classified from threshold crossings in SMG during cue, delay, and imagery phases as in the earlier data (**Figure 3.2b**; **Table 3.1**). We found a significant classification in the delay and imagery phase in PMv. Using spectral power features from experiment 2 only to examine longitudinal stability, as above with threshold crossings, showed a similar trend. In SMG significant classification was observed in all frequency bands during the cue but in the delay phase was only observed in higher frequency bands (**Figure 3.2c**, middle row; **Table 3.1**). Additional lower bands became significant in the imagery phase. In PMv, significant classification accuracy was only achieved in the cue phase at a single high-frequency band and in the imagery phase across a range of bands. No significant classification using spectral power was achieved in S1 during experiment 2.

To determine how similar activity was between experiments 1 and 2 within each task phase and each array, we performed a split training and testing using all trials of experiment 1 to train and all trials

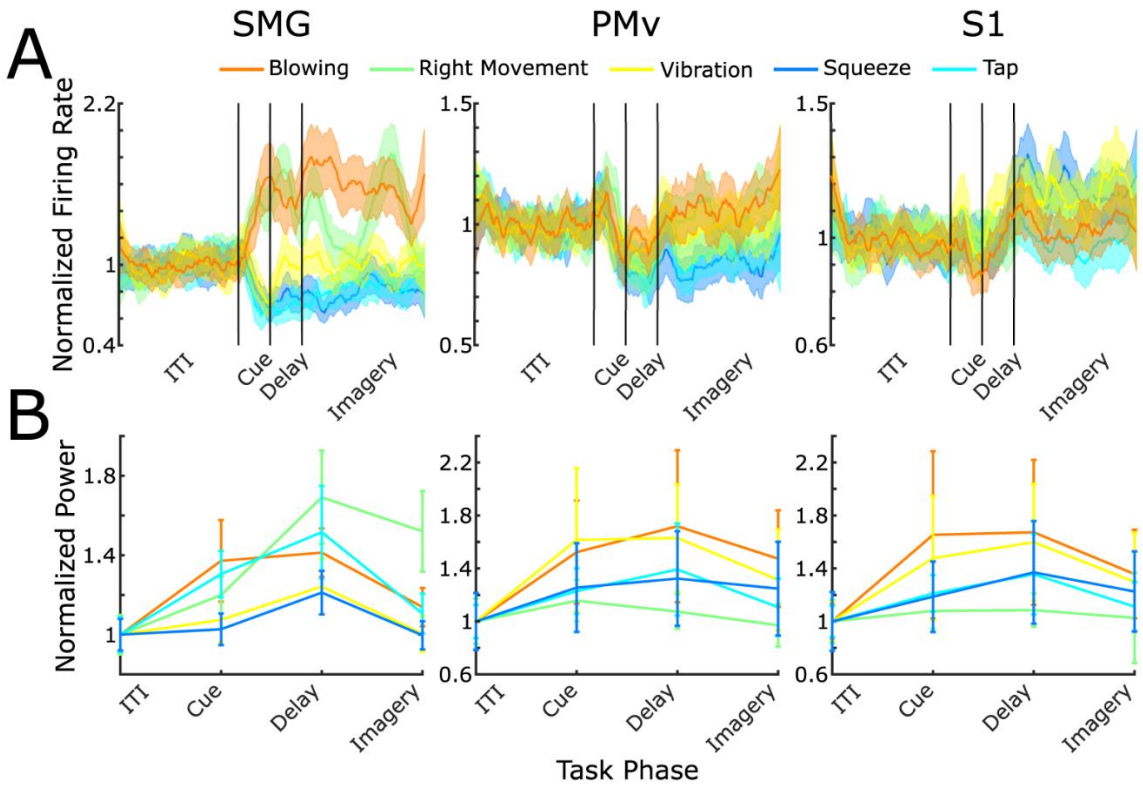


**Figure 3.3 Sample firing rates and mean power**
**a)** Mean firing rates across all trials for each sensation on an exemplary channel in each recording location. **b)** Mean power in the 150- to 300-Hz LFP band across all trials for each sensation on an exemplary channel in each recording locations. Channels show significantly different activity for multiple individual sensations. In all subplots, error bars show 95% confidence interval.

of experiment 2 to test (and vice versa). A null distribution was created using shuffled labels over *N* = 1000 repetitions of the classification. Using threshold crossings, significant classification accuracy was only observed in SMG during the imagery phase when testing on experiment 2. When testing on experiment 1, significant classification accuracy was observed only in SMG during the cue, delay and imagery phases of the task (**Figure 3.4**).

To evaluate the longitudinal stability of spectral power representations, we trained and tested on both the experiments 1 and 2 datasets, as described above for threshold crossing features. When training on experiment 1 and testing on experiment 2, SMG showed significant classification accuracy in the

cue and imagery phase across a broad range of bands and significance in one band in the delay phase. In PMv, significant classification accuracy also occurred in the cue and imagery phase. In S1, significant classification accuracy was observed in the imagery phase at only a low-frequency band (**Figure 3.4a**). When training on experiment 2 and testing on experiment 1, significant classification accuracy was observed in SMG during the cue, delay and imagery phase. In PMv, significant classification accuracy occurred during the delay and imagery phase. In S1, significant classification accuracy only occurred during the imagery phase (**Figure 3.4b**; **Table 3.1**). Longitudinal classification from both spike and LFP signals performs well especially where the signal has a high decoding accuracy within either experiment 1 or 2 alone. In the longitudinal analysis, taking all brain regions together, there are some additional task phases and array locations with significant classification accuracy in the spectral power data compared with the spike data. This indicates a tendency toward more general stability in the spectral power.

To ensure that classification accuracy could not be further improved with more data we combined threshold crossing datasets from both experiment 1 and experiment 2 to use all trials recorded ($N$ = 800) in the same classifier, with the same LDA and SVD method as before. Note, data across the two experiments is combined in this model. The significant classification accuracies in this result corroborate stability over time as in the longitudinal analysis above. However, combining data does not take into consideration changes in signal or noise over time as addressed specifically in the longitudinal analysis above. This analysis yielded significant classification accuracy for the cue, delay, and imagery phases of the task in SMG, in the imagery phase in S1 and in the imagery phase of PMv (**Figure 3.2b**, combined; **Table 3.1**). Finally, we combined the full spectral power data set as above (**Figure 3.2c**, bottom row) and found significant classification accuracy for SMG in the cue phase across a broad range of frequency bands, in the delay phase in only the higher frequency bands

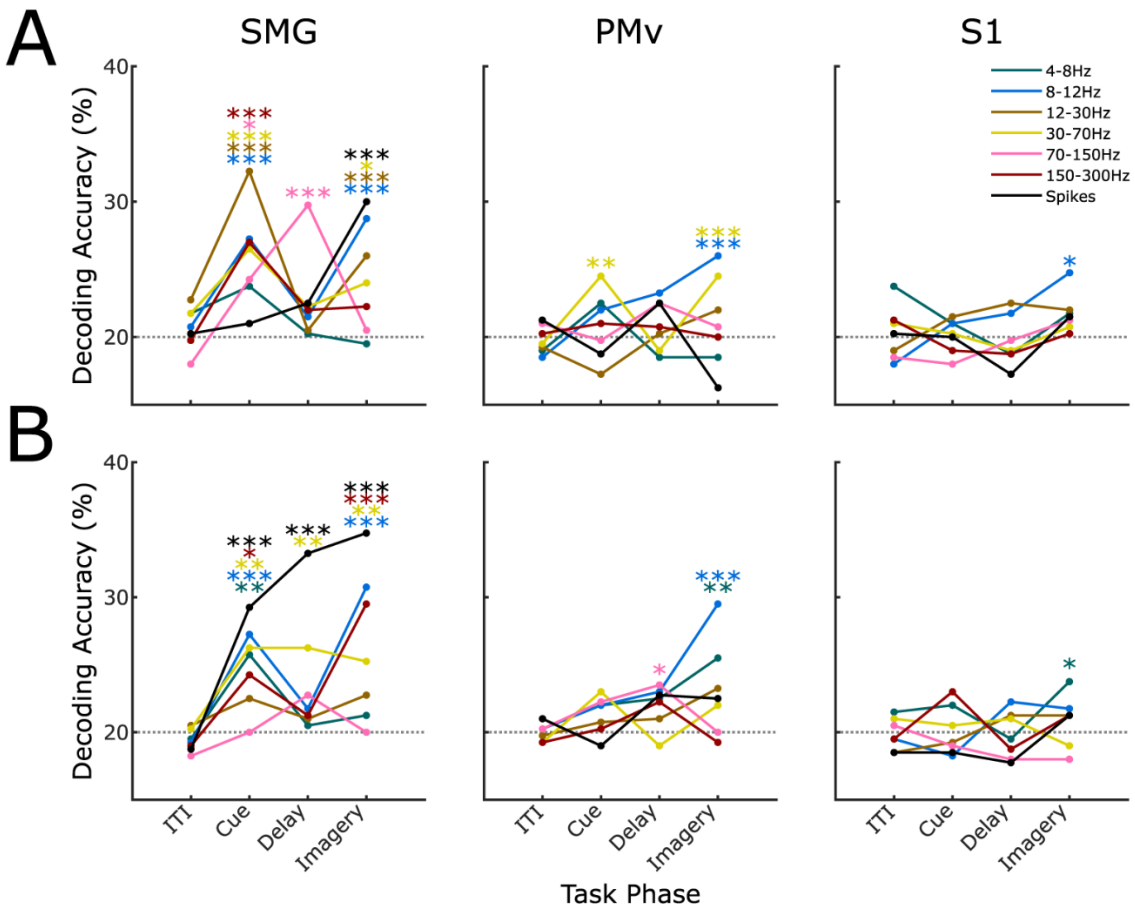


**Figure 3.4 Longitudinal decoding**
Classification accuracy calculated per phase and per brain region. **a)** An LDA with SVD model was trained on all trials in experiment 1 and tested on all trials in experiment 2. **b)** The same method was used to train on all trials in experiment 2 and test on all trials in experiment 1. Different colors indicate different frequency bands. Gray dotted line shows the classification chance level. Stars indicate significance calculated with respect to the null distribution (see **Methods**).

and imagery phase again across a broad range of bands. In PMv and S1, significant classification accuracy was achieved in the imagery phase only. For PMv, this was achieved in a broad range of frequency bands, while for S1, this was only achieved in the highest frequency band.

### 3.4 Discussion

As cortical stimulation methods are becoming more widely used it is increasingly important to understand the relationship between intervention (i.e., ICMS) and evoked perception/behavior (i.e.,

sensations). In order to achieve the goal of restoring sensation in humans, we need to produce consistent effects across participants and robustly deliver specific sensations relevant to the task. We believe understanding this begins with exploring the neural representation of the sensations that we are able to elicit, for example, uncovering the neural features that represent unique sensations. In the work presented here, we demonstrate that different sensations are uniquely represented in the neural activity of human cortex. We measured spiking activity and spectral power during somatosensory imagery with intra-cortical recording arrays in SMG, PMv, and S1 of a single human participant with a high-level spinal cord injury (see **Methods**). We demonstrate that individual sensations can be accurately classified using these signals (**Figure 3.2**; **Table 3.1**). Here, we observe activity through somatosensory imagery, a powerful tool to elicit sensation-relevant neural activity, as physical interaction with the environment is not possible because of the nature of the injury in the tetraplegic patient population. We explore sensations that the participant had experienced both naturally before the injury and reported during ICMS mapping. Previously, individual aspects of somatosensation have been studied in isolation such as responses to different textures, the frequency of vibration, individual forces, etc. In somatosensory imagery, all these components are combined as a naturalistic sensation. With recordings across human cortical areas we can further characterize the distributed response in the brain to somatosensation (Delhaye et al., 2018). We show sensations can be classified in S1 during somatosensory imagery with threshold crossing activity, when the participant vividly recalls a previously experienced sensation (**Figure 3.2a**; **Table 3.1**). Additionally, in S1 the sensations are only classifiable in the imagery phase in high-frequency spectral power of 150–300 Hz, again likely reflecting spiking activity (**Figure 3.2c**, top row; **Table 3.1**). This finding suggests S1 does not encode the planning or anticipation of sensation during imagery with no significant classification occurring in the cue or delay phase. In PMv, we found activity in the imagery phase

similar to S1, but with additional low-frequency components of 4–8 and 8–12 Hz, which may be responsible for driving coordinated networks over a larger area (Canolty et al., 2006). In experiment 2, we were able to classify sensations from threshold crossing activity in PMv during the delay phase. This result reinforces the trend seen in experiment 1 for PMv (**Figure 3.2b**), suggesting that it encodes the planning or anticipation of the sensation in addition to the sensation itself (Fogassi et al., 1996). In SMG, we saw the highest classification performance of any area tested during the cue, delay and imagery phases of the task, both in threshold crossing activity and the spectral power in high-frequency bands. This finding demonstrates SMG contains somatosensory information, both during imagery and in the planning/ anticipation of somatosensory imagery (Delhaye et al., 2018). Classification during the cue phase, which uniquely included $\theta$ band activity, suggests a representation of the semantic aspect of the cued sensation within SMG, which further supports the higher order cognitive encoding of sensorimotor control in posterior parietal cortex (Aflalo et al., 2015; Andersen and Buneo, 2002; Zhang et al., 2017). We observe a large difference in the decoding performance between SMG and S1/PMv. A hypothesis for this difference may be that since somatosensory imagery is a top-down cognitive process, without somatosensory input, the representation is stronger in SMG as this is a higher order, cognitive area in somatosensory processing. Our results show imagery produces discriminable activity in S1 and PMv; however, the reduced decoding accuracy may reflect the primary role of this neural population to process input from the somatosensory system.

We explicitly test somatosensory imagery to determine whether neural activity encodes the imagined sensation. This is motivated entirely because of the nature of injury in our patient population. We do not assume that these areas would represent the sensations in exactly the same way if they were experienced through interaction with the environment in the absence of injury. Indeed, the

representations found from somatosensory imagery have intrinsic value to efforts aimed at restoring sensation in injured people. However, it is likely that there would be a high degree of correspondence between the neural representation of sensations during somatosensory imagery and actual somatosensation (Fitzgibbon et al., 2012; Hodge et al., 1996; Rosén et al., 2001; Yoo et al., 2003). As seen in the motor system (Hardwick et al., 2018; Jeannerod, 1994), research into motor control, motor learning and motor BMIs have shown a high degree of similarity between the neural activity of imagined and executed behavior.

In the longitudinal comparison of the neural representation of sensation (**Figure 3.4**), classification accuracy decreased in most phases and locations compared with testing within the experiments (**Figure 3.2**), with the biggest decrease in performance observed in S1. While it is unclear what caused this change in classification accuracy, it is interesting to note that it was accompanied by the participant's comments during experiment 2 that the passage of time between the two experiments "made it much harder to imagine the sensation [evoked by ICMS] because I have not felt them in a while." This anecdotal evidence might suggest a link between the strength of responses in S1 to the clarity with which the sensations could be recalled, as may be intuitively expected in a somatosensory imagery task. Nevertheless, threshold crossing S1 activity was still able to yield significant longitudinal classification accuracy after 11 months, comparable to that measured initially. In SMG, the presence of significant classification across experiments may suggest a stronger representation of the task than PMv or S1. The cross-classification performance across the two experiments suggests that while each of these areas encode the sensations after 11 months, the representation over all brain areas differs over time. While physiological changes in the representation of the sensations or the quality of the imagery could contribute to this, there are many additional factors unrelated to the neurophysiology of the task that likely contribute as well. For example, small movements in the array,

degradation of the array over time and changes at the electrode-tissue interface may all account for the reduced performance.

Identifying a stable relationship between aspects of the neural signal representing sensations during somatosensory imagery and features of stimulation that evoke those sensations could allow us to efficiently identify protocols for artificially eliciting sensation. This is relevant to closed loop BMIs where during robotic or computer control, task-relevant sensations must be identified and delivered via ICMS. It remains to be investigated whether correspondence between features of the neural signal during imagery and the neural signal evoked during stimulation could reduce the time to map the relationship between sensations and stimulation. If so, somatosensory imagery could be used to improve sensory mapping by stimulation and potentially elicit more varied responses in future work. Furthermore, S1 was originally chosen as a stimulation site because of its known neurophysiological relationship to sensation. Here, we confirm a relationship between imagined sensations and S1 neurophysiology for sensations previously elicited with S1 stimulation in the same array. Somatosensory imagery of the sensations shows an even stronger relationship between neurophysiological activity and imagined sensation in SMG. Therefore, SMG may also be a potential target for ICMS to elicit sensation. Stimulation in parietal cortex has previously been shown to have connections with (Baldwin et al., 2017) and relate to behavior of (Desmurget et al., 2018; Hanks et al., 2006; Mirpour et al., 2010) the sensorimotor system.

In conclusion, we present evidence that human somatosensory imagery can be uniquely and robustly encoded in the activity of distributed cortical areas. In future work it would be essential to identify the evoked neurophysiology from certain stimulation parameters and compare this, instead of stimulation parameters alone, to the evoked sensations and representation of the sensations during imagery or experience. Such information would likely elucidate further the relationship between the

stimulation parameters, their ability to elicit certain sensations, and the representation of the sensations elicited in the brain.

# *Chapter 4*

# THE ROLE OF VISUAL INFORMATION AND THE CORTICAL HOMUNCULUS IN S1

The following chapter's contents are taken and adapted from Rosenthal et al. (2023) with modifications done to fit the dissertation format.

> Rosenthal, I.A., Bashford, L., Kellis, S., Pejsa, K., Lee, B., Liu, C., Andersen, R.A., 2023. S1 represents multisensory contexts and somatotopic locations within and outside the bounds of the cortical homunculus. Cell Reports 42, 112312. https://doi.org/10.1016/j.celrep.2023.112312

## 4.1 Introduction

The sense of touch is important for implementing dexterous, adaptable action plans (Ghez et al., 1995; Miall et al., 2021, 2019; Robles-De-La-Torre, 2006; Sainburg et al., 1995) and creating a sense of ownership and agency over one's body (Ehrsson, 2020; Jeannerod, 2003; Tsakiris et al., 2010). The primary source of information for tactile sensations is input from peripheral mechanoreceptors, but multisensory integration (Ernst and Banks, 2002; Körding and Wolpert, 2004) plays a role as well, especially visual information (Botvinick and Cohen, 1998; Ghazanfar and Schroeder, 2006; Johnson et al., 2006; Kandula et al., 2015; Tipper et al., 2001).

The primary somatosensory cortex (S1) is one of the first cortical areas to receive incoming tactile information, relayed via the cuneate nucleus and the thalamus (Delhaye et al., 2018). S1's responsiveness to physical touch and its topographic organization have been extensively documented

(Ejaz et al., 2015; Kaas et al., 2019; Kolasinski et al., 2016; Penfield and Boldrey, 1937; Sanders et al., 2019), but the extent to which multisensory information is represented in S1 remains under investigation. A large body of literature addressing this precise question has found that S1 responds to observed touch when it occurs in others but not oneself (Blakemore et al., 2005; Bufalari et al., 2007; Ebisch et al., 2008; Kuehn et al., 2018, 2013; Longo et al., 2011; Meyer et al., 2011; Pihko et al., 2010; Schaefer et al., 2009). However, a significant number of studies have failed to find evidence of this phenomenon (Chan and Baker, 2015; Keysers et al., 2004; Morrison et al., 2004; Sharma et al., 2018).

A similar but distinct question concerns whether S1 is modulated by vision when it is paired with a physical touch event. Psychophysically, the visual enhancement of touch has been well-established: tactile acuity is enhanced when a touched area is observed, even when the visual input is non-informative (Colino et al., 2017; Haggard et al., 2007; Kennett et al., 2001; Press et al., 2004; Tipper et al., 2001), although the precise conditions necessary to trigger the effect are still unclear39. EEG experiments have shown that combining visual and tactile stimuli modulates the P50 somatosensory evoked potential, which is thought to originate in S1 (Cardini et al., 2012, 2011; Deschrijver et al., 2016; Dionne et al., 2013; Taylor-Clarke et al., 2002). MEG studies have suggested that the topographic mapping of fingers shifts in S1 based on the relative timing of visual and tactile signals (Schaefer et al., 2008, 2006). Transcranial magnetic stimulation (TMS) over S1 negatively affects the ability to detect or discriminate touches, if the accompanying visual information incorporates a human hand rather than a neutral object (Bolognini et al., 2011; Fiorio and Haggard, 2005; Rossetti et al., 2012). Thus biologically relevant visual information appears to be used as a predictive signal and modulate S1 encodings of tactile events.

Like its role in integrating multisensory stimuli, S1's topographic organization appears to be more nuanced than first thought. Recent experiments suggest that although S1 maintains a gross topographic representation of the body as laid out in the earliest human cortical stimulation studies and observed many times since (Cunningham et al., 2013; Ejaz et al., 2015; Kaas et al., 2019; Kolasinski et al., 2016; Penfield and Boldrey, 1937; Sanders et al., 2019), it also contains other more complex levels of tactile representation (Arbuckle et al., 2022; Enander and Jörntell, 2019; Thakur et al., 2012). Studies of the non-human primate hand have shown that S1 neural activity contains non-linear interactions across different digits (Arbuckle et al., 2022; Qi et al., 2016; Thakur et al., 2012), supporting the idea that S1 carries information beyond a linear report of inputs from tactile receptors. In humans, S1 has recently been shown to represent body parts outside of their traditionally defined areas (Muret et al., 2022; Wesselink et al., 2022).

To interrogate S1's representations of touch across body locations and multisensory contexts, electrophysiological recordings in a human tetraplegic patient with two microelectrode arrays (Blackrock Microsystems, Salt Lake City, UT) implanted in the putative area 1 of the S1 arm region (Armenta Salas et al., 2018) were collected. The patient retained enough tactile ability after spinal cord injury to sense short stroking stimuli delivered to his arm and finger. Touch conditions occurred on either the patient's arm, finger, or an inanimate object, in a variety of multisensory contexts (**Table 4.1**). Our results provide evidence that tactile information in S1 is encoded as part of the well-established cortical homunculus as well as in a more general manner which encompasses larger areas of the body. Additionally, we find that S1 does not respond to observed touches to oneself, another person, or an object, but that vision does modulate neural activity when it is paired with physical tactile stimulation. This finding suggests that passively observing visual information depicting touches fails to meet some threshold of relevance or attention necessary to activate S1 neurons.

| Modality | Location | Touch Type | | Description |
|---|---|---|---|---|
| ***FPa** | Arm (**a**) | | *FP | The participant observed, in first person (**FP**) perspective, a real physical touch to his body. |
| ***FPf** | Finger (**f**) | | | |
| ***BLa** | Arm | | *BL | The participant fixated on a non-informative dot in virtual reality, effectively blindfolding (**BL**) him during a real physical touch to his body. |
| ***BLf** | Finger | | | |
| **VrFPa** | Arm | | VrFP | The participant observed, via virtual reality and in first person perspective (**VrFP**), a touch to his body without any physical contact. |
| **VrFPf** | Finger | | | |
| **TPa** | Arm | | TP | The participant observed, in third person (**TP**) perspective, a real physical touch to another person's body. |
| **TPf** | Finger | | | |
| **Obj** | Object | | Obj | The participant observed a real physical touch to an inanimate object (**Obj**), a wooden block. |

**Table 4.1 Experimental task conditions**
Touch modality conditions are each presented with the color code representing that touch type throughout the paper. Each modality with a physical touch stimulus is coded with '*'. All modalities with a stimulus on the arm end in 'a'; all modalities with a stimulus on the finger end in 'f.' Touches were single strokes delivered by an experimenter using a pressure-sensing rod; in *BL and VrFP trials the participant wore a Vive Pro Eye headset.

## 4.2 Methods

### *4.2.1 Participant and implant details*

A C5-level incomplete tetraplegic participant (male, 32 years old) was recruited and consented for a brain-machine interface (BMI) clinical trial including intra-cortical recording and stimulation. At the beginning of data collection, the participant was 6.5 years post-injury and 5 years post-implant. All procedures were approved by the Institutional Review Boards (IRB) of the California Institute of Technology, University of Southern California, and Rancho Los Amigos National Rehabilitation Hospital.

The participant was implanted with microelectrode arrays in three locations in the left hemisphere: the supra-marginal gyrus (SMG), ventral premotor cortex (PMv), and the primary somatosensory cortex (S1) (**Figure 4.1a**). This paper only examines data in S1, which was recorded using two 48-channel 1.5mm SIROF-tipped (sputtered iridium oxide film) microelectrode arrays (Blackrock

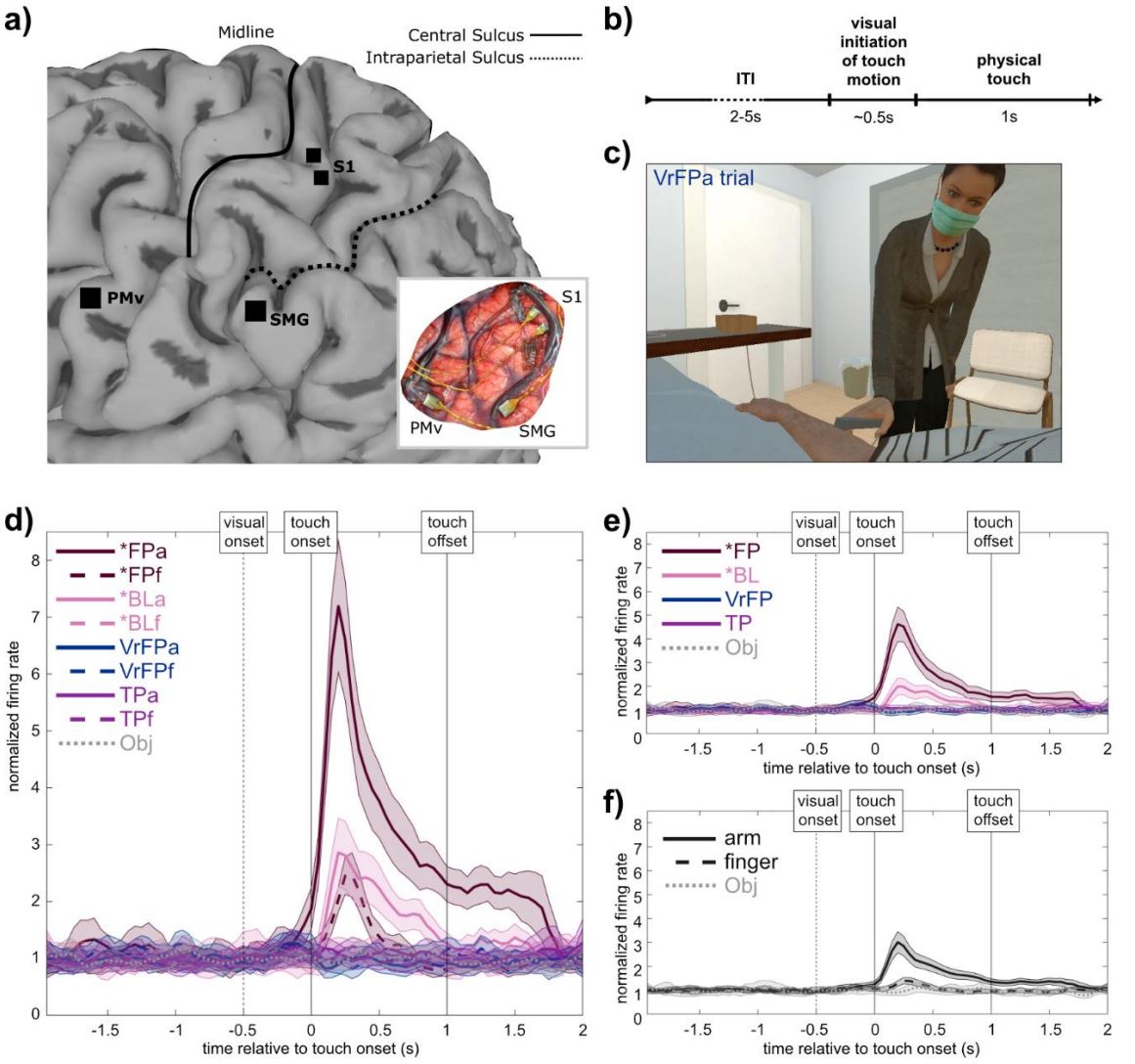


**Figure 4.1 Experimental methods and paradigm**
**a)** Microelectrode array implant locations on the cortical surface of the left hemisphere, rendered with MRI. Only data from the two S1 arrays were analyzed in this study. Inset: in situ array locations. Figure reproduced from Armenta Salas et al. (2018). **b)** Task time course. Visual initiation of touch motion was only perceived by the participant in touch types with visual content (*FP, VrFP, TP, Obj). **c)** Sample frame from a VrFPa trial, presented using a virtual reality headset. See **Supplemental video 1**. **d)** Example smoothed firing rate of one S1 channel to each tested modality of touch (n=70 trials/modality). Shaded area surrounding each line indicates standard error of the mean (SEM). **e)** and **f)** depict activity of the same channel averaged across modalities to isolate touch type and effector respectively (i.e., *FPa and *FPf in **(d)** are averaged to yield *FP in **(e)**.

Microsystems, Salt Lake City, UT). Given the curvature of sensorimotor cortex and the need to implant arrays on the gyral surface, it is likely the S1 micro-electrode arrays are located in Brodmann area 1 (BA 1). Additional details pertaining to the arrays and the specifics of surgical planning are

described in (Armenta Salas et al., 2018).

### *4.2.2 Experimental paradigm*

Two anatomical locations were examined across a set of tactile and visual conditions. The two locations selected were a "finger" location on the back of the thumb where the participant reported naturalistic sensations, and an "arm" location near the back of the elbow where the participant reported numb sensation. These locations were selected on the basis of a preliminary mapping of the participant's tactile capabilities on the arm and hand using Semmes-Weinstein filaments at varying strengths, which took place two days prior to the first experimental session.

Although the different task conditions (**Table 4.1**) did not all include both a physical and a visual component, all employed the same style of touch: a 1-second stroke over approximately 6cm of skin. The touch was delivered by a plastic rod (or a virtual facsimile of one), built in-house, which had a raised button on one end (1.5 x 2 cm) that was passed along the touch location. The rod housed a load cell which was used to record the pressure applied and align the onset of touch to neural recordings.

Each trial consisted of an inter-trial-interval (ITI) of 5s with an additional 0-3s jitter, followed by a 1s touch stimulus and 1s post-touch phase. In trials with a visual component, the visual component (approach towards the touch target) began approximately 0.5s before touch onset. The experimenter performing the touch was positioned at approximately a one o'clock position relative to the participant's head, such that the participant could clearly see the experimenter and the approach trajectory of the touch stimulus (**Figure 4.1c, Supplemental video legends**). The uniform and direct nature of the approach trajectory meant that the participant could approximately anticipate when a touch would begin using visual information once the approach began. A total of 11 conditions were examined, incorporating 6 touch types and 3 touch locations (**Table 4.1**).

### *4.2.3 Data collection*

Neural data was recorded from each microelectrode array using a 128-channel Neural Signal Processor (Blackrock Microsystems) as 30,000 Hz broadband signals. Data was collected in 8 sessions over 6 months, in two sets (see **Table 4.1** for task condition descriptions). In the first set, the participant observed real physical touches to his body in first person (*FP), the same touches delivered to someone else (third person; TP), and touches to an inanimate object (Obj). This set was collected over the first two months in 4 sessions with up to 3 weeks between sessions. In the second set, the participant experienced real physical touches without visual touch information (blind; *BL), and saw touches being delivered to him in first person using virtual reality, without any physical touch component (VrFP). The second set was collected over the third to sixth months in 4 sessions with up to 9 weeks between sessions.

Within a session, data was collected in series of 11-trial runs. Each run contained 10 trials of the same condition and one catch trial. Within the two sets, runs were pseudorandomly shuffled so there were no two runs of the same condition back to back in any session. 1-2 runs of each condition within a set were collected in each session. 70 trials (7 runs) were collected in every condition. At the start of each run, the participant was informed which type of stimuli would be delivered and was instructed to attend to the stimuli while visually fixating on the touch location except for BL trials in which he fixated on a non-informative dot centered in his field of view.

In third person (TP) trials, the third person being touched (an experimenter familiar to the participant) was positioned so their arm and hand were adjacent and parallel to the participant's own arm and hand. In object (Obj) trials, the participant observed a wooden block approximately the size of his hand being touched along its flat surface while it lay on a desk in front of him.

The conditions in set two required a virtual reality headset; a Vive Pro Eye was used to display a virtual environment run with Unity, which closely mimicked the data collection room and gave the participant a first-person perspective over a virtual body with a size, gender, and posture reflecting his own body. In the virtual environment, a virtual experimenter was animated to deliver touches in a manner resembling the real experimenter (**Figure 4.1c, Supplemental video legends**). The human avatar for the virtual experimenter was taken from the Microsoft Rocketbox Avatar Library (Gonzalez-Franco et al., 2020) (https://github.com/microsoft/Microsoft-Rocketbox/). For *BL conditions, the headset was used as a blindfold, and displayed a non-informative white dot in the center of a black field of view which the participant was instructed to fixate on.

To verify that the fundamentals of the neural signal remained unchanged across the two sets, SNR was analyzed using two different metrics. 1) In every run, the ratio of the mean waveform's peak value on each channel to the root mean square of the noise estimate for that channel was computed. 2) The ratio of the mean waveform on each channel to the standard deviation of the waveform within every run was also computed. Both these metrics were averaged across runs within each set; neither metric was different across the two sets (Wilcoxon sign rank test, [1] $p=0.28$, [2] $p=0.08$).

The mean and standard deviation of ITI firing rates taken from the time period [4s to 1s] before each touch stimulus began, were also examined. All firing rates were normalized by dividing by the mean of the baseline within a run, then averaged across all trials and runs within a set and compared across sets. Both the mean (Wilcoxon sign rank test, $p=0.18$) and the standard deviation ($p=0.53$) of ITI firing rates were not significantly different between sets.

Although outside the scope of this paper, additional conditions were collected along with the ones analyzed here. In set one, conditions in which the participant imagined the touches being delivered without any external tactile stimuli were also obtained. In set two, a touch type identical to VrFP

except that the participant's virtual body was composed of abstract blocks rather than a realistic human body was collected, and a condition in which the participant viewed an inanimate object being touched in virtual reality was also acquired.

### *4.2.4 Quantification and statistical analysis*

All analyses were performed using MATLAB R2019b (MathWorks, Natick, MA) unless otherwise indicated.

#### *4.2.4.1 Preprocessing and temporal alignment of data*

Firing rates for each electrode were extracted in 50ms bins from the broadband signal in a multi-unit, unsorted fashion (Christie et al., 2015; Dai et al., 2019), using a threshold of -3.5 times the noise RMS of the continuous signal voltage. This multi-unit channel activity was aligned within each trial to the physical or virtual moment of contact between the touch sensor and the item being touched (i.e., touch onset). In conditions with a physical touch component, touch onset was calculated using the pressure readings obtained from the rod used to deliver touches; in conditions with only a virtual touch component, touch onset was calculated using the timing of Unity animations.

To normalize firing rates, within each run and each channel, a mean baseline firing rate was calculated from the time period 4s to 2.5s prior to each touch onset and averaged across trials. The firing rates of each channel at every time point were divided by this baseline.

#### *4.2.4.2 Decoding analysis*

Linear Discriminant Analysis (LDA) pairwise classifiers were used to probe the linearly decodable information within and across task conditions (**Figure 4.2a, Figure 4.3**). Normalized firing rate data was binned into either 0.5s or 0.1s bins, depending on the analysis. Within each bin, data was randomly split equally into train/test partitions, regardless of session collected. This split occurred

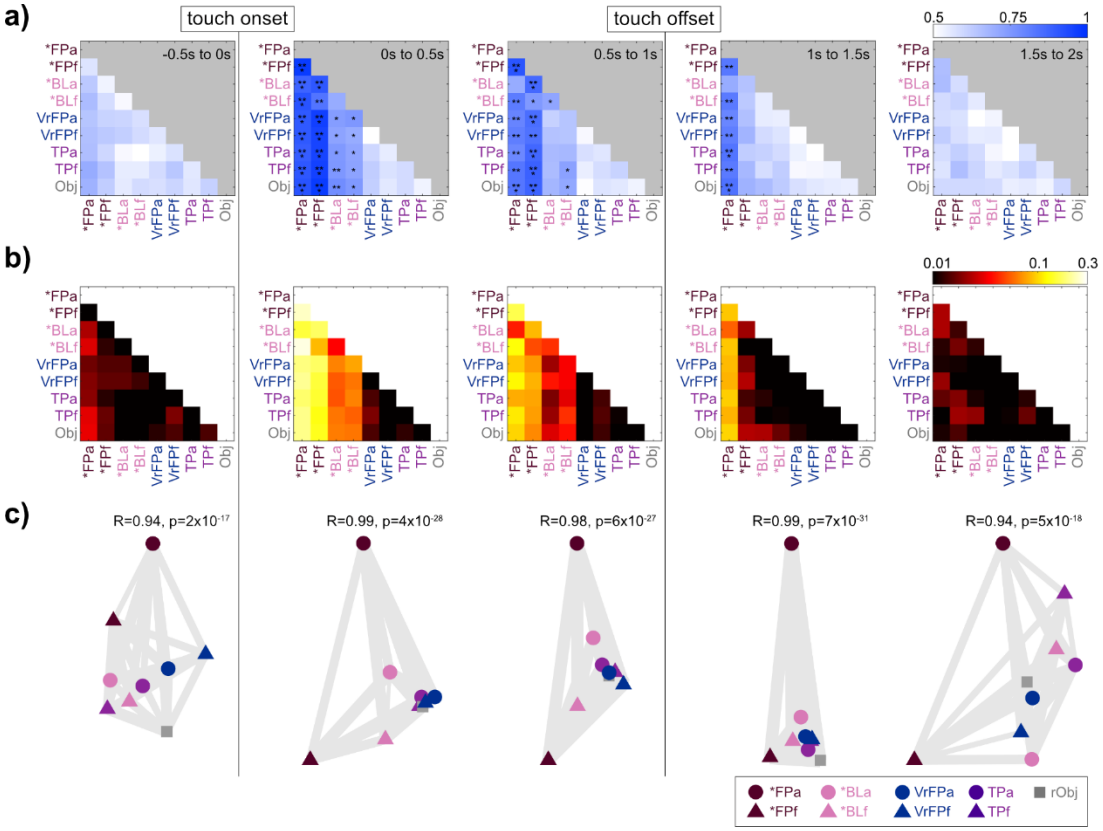


**Figure 4.2 Pairwise decoding and RSA**
**a)** Pairwise identity decoding results. At each 0.5s time bin, a LDA classifier was trained to distinguish between each pair of modalities based on the top 40 principle components of multiunit activity. The 70 trials per modality were randomly divided in half to generate train and test data 1000 times, and the accuracies of the resulting decoders were averaged together to yield the values in the confusion matrices. Asterisks represent significantly different accuracies relative to a null distribution which was generated by training the same decoder on data with shuffled labels 1000 times. * = significantly different 95% confidence intervals (CIs); ** = 97.5% CIs; *** = 99% CIs. See also **Supplemental video legends**. **b)** Representational similarity analysis was performed on touch-onset-aligned multi-unit S1 channel activity, and resulting representational dissimilarity matrices (RDMs) are shown. Distances between conditions (plotted on log axis) are cross-validated Mahalanobis distance with multivariate noise correction; a distance of 0 indicated conditions are statistically indistinguishable. **c)** Multi-dimensional scaling (MDS) plots of RDMs in **(b)**. Axes are arbitrary but have been rotated for consistency across time bins. Gray lines between condition icons are "rubber bands" whose thickness is based on the goodness of fit of the scaling. A relatively thinner, more "stretched" band between conditions indicates that in a plot that fully captures neural geometry, the conditions would be closer together.

1000 times and was balanced each time to include equal numbers of trials from every condition tested (70 trials per condition = 35 trials each in train and test).

Singular value decomposition (SVD) was used to perform dimensionality reduction on the initial 96 multi-unit channels of the training dataset. Average firing rate data from both train and test datasets

in each bin was projected on the top 40 features capturing the most variance in the training data.

LDA classifiers were fit to the resulting data using MATLAB's *fitcdiscr* function across the 1000 iterations. The overall performance of each classifier was taken as the average performance and 95% confidence intervals on this estimate were taken from the distribution of accuracies across iterations. This analysis was repeated on a null dataset in which condition labels were shuffled across trials in order to generate chance-level performance of the classifier. Significance was calculated by comparing the accuracy percentile values of the classifiers with their null counterparts.

*4.2.4.3 RSA and MDS*

Representational Similarity Analysis (RSA) was employed on normalized firing rate data to assess the relationships between touch conditions (**Figure 4.2b,c)** (Kriegeskorte, 2008; Nili et al., 2014). Cross-validated Mahalanobis distance with multivariate noise normalization was used as the measure of dissimilarity (Walther et al., 2016). The noise covariance matrix was estimated from the data and regularized towards a diagonal matrix to ensure that it would be invertible. The cross-validated Mahalanobis distance is an unbiased measure of square Mahalanobis distance with the added benefit of having a meaningful zero-point (Diedrichsen et al., 2021; Walther et al., 2016). The larger the Mahalanobis distance between two conditions, the more discriminable their neural patterns. If the patterns are fully indiscriminable, their distance is 0. This continuous measure is directly related to discrete classification performance with pairwise LDA. Cross-validated Mahalanobis distance is thus less affected by common activation patterns across conditions in comparison to other measures such as Pearson correlation. The python package *rsatoolbox* (https://github.com/rsagroup/rsatoolbox) was used to compute noise covariance and generate representational dissimilarity matrices (RDMs).

Data was cross-validated across 7 splits, divided by the 10-trial runs the data was originally collected in, and RDMs were generated independently on data divided into 0.5s bins. The resulting RDMs were symmetric across the diagonal, with meaningless values on the diagonal itself.

RDMs were visualized with multi-dimensional scaling (MDS) using the MATLAB toolbox *rsatoolbox* (https://github.com/rsagroup/rsatoolbox_matlab) (Nili et al., 2014). MDS allows for distances in RDMs to be visualized intuitively in a lower-dimensional space while preserving these distances as much as possible. The MDS visualizations used a metric stress criterion to arrange conditions without assuming any category structure a priori. The stress is visualized on MDS plots (**Figure 4.2c**) in the form of grey "rubber bands" stretched between points–the thinner the band, the more the true distances between points are distorted by the low dimensional MDS mapping to be further apart than in the high dimensional RDM.

*4.2.4.4 Tuning and onset analysis*

Tuning properties of multi-unit channels were assessed via linear regression analysis. In each 500ms bin corresponding to 1s before touch onset to 2s after touch onset, normalized firing rates for each channel were fit to a linear regression model based on the following equation:

$$F = \beta_0 + \beta_1 X_1 + \beta_2 X_2 + \cdots \beta_C X_C$$

where F = vector of firing rates on each trial, X = one-hot-encoded matrix signaling condition identity for each trial, $\beta$ = estimated regression coefficients indicating level of tuning to each condition, and C = number of conditions tested. In addition to data from every trial, F also included 70 entries (to match the number of trials per condition), corresponding to $\beta_0$, containing the baseline firing rate of the channel across all trials. This baseline was calculated as a mean of channel activity 4s to 2.5s before touch onset in every trial. For each channel and condition fit with linear regression, a student's

t test was performed to assess the null hypothesis $\beta = 0$. If the null hypothesis was rejected, the channel was determined to be tuned to that condition in comparison to its baseline firing rate. P values were corrected for multiple comparisons using the Bonferroni-Holm method within each channel.

A bootstrap analysis was run for 1000 iterations, in which all conditions were randomly sampled with replacement to yield 70 trials each, to assess significant differences in numbers of tuned channels across conditions (**Figure 4.4**).

The channels identified as tuned to any condition in the period of 1s before touch onset to 2s after touch onset were analyzed to determine the average timing onsets and offsets of their tuned responses. Within a condition, firing rates of all tuned channels were averaged together in 50ms bins, and the 95$^{th}$ percentile of the distribution of average baseline firing rates was computed. The onset time for the condition was the middle of the first time bin in which the firing rate rose above the 95$^{th}$ percentile of the average baseline. The offset time was calculated as the middle of the first time bin in which the firing rate dipped below the 95$^{th}$ percentile of the average baseline, after onset. 95% confidence intervals were constructed for the onset and offset times by bootstrapping over trials within the tuned channels 10,000 times.

### 4.3 Results

S1 responses to visual and tactile stroking stimuli along the arm and finger in a human tetraplegic participant were recorded via two intra-cortical microelectrode arrays. Within arm and finger locations, neural responses to four touch types were examined **(Table 4.1; Figure 4.1**). A fifth touch type (Obj) used an inanimate object as a control rather than a body location, resulting in a total of 9 conditions across locations and touch types. 70 trials were collected in each condition.

Multi-unit channel activity (**Figure 4.1a)** recorded during these trials was aligned to the physical or virtual moment of contact between the touch sensor and the item being touched (touch onset). In visual conditions (*FP, VrFP, TP, Obj), visual information predicting the touch was available beginning approximately 0.5s before touch onset, as the experimenter could be seen beginning the motion towards the touch target (**Figure 4.1b, Supplemental video legends**). In totality, the task comprised 9 conditions (**Table 4.1**); the average firing rate of a single channel to each condition is plotted as an example (**Figure 4.1d**). The task was designed such that data could be averaged across location (**Figure 4.1e**) or averaged across touch type (**Figure 4.1f**) to better isolate neural responses to these factors.

### *4.3.1 Condition identity decoding*

Linear discriminant analysis (LDA) was performed on the top 40 dimensions of the multi-unit channel data, sub-selected over 1000 train/test divisions for equal class sizes and averaged together (**Figure 4.2a**). Classifiers were trained on every pair of conditions, using average firing rates binned in 0.5s increments. No significant decoding occurs prior to touch onset. In the first 0.5s following touch onset, conditions containing a physical touch (*FP, *BL) can be meaningfully distinguished from purely visual conditions (VrFP, TP, Obj) in all cases, and can be significantly distinguished from one another in every case except *BLa vs *BLf (accuracy = 70% [60-80%]), which only becomes significant 0.5s later (72% [61-81%]). *FPa vs *BLa is highly decodable with an accuracy of 87.7% [80-94.3%] despite the two classes only varying on the basis of visual information; similarly, *FPf vs *BLf obtains an accuracy of 83.7% [74.3-91.4%].

Overall in the first time bin post touch onset, *FPa and *FPf are highly distinguishable from other conditions, especially those without physical touch. *BLa and *BLf are less significantly distinguishable. In the following time bin (0.5-1s), this relative disparity in classification accuracies

remains true, but classifications are overall weaker (pairwise one-sided t test across all accuracies, p=3x10-9).

In the [1-1.5s] bin which occurs immediately post touch offset, *FPa is the only condition that can be distinguished from the other conditions. 1.5s post touch onset, no classifiers obtain significant decoding accuracy.

To examine decoding on a finer time scale, the same LDA classifiers as described above were run in touch-onset aligned 0.1s bins (**Supplemental video legends**). No significant decoding occurs before the 0-0.1s bin. In this bin, *FPa can be significant decoded from all conditions apart from *FPf and *BLa, but no other classifiers are significant. In the following 100ms (0.1-0.2s post touch onset) *FP/*BL can be significantly distinguished from all other conditions with the exception of *FPf vs *BLf. By 0.3-0.4s post touch onset, decoding is overall weaker than in the first bin suggesting the time period of 0-0.2s following touch onset contains the strongest touch representations. By 0.7-0.8s post touch onset, nearly all classifiers cease to be significantly accurate.

### *4.3.2 Representational Similarity Analysis (RSA)*

To better visualize the relationships between different task conditions, RSA (Kriegeskorte, 2008) was used on the same multi-unit activity as analyzed with the linear classifier (**Figure 4.2b**). Representational dissimilarity matrices (RDMs) were computed based on the cross-validated Mahalanobis distance with multivariate noise correction (Walther et al., 2016). For visualization purposes, multi-dimensional scaling (MDS) was used to scale the relationships captured in the RDMs into two dimensions (**Figure 4.2c**) (Nili et al., 2014) .

There is a high level of similarity between pairwise decoding (**Figure 4.2a**) and the RDMs (**Figure 4.2b**) during touch encoding (for the three consecutive time bins post touch onset, $r>0.89$; $p<1x10^{-12}$

in all cases, Bonferroni corrected). This similarity is expected since both methods assess the discriminability of neural activity averaged across conditions.

In the 0.5s prior to touch onset, distances between conditions form a pattern which shares a mild correlation with activity post touch onset; activity is most correlated between the -0.5-0s RDM and the 1-1.5s RDM (**Figure 4.2b**, Pearson correlations between -0.5-0s RDM and RDMs 0-2s, in chronological order: r = 0.67, 0.61, 0.70, 0.38; p = $3x10^{-11}$, $3x10^{-9}$, $1x10^{-12}$, $5x10^{-4}$, Bonferroni corrected).

Once touch occurs, the initial RDM within 0-0.5s post touch onset contains a strong pattern that remains stable during the touch and afterwards, although it becomes weaker as time elapses (Pearson correlations between 0-0.5s RDM and RDMs 0.5-2s, in chronological order: r = 0.96, 0.86, 0.62; p = $2x10^{-43}$, $1x10^{-24}$, $9x10^{-10}$, Bonferroni corrected).

Within the 0-0.5s bin, touch types with only visual stimuli (VrFP, TP, Obj) are less distinguishable and tightly grouped together, while the physical touch types (*FP, *BL) are more distinct from one another and therefore more spread out (two-sample t test on distances within VrFP/TP/Obj vs distances within *FP/*vBL: $p=9x10^{-5}$).

*FP and *BL vary in their level of separation from the non-physical touch types (**Figure 4.2c**, 0-0.5s bin). *FP (mean=0.17; std=0.03) is more distant to the non-physical touch types than *BL (mean=0.04; std=0.03). These sets of distances are significantly different from each other (paired t test, $p=3x10^{-5}$). Additionally, during and immediately after the touch, *FP/*BL arm representations are grouped distinctly from the finger representations: on the MDS plots (**Figure 4.2c**), arm conditions are consistently grouped separately (above) finger conditions.

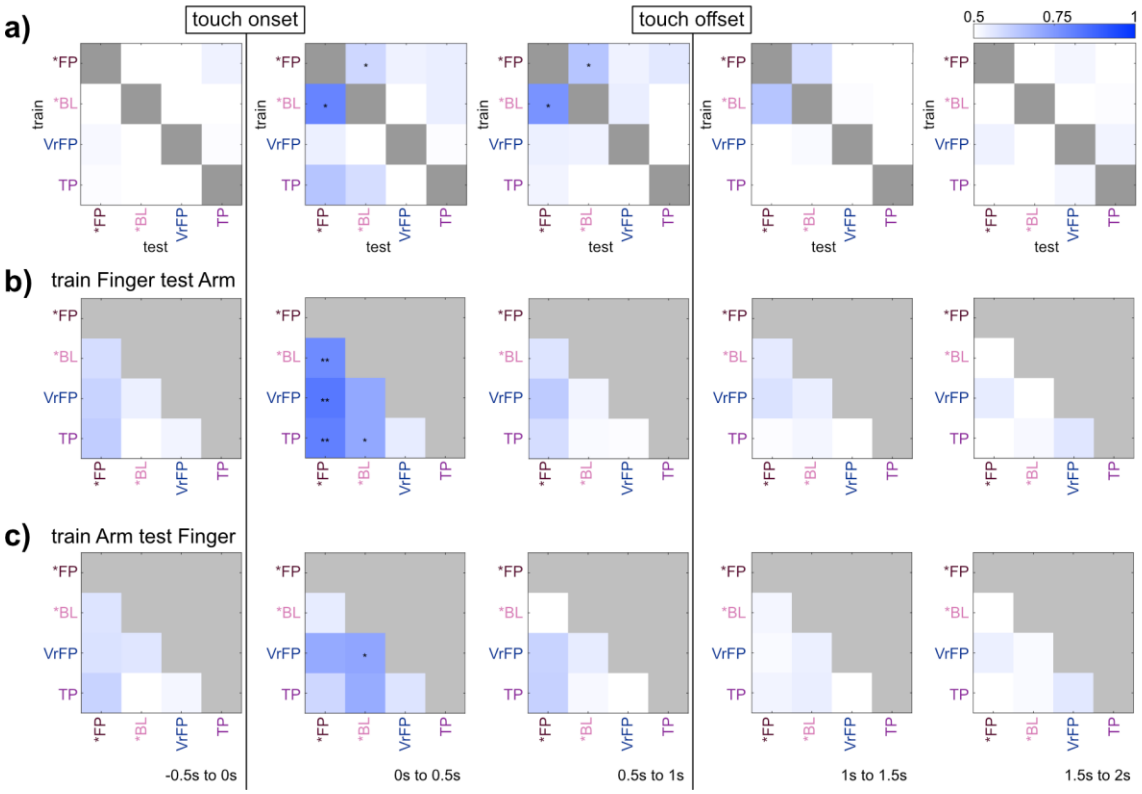


**Figure 4.3 Generalization decoding results**
**a)** Effector was decoded across all pairs of touch types. For example, the bottom left square of each grid represents the average accuracy when a decoder is trained to distinguish Arm v Finger on TP trials and tested on *FP trials. See also **Supplemental video legends**. **b)** Pairs of touch types were decoded, training on Finger trials and testing on Arm trials. For example the bottom left square of each grid represents the average accuracy when a decoder is trained to distinguish TP vs *FP on Finger trials and tested on Arm trials. See also **Supplemental video legends**. **c)** The same procedure as in **(b)** except that training occurred on Arm trials and testing on Finger trials. See also **Supplemental video legends**. All decoders used 140 trials in training and testing respectively, 70 of each effector. All statistics and plotting conventions as in **Figure 4.2a**.

### *4.3.3 Location and touch type generalization decoding*

To investigate if body location information generalizes across touch types, LDA classifiers were trained to differentiate arm/finger conditions within one touch type and tested on another (**Figure 4.3a**). During the touch (0-1s), body location information generalizes within physical touch conditions; it is possible to train the classifier on *FP and decode body location from *BL, or vice versa. The strongest decoding is achieved in the 0-0.5s bin by the decoder that trained on *BL and tested on *FP (accuracy = 79.6% [68.6-90%]). Post touch offset, generalization is no longer possible.

When the same decoding problem is performed in 0.1s bins (**Supplemental video legends**), the only significant accuracies is at 0.1-0.2s post touch onset for the same subset of conditions significant in the 0-0.5s bin, indicating a small window of time when body location can generalize strongly across touch types. The opposite question was also interrogated: can a classifier trained on one body location successfully decode the type of touch presented using another body location? In this case, for both classifiers that trained on finger data and tested on arm data (**Figure 4.3b**), and classifiers that trained on arm data and tested on finger data (**Figure 4.3c**), the only significantly decodable instances occur in the 0-0.5s time bin.

Decoding is notably asymmetric between training on finger/testing on arm and the opposite paradigm: *FP can be strongly distinguished from all other conditions when training on finger and testing on arm, but cannot be significantly distinguished from any conditions when training on arm and testing on finger. Additionally, there are smaller asymmetries in significance across the two paradigms when distinguishing *BL from VrFP or TP. Decoding in 0.1s time bins is overall weaker, and only is significant in the 0.2-0.3s time bin for training on finger, testing on arm (**Supplemental video legends**), while training on arm, testing on finger never reaches significance at any time point (**Supplemental video legends**).

### *4.3.4 Individual channel tuning analysis*

To investigate the tuning properties of individual channels within the S1 arrays, linear regression analysis was performed in 0.5s bins aligned to touch onset. The most channels are tuned to *FPa (34 [95% CI=30, 45] out of 96 channels total), a number significantly greater than the number of channels tuned to *FPf (21 [18, 26]) or *BLa (13 [10, 22]; **Figure 4.4a**). *FPf elicits more tuned channels than *BLf, which trails at 8 [6, 16] channels. Of the non-physical touch conditions, only 1 [1, 8] channel is tuned to VrFPf. The number of time bins that tuned channels are responsive to a given condition is

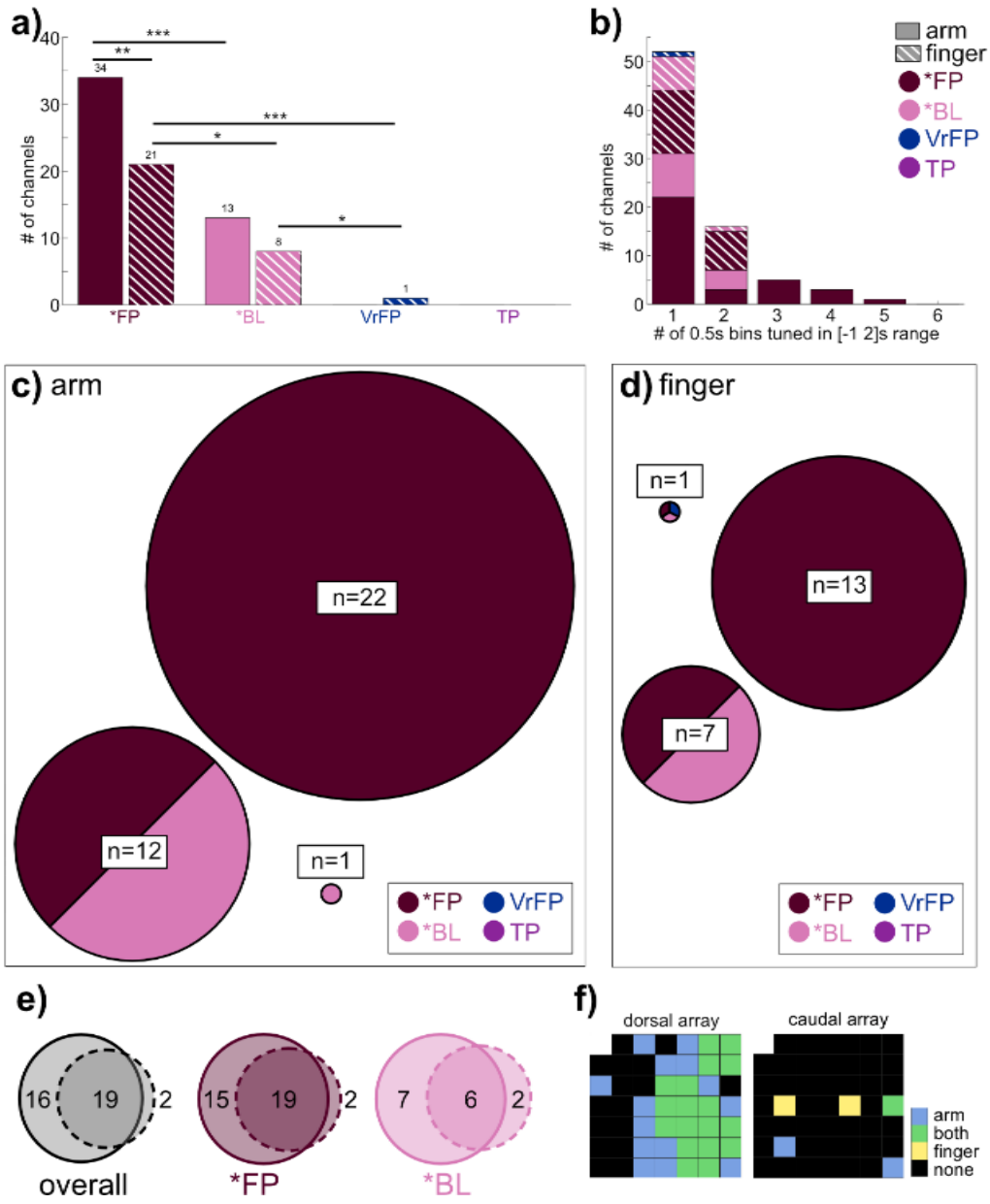


**Figure 4.4 Tuning analysis**
Channels selective for any touch modality ($p<0.05$, Bonferroni-corrected linear regression analysis) at any time bin in the -1 to 2s range relative to touch onset were examined. **a)** Total number of channels tuned within arm and finger touch conditions. Asterisks indicate non-overlapping 95% CIs. **b)** Histogram indicating the range of time that channels were tuned. Tuning was performed in 0.5s non-overlapping time bins (maximum bins a channel could be tuned to in the -1 to 2s range was 6. **c)** Circles indicate the specific set of modalities each channel was tuned to, within arm touch modalities, and have a diameter proportional to the number n channels tuned to that set. **d)** Plotting as in **(c)** but based on finger touch conditions. **e)** Distribution of channels tuned to arm (solid line circle), finger (dashed line circle), or both, across all touch conditions (left) or within touch types (middle, right). f) Array map of implanted electrodes, indicating locational tuning across all conditions.

quantified (**Figure 4.4b**). No tuning to finger conditions occurs for longer than 2 bins (1s). *BLa tuning follows the same rule, but *FPa trials elicits up to 5 bins (2.5s) of responsive activity.

The overlap across tuned arm conditions within channels was calculated (**Figure 4.4c**). 22 channels are tuned to *FPa solely, while 12 channels are tuned to *FPa and *BLa together. Similarly, 13 channels are tuned to *FPf solely, while 7 channels are tuned to *FPf and *BLf together. In finger conditions (**Figure 4.4d**), fewer channels are tuned overall. Within arm and finger, channels are nearly all tuned to *FP conditions (**Figure 4.4c, d**).

The overlap of tuned channels across all arm and finger conditions was determined (**Figure 4.4e**). Overall, most channels are tuned to both arm and finger (n=19), while 16 channels are only tuned to arm conditions. Only 2 channels are tuned to solely finger conditions. Within touch types, a similar pattern emerges. In *FP, 19 channels are tuned to both arm and finger, 15 to just arm, and 2 channels to just finger. In *BL, 6 channels are tuned to arm and finger, 7 to just arm, and 2 to just finger. Lastly, the position of tuned channels across all arm and finger conditions was plotted on diagrams of the microelectrode arrays (**Figure 4.4f**). Channels tuned to both arm and finger are clustered together, surrounded by channels tuned to arm only. The two exclusively finger-tuned channels are located on the opposite array from the other channels.

The average tuned response curves of channels tuned to *FP and *BL conditions were examined (**Figure 4.5**), calculated as deviation from the distribution of baseline activity: *FPa onset = -25ms [95% CI= -75, 75]; *FPf onset = 125ms [75, 125]; *BLa onset = 25ms [25, 75]; *BLf onset = 75ms [75, 125]. The average offset times of tuned activity were also determined, relative to onset of the touch stimulus: *FPa offset = 1125ms [575, 1575]; *FPf offset = 825ms [625, 875]; *BLa offset = 875ms [575, 925]; *BLf offset = 875ms [525, 925].

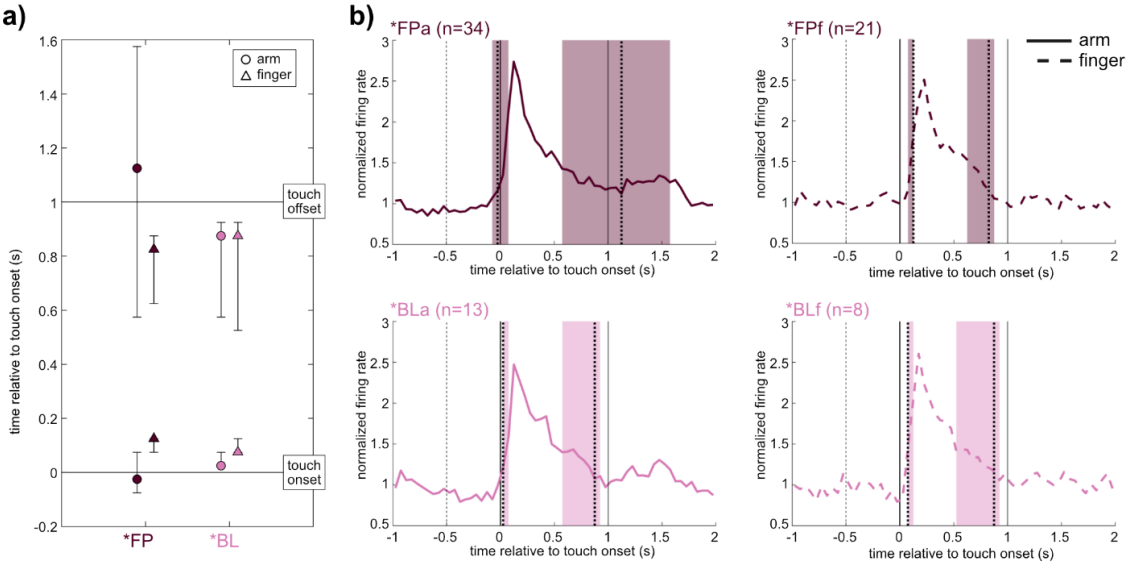


**Figure 4.5 Neural dynamics of tuned channels**
**a)** Onset and offset of channel tuning. Onset of tuning was calculated based on the average normalized firing rate across all tuned channels and condition trials, as the first time bin where average activity exceeded the 95$^{th}$ percentile of the distribution of average baseline responses. Offset was calculated on the same data as the first time bin to dip below the 95$^{th}$ percentile of baseline activity after the peak firing rate. Error bars represent 95% CI obtained by bootstrapping 10,000 times over trials. **b)** Average responses to individual conditions in tuned channels, relative to touch onset (vertical black line at 0s); touch offset is plotted as a vertical black line at 1s. Vertical dotted lines indicates onset and offset of response with colored background depicting 95% CIs. n=number of tuned channels.

While there is substantial variance across trials and electrodes, a major trend emerges from this analysis. Within *FP and *BL, arm onset times always occur before finger onset times, while offset times are similar across conditions with the exception of the wide variance of *FPa (**Figure 4.5a**). Within arm and within finger, onsets times are not statistically different although the mean of *FPa onsets occurs slightly prior to touch onset. In all conditions (**Figure 4.5b**), activity peaks sharply immediately following touch onset, followed by a gradual decrement of activity back to baseline.

## 4.4 Discussion

To examine how S1 represents tactile events based on their location and their multisensory context, electrophysiology data from the putative area 1 of the S1 arm region were examined (**Figure 4.1a)**. Within arm and finger locations, touch types varying in their tactile and visual content were tested

(**Table 4.1**). It is worth noting that the participant's long-term tactile impairment could have resulted in representations of touch in S1 that are altered relative to healthy humans. This is unlikely to be a major effect on the findings of this study, because recent work has shown that topographic representations in S1 are highly preserved in tetraplegic people, even years post-injury, although these representations can weaken over time (Kikkert et al., 2021; Makin and Bensmaia, 2017).

Analysis of this rich, exploratory dataset suggested two main conclusions about local neural activity where the multi-electrode arrays were implanted: 1) This S1 area is specialized for arm representations but is capable of representing touch information from the finger in a more general manner; 2) This S1 area is modulated by vision during physical touches, but is not activated by vision on its own.

### *4.4.1 Neural activity is specialized for arm touches and represents finger touches more generally*

Immediately after touch onset in FP* and BL*, arm conditions are separated from finger conditions, based on neural activity visualized using MDS (**Figure 4.2c**). This division based on touch location continues until the touch ceases. *FP and *BL are both separable by touch location, although *BL is significantly less separable. This pattern is also evident in the linear decoding analysis, where *FPa vs *FPf is immediately highly decodable upon touch onset, while *BLa vs *BLf is only significantly decodable one time step (0.5s) later (**Figure 4.2a**). *FPa can be distinguished from all other conditions for much longer than any other condition–up to 1.5s post touch onset–and is the first condition to become decodable in the 0.1s bin classifier (**Supplemental video legends**).

Despite *FP seeming to contain more robust location information than *BL, classifiers trained on either *FP or *BL and tested on the other to distinguish arm from finger trials achieve significant decoding (**Figure 4.3a**). Locational information is therefore sufficiently present in *BL conditions to

allow for generalization to and from *FP conditions. Through analysis of the 0.1s bin decoders, it appears the bulk of this locational information is present 0.1-0.2s post touch onset.

While arm and finger touches are both represented in S1, an asymmetry becomes apparent when training classifiers to decode touch type while generalizing across body locations. In particular, *FP trials can be distinguished from all other touch types when classifiers are trained on finger data and tested on arm data (**Figure 4.3b**), but the reverse is not true (**Figure 4.3c**): *FP trials are indistinguishable from other touch types when classifiers are trained on arm data and tested on finger data. As the data were recorded in a putative arm area, it is likely that this asymmetry is due to different levels of encoding specificity. Arm touches may be represented in a highly specific manner that does not generalize to other touch locations, while finger touches (and potentially touches from other areas) may be represented more generally as they are outside of their primary topographic S1 location.

The tuning analysis further demonstrates the differences in arm and finger neural representations. More channels overall are tuned to arm than finger conditions (**Figure 4.4a**), and *FPa trials elicit tuning for up to 5 time bins (2.5s) while *FPf tuning only lasted up to two time bins (1s; **Figure 4.4b**). The vast majority of tuned channels are either tuned to solely arm conditions or both arm and finger conditions (**Figure 4.4e**). Only two channels are tuned to solely finger conditions, suggesting the bulk of the neural population recorded is not selective to finger touches specifically, but may be activated by body touches more generally in addition to arm touches specifically. *FP and *BL each contain roughly equivalent numbers of channels tuned to solely arm or to both finger and arm, and very few channels tuned solely to finger (**Figure 4.4e**). Onset analysis of *FP and *BL reveal a trend that appears to mesh with this pattern–*FPa onset occurs 0.15s before *FPf onset, and *BLa onset occurs

0.05s before *BLf (**Figure 4.5a**). In other words, arm conditions elicit sharply tuned neural responses that begin before the tuned responses to finger conditions (**Figure 4.5b**).

To summarize, neural activity elicited by physical touches delivered to the arm forms patterns distinct from the activity elicited by touches to the finger. Individual channels tend to be tuned to both arm and finger, or just arm conditions, but rarely just finger conditions. Tuned activity starts earlier for arm conditions than finger conditions. This evidence builds a picture of a region of S1 which is primarily geared towards representing arm touches. A neural sub-population of this region is also is capable of representing finger touches, albeit less strongly or specifically.

There could be several reasons for this difference between the two tested locations. One is that, due to the spinal cord injury, the participant was able to sense one location more strongly and naturalistically than the other. The patient reported finger sensations to be more natural, yet neural finger representations were weaker. This makes the participant's uneven tactile impairment an unlikely culprit for the differences in location encoding.

If the differences between arm and finger representations are not primarily due to differences in spinal cord damage and tactile impairment, then they are likely due to differences in the neural representations of these locations. The distribution of tuned channels appear geographically distributed when mapped to the implanted micro-electrode arrays–the upper array contains the bulk of activity, with a nucleus of channels tuned to both arm and finger conditions and a surrounding of channels tuned solely to arm conditions (**Figure 4.4f**). The only two finger-specific channels are located on the lower array. Cortical curvature may have resulted in electrodes recording from varying cortical layers within S1.

From prior work with this participant, it is known that intra-cortical microstimulation (ICMS) of the S1 arrays studied here elicits cutaneous and proprioceptive sensations primarily in the arm, with a much smaller number of sensations in the fingers (Armenta Salas et al., 2018). It is likely the arrays, especially the dorsal array (**Figure 4.4f**), are located in the arm region of area 1 within S1. The neural response to finger touches detailed here contribute to the growing literature suggesting that although S1 overall does maintain a gross representation of the body along the lines of the homunculus laid out in the earliest human cortical stimulation studies and observed many times since (Ejaz et al., 2015; Kaas et al., 2019; Kolasinski et al., 2016; Penfield and Boldrey, 1937; Sanders et al., 2019), it also contains other more complex levels of tactile representations (Arbuckle et al., 2022; Enander and Jörntell, 2019; Muret et al., 2022; Qi et al., 2016; Thakur et al., 2012). Most recently, Muret et al. (2022) used MRI to show that different body locations are represented in S1 in areas beyond their primary topographic area both in area 3b specifically and S1 overall. Our findings support and expand this finding, indicating that S1 area 1 encodes highly specific and rapid responses to touches through its established topography, but tactile information from other anatomical areas outside this topography may activate area 1 in a more general manner.

### *4.4.2 Visual information modulates neural activity if accompanied by a physical stimulus*

S1 neural activity is restricted to conditions which contain a physical tactile stimulus, and less than 2% of channels are tuned to visual-only conditions **(Figure 4.4a**). Although several variations on visual touches without physical stimuli were tested (VrFP, TP, Obj), they are not represented in a discriminable manner from one another in S1 (**Figure 4.2**). VrFP and TP do not elicit representations of touch location information in S1 activity, whether decoded in an identity or generalization problem (**Figure 4.2a, Figure 4.3a**). Across all methods in this study, there is no detectable encoding of tactile information in S1 from purely visual stimuli.

In contrast, *FP trials contain visual information paired with a physical stimulus and, immediately after touch onset, they can be easily discriminated from all non-physical conditions and from *BL trials which contain the same physical stimulus minus the visual content (**Figure 4.2a**). The strong performance of *FPa vs *BLa and *FPf vs *BLf classifiers indicate the presence of visual information is sufficient to change the touch encoding in S1. Visual information also appears to affect the length of time a touch representation occurred in S1, as *FPa is decodable for much longer than any other condition.

RSA demonstrates that the pattern of responses immediately prior to touch onset is mildly correlated with activity during the touch itself, suggesting there is some effect of a visual approach of a tactile stimulus before an expected touch occurs (**Figure 4.2b**). However, a much stronger stable pattern of activity emerges once the touch actually begins, as indicated by the correlations between the RDM of the first 0.5s to the following RDMs. This relationship is evident in the MDS plots generated based on neural activity (**Figure 4.2c**). In the second following touch onset, *FP and *BL conditions are separated from all other touch types and from each other. In particular, *FPa and *FPf are highly dissociated from the other conditions. The presence of visual information generalizes across touch location to some extent–a classifier trained on finger trials can distinguish *FP vs *BL in arm trials, but not vice versa (**Figure 4.3b,c**). The ability to decode visual information in a manner than generalizes across body location also appears to be present quite late relative to touch onset; the 0.1s bin decoder only achieves any significance in the 0.2-0.3s time bin relative to touch onset. These findings speak to a more general distinction between visual and blind physical touches existing in S1 finger touches, which is overridden by more specific information in arm touches that are not able to generalize to other body parts.

There are large populations of channels tuned to *FPa and *FPf, and within these populations there are sub-groups also tuned to *BLa and *BLf respectively (**Figure 4.4c, d**). Blind and visual touches appear to activate the same population of neurons, but touches with a visual component activate additional neurons on top of this population.

These results suggest that visual information is enough to distinguish two otherwise identical physical touches in S1, but visual information on its own, whether it relates to oneself (VrFP), another person (TP) or an inanimate object (Obj) is not sufficient to engage S1. This finding is especially intriguing because while it is clear that visual information affects experiences of touch (Botvinick and Cohen, 1998; Gazzola et al., 2012; Press et al., 2004), a rapidly evolving scientific literature is still deciding the role of vision in modulating S1 (Blakemore et al., 2005; Chan and Baker, 2015; Keysers et al., 2004; Kuehn et al., 2013; Longo et al., 2011; Meyer et al., 2011; Morrison et al., 2004; Schaefer et al., 2009; Zhou and Fuster, 2000).

The results presented here examine the effect of vision on S1 using human electrophysiology, specifically in a highly localized sub-region of S1, with high spatial resolution of spiking activity. The bulk of prior literature has used fMRI, MEG, and EEG to address this question, data which capture whole brain dynamics at a relatively low spatial resolution, and likely include membrane potentials that do not produce spikes. These experiments have for the most part examined S1 as a whole, and results have varied, finding either that S1 has no response to observed touch (Chan and Baker, 2015; Keysers et al., 2004; Morrison et al., 2004) or does respond to observed touch (Blakemore et al., 2005; Longo et al., 2011; Meyer et al., 2011; Schaefer et al., 2009; Zhou and Fuster, 2000). From the studies examining Brodmann areas more specifically, we see evidence that area 3b (Kuehn et al., 2018) and areas 1 and 2 (Kuehn et al., 2013) are capable of responding to observed

touch. One potential method to reconcile these findings and the results found here in area 1 would be to examine the type of task employed.

The majority of experiments finding S1 modulation to observed touches employ a touch-relevant task during data collection, whether it be counting touches (Ebisch et al., 2008; Schaefer et al., 2009), answering qualitative questions about the touch type (Bufalari et al., 2007; Kuehn et al., 2018, 2013; Longo et al., 2011), or rating touch intensity (Blakemore et al., 2005). The experiments which find no effect of observed touch on S1 tend to employ either non-touch-related tasks (Chan and Baker, 2015) or simply ask participants to passively observe the stimuli (Keysers et al., 2004; Morrison et al., 2004). Thus it is possible that a relevance threshold, modulated by higher order brain areas, must be exceeded in order for S1 to represent observed touches (Dionne et al., 2013). If this is true, the fact that S1 does not respond to visual stimuli when the participant passively observes touches in this study agrees with the existing literature, despite the differences in data types. This effect could also explain why visual information does modulate tactile representations of physical touch–the physical component of the touch activates S1 as it would in a blind touch, but additionally higher order areas integrate the visual input as sufficiently relevant to the tactile input such that vision affects S1 simultaneously.

What might be the role of this modulation? It is known that vision modulates experiences of touch in a variety of ways, including effects like visual enhancement of touch (Colino et al., 2017; Haggard et al., 2007; Kennett et al., 2001; Press et al., 2004; Tipper et al., 2001) in which non-informative vision of a body part improves tactile perception. Our results suggest that touch-relevant visual information elicits an earlier tuned response over more neurons, and results in a representation of touches that are highly distinguishable in terms of location and multisensory content. All of these attributes have the potential to contribute to visual enhancement of touch. Indeed, these results agree with prior literature

which has suggested that S1 is modulated by paired visual and tactile stimuli (Cardini et al., 2012, 2011; Deschrijver et al., 2016; Dionne et al., 2013, 2010; Eck et al., 2013; Schaefer et al., 2006; Taylor-Clarke et al., 2002; Zhou and Fuster, 2000), and has also shown that S1 is a necessary component of body-centered visuotactile integration (Bolognini et al., 2011; Fiorio and Haggard, 2005; Rossetti et al., 2012) and reflects predictions of tactile events from visual signals (Kimura, 2021).

S1 can be modulated by concepts as high-level as affective significance, as was shown in a study which examined the effect of perceived gender of a person delivering a caress to heterosexual men (Gazzola et al., 2012). S1 is also affected by motor planning, presumably expecting the sensory consequences of upcoming actions (Ariani et al., 2022; Gale et al., 2021), and by imagining touch sensations (Bashford et al., 2021; Yoo et al., 2003). It is likely that when S1 is modulated by visual information, it is not directly interacting with the visual system but instead affected by upstream areas which are implementing some version of a forward model to determine expected tactile inputs.

### *4.4.3 Conclusion*

This study represents a broad exploration of how different types and locations of touch affect a small area in the putative arm region of S1. It contributes to the growing body of literature suggesting that area 1 within S1 contains highly specific topographic organization as classically depicted, but additionally encodes touches outside this topography in a less specific manner. We also find that visual information depicting touches, either to oneself, to another person, or to an object, are not sufficient to activate S1 in a measurable way. However, a blindly sensed physical touch and a visually seen physical touch are represented distinguishably in S1–both elicit strong responses that share commonalities, such as how touch location is encoded, but they are not identical.

Taken as a whole, these findings demonstrate that S1 contains a nuanced and complex encoding of tactile experiences that is to some degree multisensory. Future endeavors should aim to examine these same conditions in a larger population of individuals, both healthy and with a variety of levels of sensorimotor impairment. There are many practical applications for a better understanding of S1, including the improvement of restorative devices seeking to artificially generate tactile sensations in deafferented limbs and prosthetics (Armenta Salas et al., 2018; Christie et al., 2019a; Flesher et al., 2016; Pandarinath and Bensmaia, 2022). By better understanding how naturalistic tactile sensations are encoded in S1, and how they interact with cues from other sensory modalities, we can improve our ability to generate biomimetic artificial stimuli.

### *4.4.4 Limitations of the study*

The dataset examined here, while informative, is limited in several ways. Recordings from more locations of S1 would have allowed for a better understanding of the differences between Brodmann areas 1, 2, 3a, and 3b within S1, as well as differences along the topographic map within areas. Examining only two body parts leaves room for the possibility that other body parts are represented differently than the ones tested; since array localization was based on subjective ICMS responses (Armenta Salas et al., 2018) these locations have some uncertainty and limited precision. Visual information within the task may have contributed to a variety of processes, including expectation/prediction of touch onset, face processing, peri-personal space processing, and attentional factors. The different conditions tested here may be more or less salient, but these differences occur as part of our biologically relevant task design, and part of the experiment was explicitly addressing how different visuotactile contexts affect S1. Data from only one participant can confound individual differences with population trends, and while unlikely, it is possible the participant's spinal cord injury has caused some remapping of S1 (Kikkert et al., 2021; Makin and Bensmaia, 2017). Finally,

due to restrictions on data collection, recordings were collected over the course of six months and some conditions were tested in separate sessions, which may have affected decoding and introduced confounds associated with neural recordings drifting over time.

## 4.5 Supplemental video legends

**Supplemental Video 4.1 Sample stimulus from the VrFPa condition**
Related to **Figure 4.1c.** Stimulus was presented using a virtual reality headset. The virtual reality environment was constructed to mimic the room in which the experiment was performed.

**Supplemental Video 4.2 Pairwise identity decoding at 0.1s resolution**
Related to **Figure 4.2a.** All decoding, statistics and plotting conventions as in **Figure 4.2a**., except decoding bins are 0.1s wide instead of 0.5s. Bins are aligned relative to touch onset.

**Supplemental Video 4.3 Generalization decoding of effector across all pairs of touch types at 0.1s resolution**
Related to **Figure 4.3a.** All decoding, statistics and plotting conventions as in **Figure 4.3a**., except decoding bins are 0.1s wide instead of 0.5s. Bins are aligned relative to touch onset.

**Supplemental Video 4.4 Generalization decoding of touch type, training on Finger trials and testing on Arm trials at 0.1s resolution**
Related to **Figure 4.3b.** All decoding, statistics and plotting conventions as in **Figure 4.3b**., except decoding bins are 0.1s wide instead of 0.5s. Bins are aligned relative to touch onset.

**Supplemental Video 4.5 Generalization decoding of effector, training on Arm trials and testing on Finger trials, at 0.1s resolution**
Related to **Figure 4.3c.** All decoding, statistics and plotting conventions as in **Figure 4.3c**., except decoding bins are 0.1s wide instead of 0.5s. Bins are aligned relative to touch onset.

# *Chapter 5*

# THE INTEGRATION OF ICMS AND VISUAL CONTEXT

## 5.1 Introduction

Tactile sensation is highly important for executing dexterous, adaptable movements (Ghez et al., 1995; Miall et al., 2021, 2019; Robles-De-La-Torre, 2006; Sainburg et al., 1995) and providing a sense of embodiment within one's own body (Giummarra et al., 2008; Jeannerod, 2003; Tsakiris et al., 2010). In cases of spinal cord injury (SCI), motor and somatosensory abilities are impaired or fully lost below the level of the injury. Brain-machine interfaces (BMIs) provide a potential method to restore these abilities, by decoding motor intentions from neural activity (Collinger et al., 2013; Dekleva et al., 2021; Moses et al., 2021), and by using intra-cortical microstimulation (ICMS) in the primary somatosensory cortex (S1) to elicit artificial tactile sensations (Armenta Salas et al., 2018; Flesher et al., 2016).

Motor BMIs have become more accurate and sophisticated over the last 15 years (Dekleva et al., 2021; Keshtkaran et al., 2022; Simeral et al., 2021; Willsey et al., 2022). In contrast, broadly viable somatosensory BMIs remain at the proof-of-concept stage (Flesher et al., 2021), although some principles mapping the relationship between ICMS and sensations have emerged. A higher ICMS current amplitude elicits sensations more often than a lower current amplitude, and the sensations tend to be rated as more intense (Armenta Salas et al., 2018; Flesher et al., 2016; Hughes et al., 2021a). The perceived location of elicited sensations reflects the topographic organization of S1 according to where the stimulation microelectrode arrays are implanted (Armenta Salas et al., 2018; Flesher et al., 2016). However, it remains poorly understood how to achieve reliable, replicable sensations with

controllable qualia because experiences of ICMS can vary widely across electrodes, participants, and experiments, even when stimulation parameters are kept constant (Armenta Salas et al., 2018; Callier et al., 2020; Flesher et al., 2016).

A somatosensory BMI implemented in the real world will necessitate ICMS being processed by the brain as part of a complex multisensory environment (Risso and Valle, 2022). To this end, understanding how ICMS is integrated with, and influenced by, other sensory inputs to produce perceptual experiences is highly important. Studies have shown that artificial tactile sensations have slower reactions times compared to real tactile inputs or visual stimuli (Caldwell et al., 2019; Christie et al., 2022; Godlove et al., 2014). However, while relative processing speeds between sensory modalities have been investigated, the dynamics of how they are integrated together are still unclear.

Given that visual and tactile stimuli are often paired together in the real world, the characteristics of the temporal binding window, or the period of time in which two stimuli are perceived as simultaneous events, needs to be mapped out with respect to ICMS and visual stimuli. It has been shown that the optimal timing needed to perceive peripheral nerve stimulation and visual stimuli as simultaneous is not always the same. This timing appears to change based on whether the stimulation occurs in the upper or lower limb, with stimulation in the leg needing to occur earlier than in the hand (Christie et al., 2019b). Yet the temporal binding window between ICMS and vision remains unclear, and it is unknown what timings would be optimal to perceive ICMS and a visual cue as simultaneous.

In addition to timing considerations, it is also possible that vision can affect the qualia of ICMS-elicited sensations. Some work in lower limb amputees has shown that visual information can bias the localization of sensations elicited through peripheral nerve stimulation (Christie et al., 2019a). However, there has been little research on the potential effects of visual context on the neural processing and perceptual results of ICMS.

In this work, we explore the behavioral and neural results of pairing ICMS and visual stimuli in a tetraplegic patient implanted with microelectrode arrays in the primary somatosensory cortex (S1) (**Figure 5.1a**). In order to understand the importance of biologically relevant visual information to the perception of ICMS sensations, two visual conditions are used which differ in their level of realism (**Figure 5.1b**). The visual stimuli are presented at varying temporal offsets relative to ICMS in order to better characterize the temporal binding window between ICMS and vision, and recordings of S1 are examined during catch trials to examine the effects of ICMS-related visual information on early tactile processing. We find evidence that both visual context and ICMs current amplitude are capable of biasing qualitative aspects of ICMS-elicited sensations, and that the temporal binding window changes based on the biological relevance of visual context. Additionally, vision and ICMS are perceived as optimally synchronous when ICMS precedes vision in both visual conditions. Finally, we show that S1 represents information from visual stimuli relevant to ICMS in a context-independent manner. This study lays the groundwork for the implementation of BMIs using ICMS to elicit naturalistic sensations which can be temporally and perceptually integrated with the real-world environment.

## 5.2 Methods

### *5.2.1 Participant*

As part of a brain-machine interface (BMI) clinical trial involving intra-cortical recording and stimulation, a C5-level tetraplegic participant (male, 32 years old) was recruited and consented. The participant's microelectrode array implants were placed in three locations in the left hemisphere: the supra-marginal gyrus (SMG), ventral premotor cortex (PMv), and primary somatosensory cortex (S1). This work only examines the arrays in S1 (**Figure 5.1a**). The implants in S1 were two 48-channel 1.5mm SIROF-tipped (sputtered iridium oxide film) microelectrode arrays (Blackrock

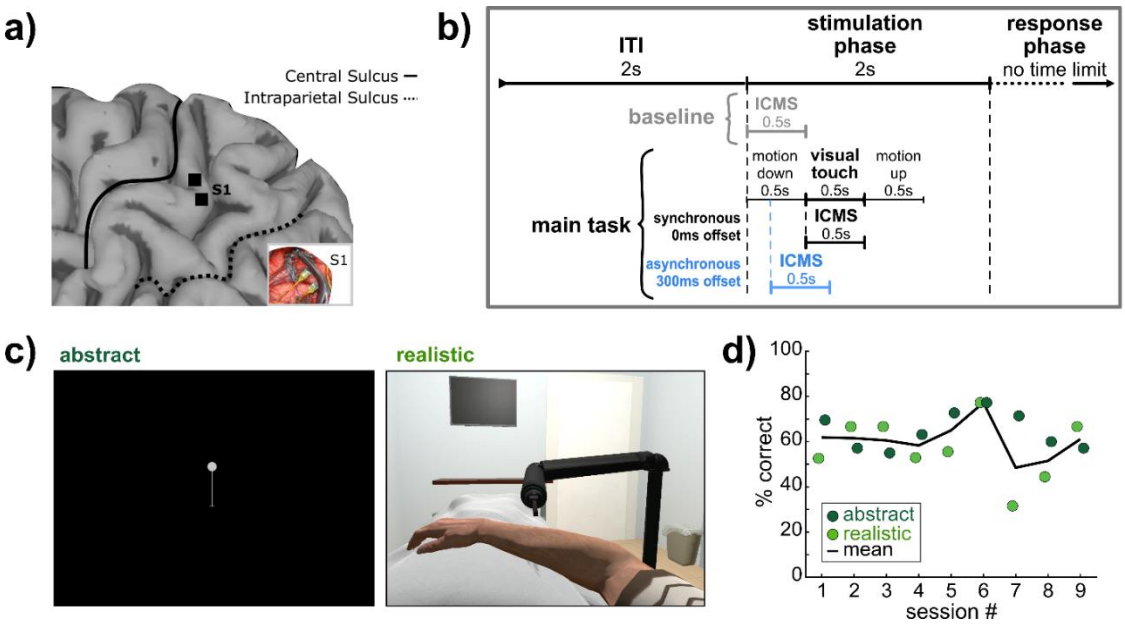


**Figure 5.1 Experimental methods and paradigm**
**a)** Microelectrode array implant location in a human tetraplegic patient (n=1), visualized using MRI on the cortical surface of the left hemisphere. Inset: in situ array location. Figure modified from Armenta Salas et al. (2018). **b)** Task time course. In the baseline, only ICMS was delivered. In the main task (either abstract or realistic), a visual cue was temporally linked to the ICMS at a given offset (either -300, -150, 0, 150, or 300ms); 300ms offset is depicted. **c)** Sample frames from visual cues. In the abstract condition, the dot moved down to contact the end of the line. In the realistic condition, the robotic arm moved down to contact the virtual body. See **Supplemental Video 5.1**, **Supplemental Video 5.2**. **d)** Behavioral accuracy across experimental sessions, quantified as the percentage of the trials where the participant reported a sensation, in which the participant's reported order of stimuli (either vision first, ICMS first, or simultaneous) matched the ground truth stimulus order. The average number of trials felt per session was 18.2 (std=1.2) for realistic runs and 19.7 (std=3.2) for abstract runs. Black line = mean across abstract and realistic runs. See also **Supplemental Figure 5.1** for accuracy by ICMS current.

Neurotech, Salt Lake City, UT). Given the constraints of implanting arrays on the surface of cortex and the anatomy of S1, it is likely the microelectrode arrays in S1 are located in Brodmann area 1 (BA 1) (Pandarinath and Bensmaia, 2022). Additional information on the arrays and surgical methodology is available in (Armenta Salas et al., 2018).

At the first experimental session, the participant was 5.5 years post-implant and 7 years post-injury. All procedures were approved by the Institutional Review Boards (IRB) of the California Institute of Technology, University of Southern California, and Rancho Los Amigos National Rehabilitation Hospital.

### *5.2.2 Experimental paradigm*

Each experimental session consisted of three runs: the baseline, the realistic condition, and the abstract condition (**Figure 5.1b**). During all runs, visual stimuli were shown to the participant using a Vive Pro Eye virtual reality headset (HTC Corporation, Taoyuan City, Taiwan) which was programmed using Unity.

In the baseline condition (18 trials total per session), which always occurred first, the participant viewed grids of the upper body and hand on a gray background which remained static throughout the task. Each trial contained a 2s ITI, a 2s stimulation phase, and a response phase without a time limit. In each trial, 0.5s of ICMS was delivered immediately upon entering the stimulation phase, at one of three amplitudes (30, 60, 100 µAmps) which were evenly sampled (5 trials each). All stimulation occurred on the same single channel, at 300 Hz, with a pulse-width of 200ms and an interphase of 60ms. The baseline also contained 3 catch trials where no stimulation was delivered. During the response phase, the participant was given an auditory cue (a beep) to verbally indicate whether or not he experienced a tactile sensation from ICMS. In the affirmative case he used the grids as references to indicate the sensation location. He also relayed the duration ('Short,' 'Medium,' or 'Long'), a qualitative descriptor of the sensation (free word choice), and the intensity (on a subjective scale).

In the realistic and abstract conditions (40 trials total per session each), the experimental phases and ICMS parameters were identical to the baseline, except a visual component was now included (**Figure 5.1c**). In the abstract condition, the participant viewed a 2D black dot positioned at the top of a black line on a gray background (**Supplemental Video 5.1**). In the realistic condition, the VR headset was used to give the participant a first-person perspective of a body with a size, gender, and posture reflecting his own body, which was taken from the Microsoft Rocketbox Avatar Library (Gonzalez-Franco et al., 2020) (**Supplemental Video 5.2**) (https://github.com/microsoft/Microsoft-

Rocketbox/). The body was located in a VR environment which closely mimicked his vantage point in the real room in which he was located. The only object without a real analog was a virtual robotic, articulated arm with a narrow rod protruding from the end that was positioned over his virtual arm.

During the stimulation phase, both a visual and ICMS cue (same parameters as in the baseline) were delivered. In the realistic condition, the visual cue was the robotic arm performing a single tap of the participant's virtual arm, and in the abstract condition it was the dot moving along the line to tap the bottom (**Figure 5.1c**, **Supplemental Video 5.1**, **Supplemental Video 5.2**). In both conditions, the virtual cue was composed of 0.5s motion downwards, 0.5s contact ("visual touch"), and 0.5s motion upwards to the original position (**Figure 5.1b**).

The visual point of contact either to the virtual first-person body or to the end of the abstract line was depicted at varying times relative to the ICMS cue (-300, -150, 0, 150, 300ms). In 12 of the 40 trials in a section, they were presented simultaneously (0ms). In 12 trials, visual contact occurred before ICMS began (-300 or -150ms; 6 trials each). In 12 trials, visual contact occurred after ICMS began (300 or 150ms; 6 trials each). There were also 4 catch trials where the visual cue was delivered without ICMS. ICMS amplitudes (30, 60, 100μA) were sampled evenly within timing conditions.

Within conditions, trials were pseudo-randomly shuffled. The order of the realistic and abstract conditions was alternated across days.

### *5.2.3 Data collection*

In total, nine experimental sessions were collected on unique days over a 6-month period. Neural data was recorded from the S1 microelectrode arrays using a Neural Biopotential Signal Processor as 30,000 Hz broadband signals, and a CereStim96 device was used to deliver ICMS in S1 (Blackrock Neurotech, Salt Lake City, UT).

A central computer used custom MATLAB (MathWorks, Natick, MA) code with synchronized ICMS and visual outputs, the latter of which were displayed on a virtual reality headset (Vive Pro Eye, HTC Corporation, Taoyuan City, Taiwan). Latencies to stimulus delivery were calculated and compensated for, resulting in a negligibly small unintended temporal offset of ICMS occurring 5ms on average (std = 2ms) before visual outputs across sessions.

### *5.2.4 Quantification and statistical analysis*

All analyses were performed using MATLAB R2019b (MathWorks, Natick, MA) unless otherwise noted. Throughout the analysis, when multiple comparisons were performed, Bonferroni-Holm correction was performed to correct the p-values.

#### *5.2.4.1 Data preprocessing*

Data from the arrays in S1 were passed through a 180Hz notch filter in order to remove an electrical artifact which occurred throughout all recording sessions. Multi-unit firing rates were computed from each channel's broadband signals in 50ms bins without spike sorting (Christie et al., 2015; Dai et al., 2019), with a threshold of -3.5 times the noise RMS of the continuous signal voltage. These firing rates were aligned within each trial to the ICMS and visual stimuli presented. Firing rates were normalized within each run and each channel by calculating the mean baseline firing rate across the entire 2s ITI period, and dividing all firing rates in the session by this value.

#### *5.2.4.2 Gaussian curve fitting*

The percentages of trials where the participant reported simultaneous ICMS and visual percepts were fit to Gaussian curves (**Figure 5.3b,c**). Gaussians were fit to the raw percentages reported in **Figure 5.3a**, using MATLAB's *fit* function, and restricted to peaks bounded by [0, 100] since the physical limits of simultaneous reports are 0% and 100%. A parametric bootstrap with 1000 iterations was used to assess variance (Christie et al., 2022). In the bootstrap, a binomial distribution $B(n,p)$ was fit

to the raw data at every time point, in which *n*=the number of trials at that time point and *p*=the percentage of trials that were reported as simultaneous. On every iteration of the bootstrap, these binomial distributions were sampled using MATLAB's *binornd* function and Gaussian curves were fit to the resulting synthetic data. 95% confidence intervals on the Gaussians and their peaks were computed by examining the distribution of Gaussians generated over the bootstrap.

The point of subjective simultaneity was taken as the peak of the fitted Gaussians. The just-noticeable difference (JND) was taken as average of the absolute value of the times when the fitted Gaussians crossed the 25% line on either side of the peak.

A Gaussian model was chosen for its simplicity, given that only 5 temporal offsets were sampled in the data (-300, -150, 0, 150, 300ms). A more complex model runs the risk of overfitting to the data, and would require a larger number of time samples to better characterize the shape of the temporal binding window.

*5.2.4.3 Tuning analysis*

The tuning of multi-unit activity in each visual condition was assessed using the catch trials (n=36) collected during the realistic and abstract conditions, in which the visual cue was presented and the participant expected an ICMS-elicited sensation, but no ICMS was delivered. Tuning was computed via linear regression analysis in 250ms bins. In each time bin, normalized firing rates were compared to baseline firing rates, which were computed as the mean firing rates in the ITI, 1750ms to 75ms before the onset of the "stimulation" phase (**Figure 5.1b**). Data for each channel was fit to a linear regression model based on this equation:

$$F = \beta_0 + \beta_1 X_1 + \beta_2 X_2 + \cdots \beta_C X_C$$

where $F$ = vector of firing rates on each trial, $X$ = one-hot-encoded matrix of time bin identity for each trial, $\beta$ = estimated regression coefficients indicating level of tuning in each time bin, and $C$ = number of time bins tested. $F$ also included 36 additional entries corresponding to $\beta_0$ (to match the total number of catch trials tested), which contained the baseline firing rate calculated as indicated above. The null hypothesis $\beta = 0$ was assessed using a student's t test within each channel and time bin, and if the null hypothesis was rejected then the channel was determined to be tuned to the visual information in comparison to the baseline firing rate. Within each channel, P values were corrected for multiple comparisons across time bins using the Bonferroni-Holm method.

To assess significant differences in numbers of tuned channels across time bins and conditions, a bootstrap analysis was run for 1000 iterations. In each iteration, the catch trials were randomly sampled with replacement to yield 36 trials which were then reassessed for tuning in each channel and time bin (**Figure 5.4a**).

*5.2.4.4 RSA and MDS*

Normalized firing rate data, binned in 0.5s phases, was examined using Representational Similarity Analysis (RSA, **Figure 5.4d**) (Kriegeskorte, 2008; Nili et al., 2014). The python package *rsatoolbox* (https://github.com/rsagroup/rsatoolbox) was used to compute representational dissimilarity matrices (RDMs). The measure of dissimilarity used was cross-validated Mahalanobis distance with multivariate noise normalization (Walther et al., 2016), in which the noise covariance matrix is estimated and regularized towards a diagonal matrix to ensure that it is invertible. The cross-validated Mahalanobis distance is an unbiased measure of square Mahalanobis distance which also has a meaningful zero-point (Diedrichsen et al., 2021; Walther et al., 2016). A distance of zero between two conditions indicates the underlying neural data is fully indiscriminable, and the larger the Mahalanobis distance, the more these neural patterns are discriminable.

Data was cross-validated across 9 splits, each containing the 4 catch trials collected per run for each condition and divided into 0.5s bins ('ITI,' 'Down,' 'Touch,' 'Up'). 'ITI' was composed of the last 0.5s of the ITI before the 'Down' phase began. The RDM generated from this data is symmetric across the diagonal, with meaningless zeros on the diagonal itself (**Figure 5.4d**).

To better visualize the relationships in the RDM, multi-dimensional scaling (MDS) was applied using the MATLAB toolbox *rsatoolbox* (**Figure 5.4e**, https://github.com/rsagroup/rsatoolbox_matlab)(Nili et al., 2014). MDS allows for distances in RDMs to be mapped to the 2D plane as faithfully as possible, using a metric stress criterion to arrange points without any assumptions of category structure. The stress between points is visualized with grey lines between points, stretched like rubber bands – the thinner the band, the more the true distances between points should be closer together to be fully accurate to the original high dimensional RDM.

### 5.3 Results

To understand the relationship between ICMS and visual context, behavioral and neural responses were recorded from a human tetraplegic patient (n=1) implanted with microelectrode arrays in S1 (**Figure 5.1a**) (Blackrock Neurotech, Salt Lake City, Utah) as ICMS was delivered. Experimental sessions were composed of three conditions: the baseline, a realistic condition, and an abstract condition (**Figure 5.1b, c**). During the baseline, the participant reported when a sensation was elicited, that sensation's anatomical location and intensity, and a one-word descriptor for the sensation's qualitative nature. During the main task, the participant reported the same information, but also was tasked with reporting the relative order of ICMS and a visual cue which either depicted an abstract or realistic touch (**Figure 5.1c**, **Supplemental Video 5.1**, **Supplemental Video 5.2**). The visual cues were delivered at varying offsets relative to ICMS (-300, -150, 0, 150, 300ms). In all conditions, the participant only reported sensations localized to the right arm, between the wrist and the shoulder.

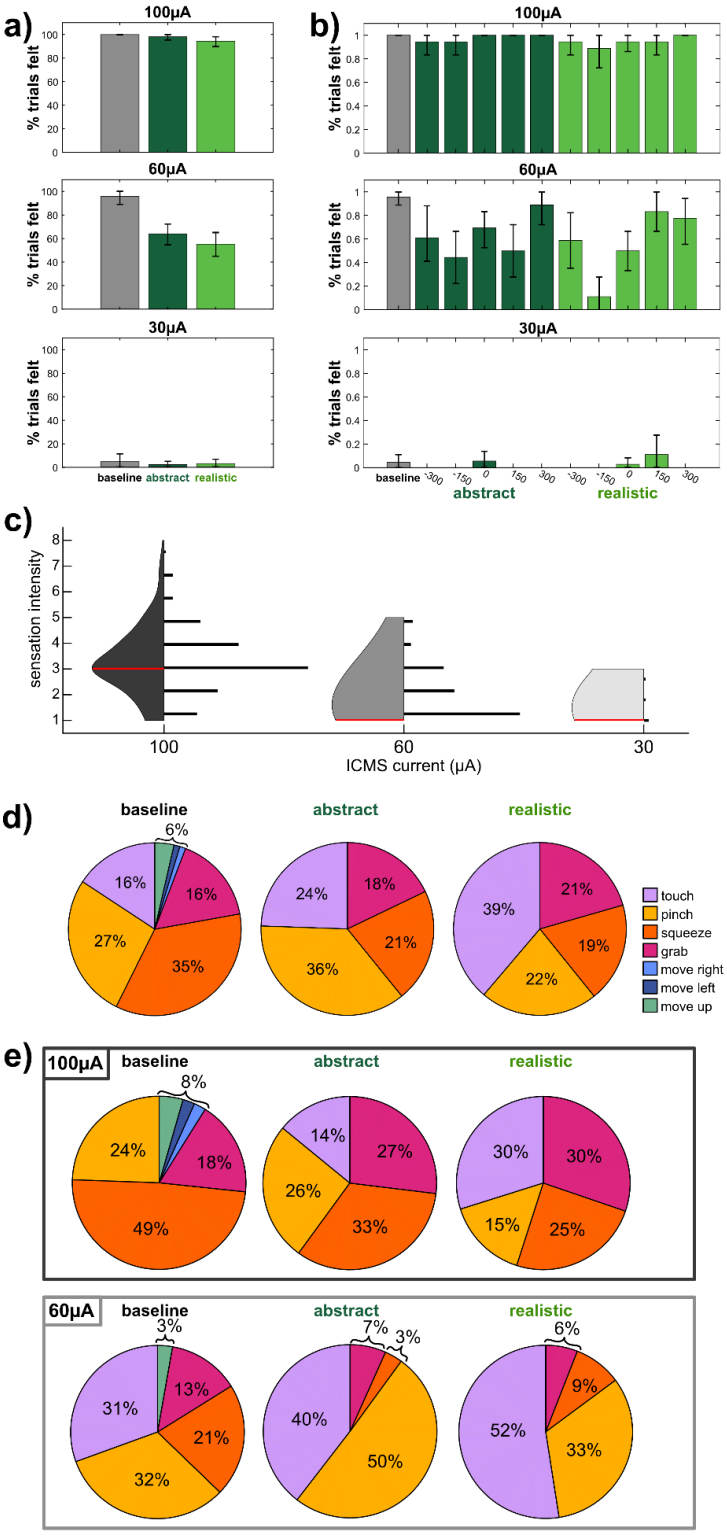


**Figure 5.2 ICMS-elicited tactile percepts**
**a)** Percentage of trials eliciting a sensation across conditions, sorted by ICMS current. Error bars represent bootstrapped values across 1000 iterations sampling from trials with replacement. **b)** Data and analysis identical to **(a)** except abstract and realistic trials are separated by timing offsets between the visual stimulus and ICMS. A negative timing offset indicates the visual stimulus preceded ICMS. **c)** Violin plot and histogram of reported sensation intensity separated by ICMS current and combined across abstract and realistic trials. Red line = median value. Histograms are to scale with the number of trials (n for 100µA = 83, 60µA = 67, 30µA =3 trials). **d)** Pie charts of sensation descriptors by condition. Only one word was used to describe each sensation. (baseline n=90, abstract n=177, realistic n=164 trials). **e)** Data and analysis identical to **(d)** except analysis is separated by ICMS current. Top = 100µA (baseline n=45, abstract n=106, realistic n=102 trials). Bottom = 60µA (baseline n=43, abstract n=69, realistic n=59 trials).

Throughout all runs, catch trials in which no ICMS was delivered were pseudo-randomly intermixed. Behavioral accuracy was computed by comparing the participant's assessments of relative ICMS and visual stimulus order with the ground truth. There was no learning effect: accuracy did not meaningfully change over the different session days (**Figure**

**5.1d**, F-test vs constant model, p=0.58). Additionally, behavioral performance was unaffected by visual condition (**Figure 5.1d**, logistic regression test p=0.34), indicating the conditions were equivalent in terms of difficulty. Performance was also not affected by the current amplitude (**Supplemental Figure 5.1**, p=0.72), but was affected by the relative offsets of the visual and ICMS (p=0.005). An effect of timing is unsurprising as the larger timing offsets (-300, 300ms) are easier to detect than the shorter ones (-150, 150ms).

### *5.3.1 ICMS-elicited tactile sensations*

On each trial, the participant reported whether or not he sensed a tactile percept. Three different ICMS current amplitudes were tested (100, 60, 30μA), and catch trials were also collected where no ICMS was delivered. The participant never reported a sensation in a catch trial. There was a strong effect of ICMS current amplitude on the probability of the participant reporting a percept on a trial in the baseline trials (logistic regression test, $p=1.1x10^{-33}$) as well as in both visual conditions of the main task (logistic regression test, $p=3.2x10^{-33}$, **Figure 5.2a**). At 100μA, sensation detection was essentially at ceiling in all conditions (baseline mean=100%, 95%CI=[100,100]; abstract mean=98.2%, [95.4,100]; realistic mean=94.4%, [89.8,98.2]). At 30μA, sensation detection was at floor in all conditions (baseline mean=4.4%%, 95%CI=[0,11.1]; abstract mean=1.2%, [0, 6.5]; realistic mean=2.8%, [0,4.6]).

In 60μA ICMS trials, in contrast, an effect of condition on the probability of reporting a sensation was evident (**Figure 5.2a**, baseline mean=95.6%, 95%CI=[88.9,100]; abstract mean=63.9%, [54.6, 72.2]; realistic mean=55.1%, [44.9,65.0]). The probability of a trial yielding a sensation was not different between realistic and abstract conditions (logistic regression test, p=0.12), but the baseline elicited more sensations than either the realistic or abstract conditions. Within 60μA ICMS realistic and abstract trials, there was also an effect of the varying ICMS/visual temporal offsets (logistic

regression test, p=5. $5x10^{-4}$, **Figure 5.2b**). In particular, rates of reported sensations were low in the realistic condition when vision preceded ICMS by 150ms (mean=11.1%, [0, 28.0]).

When the participant reported a sensation, he also reported the intensity of the sensation using a subjective number scale (**Figure 5.2c**) and a single word descriptor about how the sensation felt (**Figure 5.2d,e**). Within realistic and abstract trials, there was no effect of condition or stimulus timing on intensity ratings, but there was an effect of ICMS current amplitude (3-way ANOVA, condition p=0.69, timing p =0.49, current p = $1.5x10^{-17}$, all interaction effects p>0.05). Comparing 100µA and 60µA specifically, the greater amplitude led to greater intensity ratings (unpaired t-test, p=$1.2x10^{-21}$).

The single words used by the participant were generated entirely by him with no suggested vocabulary. Across the 9 experimental sessions, the word "touch" was used to describe the sensation in realistic trials a higher proportion of the time than in the baseline (**Figure 5.2d**, Wilcoxon rank sum test, p=0.016), but the difference between abstract and baseline uses of "touch" was insignificant (p=0.13). This trend remained true when examining only 100µA trials (**Figure 5.2e**, realistic vs baseline p=$8x10^{-4}$, abstract vs baseline p=0.24) but not within 60µA trials (**Figure 5.2e**, realistic vs baseline p=0.21, abstract vs baseline p=0.21). Additionally, the word "touch" was used more in 60µA trials than 100µA trials, across all conditions (p=0.014).

### *5.3.2 The temporal binding window between vision and ICMS*

In every trial of the realistic and abstract conditions that the participant reported an ICMS-elicited sensation, he also reported the perceived order of the ICMS and visual cue. Specifically, he was instructed to report when the "visual touch" occurred relative to the ICMS (**Figure 5.1b**), and could either state that one stimulus came before the other or that they occurred simultaneously (**Figure 5.3a**). In both conditions, the participant was able to detect the correct order in the -300 and 300ms offset trials with near perfect accuracy. In the -150, 150ms and 0ms offset trials, answers had more

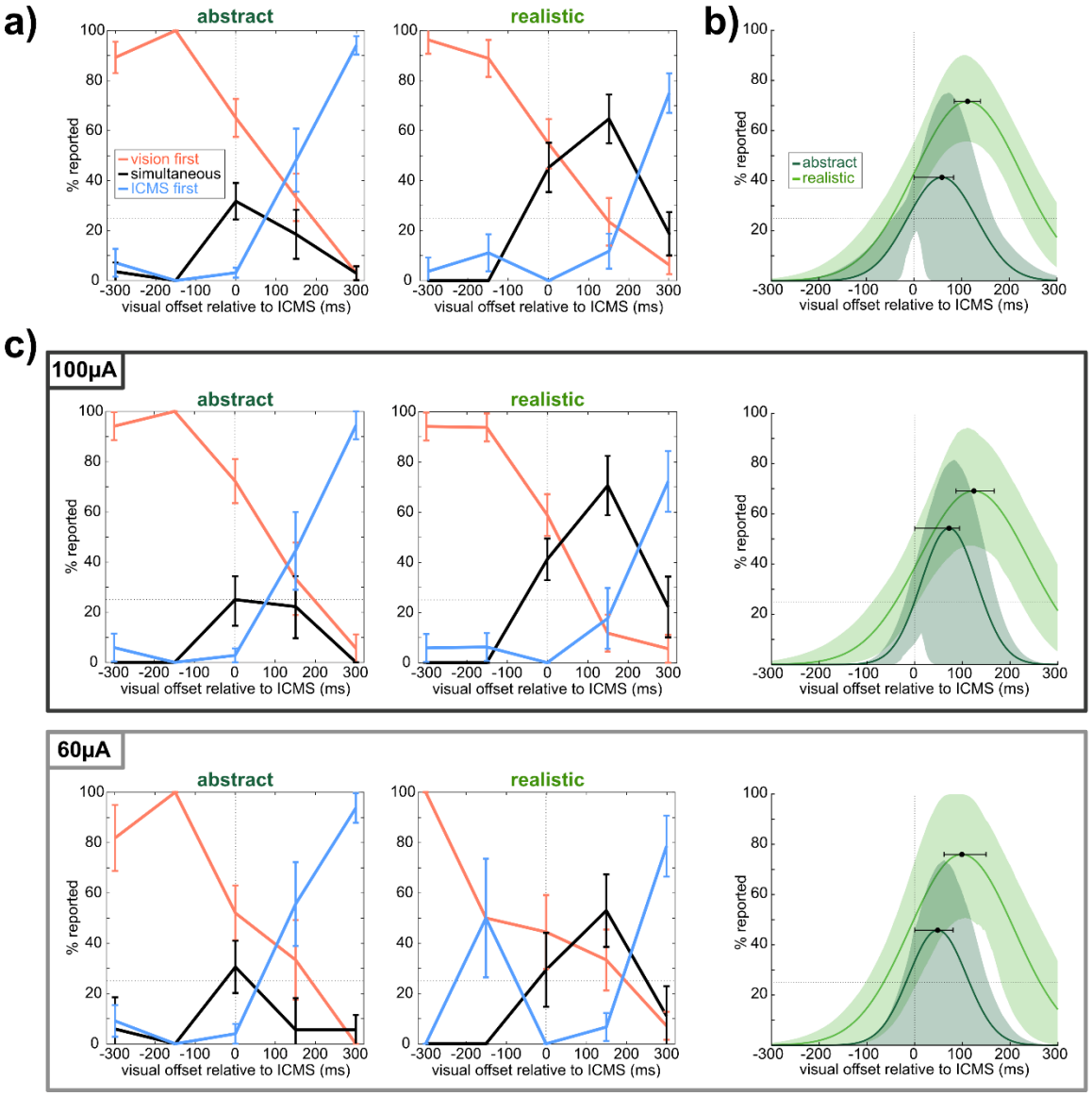


**Figure 5.3 The temporal binding window between vision and ICMS**
**a)** Reports of stimulus order relative to the ground truth. A negative timing offset indicates the visual stimulus preceded ICMS. Horizontal dotted line indicates 25% mark. Error bars represent SEM. **b)** Gaussian curves fit to the "simultaneous" points (black lines) in **(a)**. Black dots indicate curve peaks. Shaded area and error bars on peaks represent 95% CIs generated through a parametric bootstrap fit to 1000 synthetic versions of the data modeled with a binomial distribution (see Methods). **c)** Data and analysis identical to **(a)** and **(b)** except results are separated by ICMS current.

variability and were more likely to be "simultaneous" than in the -300 and 300ms offset trials. Across sessions, rates of "simultaneous" answers in the 150ms offset were higher in the realistic than the abstract condition (paired t-test, p=0.001), but not different across visual conditions in the other

offsets ($p>0.1$ for all tests). The area under the "simultaneous" curves was different between realistic and abstract trials (paired t-test, $p=3.6x10^{-4}$).

To better quantify when stimuli were perceived as occurring synchronously, the "simultaneous" curves (**Figure 5.3a**) were fit to Gaussians which allowed for interpolation between the 5 offsets tested (**Figure 5.3b**). The variability in the data was assessed using a parametric bootstrap (see Methods)(Christie et al., 2022). The point of subjective simultaneity (PSS), defined as the peak of the fitted Gaussians, occurred when ICMS preceded the visual cue for both visual conditions (abstract=58.6ms, 95% CI = [$6x10^{-42}$, 83.4]; realistic=112.5ms [84.7, 139.4]). The just-noticeable difference (JND) in realistic trials (161.7ms [124.8, 190.1]) was larger than in abstract trials (72.5ms [17.8, 101.5]). The 25% point on the left side of the Gaussian was not different between realistic (-49.1ms [-91.1, -14.2]) and abstract (-13.9ms [-47.1, 21.5]) conditions. The 25% point on the right side was not the same across conditions: the realistic condition (274ms [204.7, 326.1]) had a larger offset than the abstract condition (131.1ms [-151.6 190.9]).

The temporal analysis was repeated, separating out trials into 100µA and 60µA ICMS (**Figure 5.3c**). Within the raw data for each ICMS current amplitude, the areas under the "simultaneous" curves were different between realistic and abstract conditions (100µA: $p=6x10^{-4}$; 60µA: $p=0.012$). The PSS for each ICMS current amplitude followed the same pattern as the overall data but the differences between conditions were lessened: for 100µA, realistic PSS = 124.2ms [87.0 166.8]; abstract PSS = 72.3ms [$8x10^{-27}$, 94.2ms]. For 60µA, realistic PSS = 98.8ms [61.5 149.5]; abstract PSS = 48.2ms [0, 80.3ms]. The JND for 100µA was 164.0ms [87.6, 167.2] in realistic trials and 72.4ms [29.4, 90.5] in abstract trials; the JND for 60µA was 164.0ms [114.2, 202.2] in realistic trials and 66.6ms [11.0, 92.2] in abstract trials.

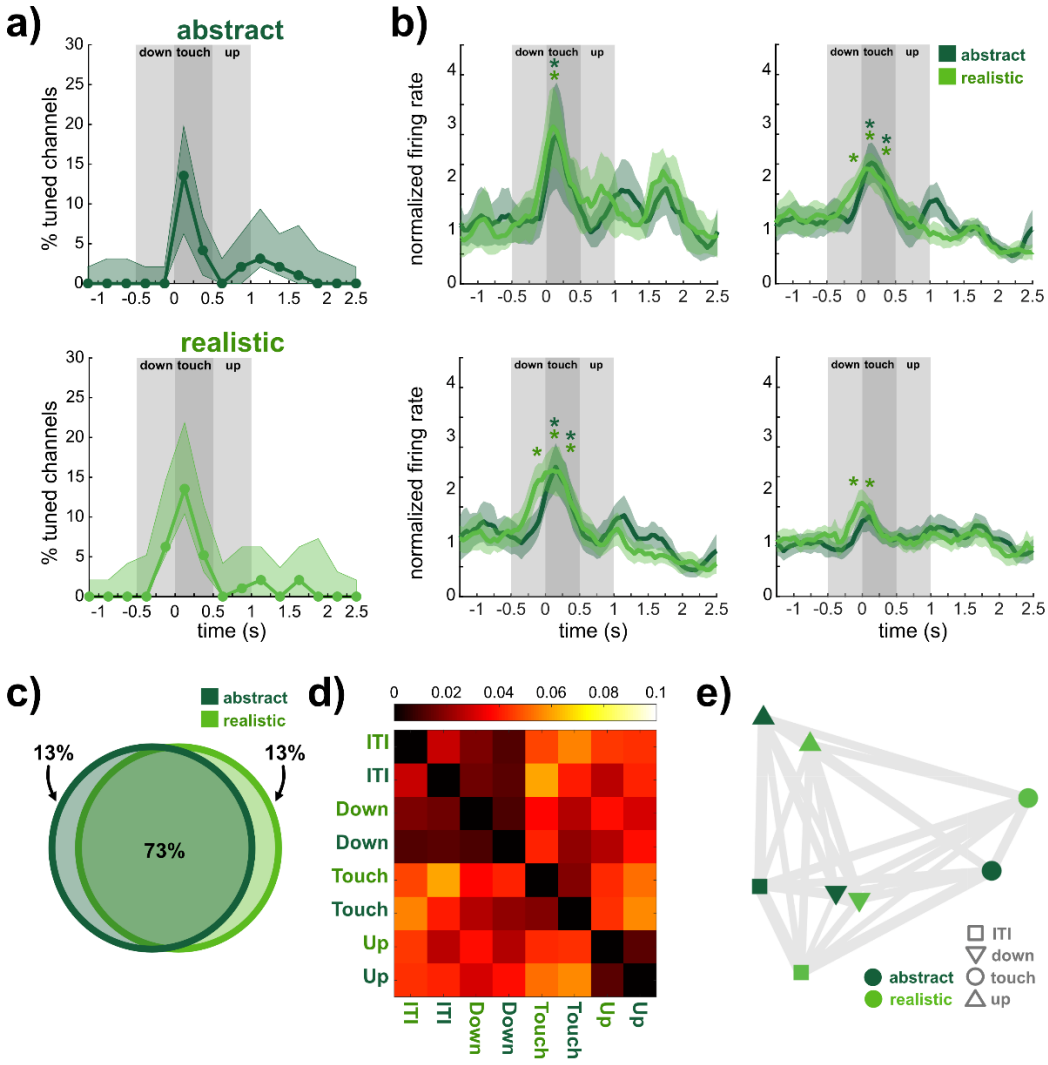


**Figure 5.4 Neural activity during catch trials**
**a)** Percentage of channels tuned during catch trials relative to baseline (n=96 channels), separated by condition. Time is aligned to the onset of the "touch" phase of the visual stimulus. Shaded area indicates 95% CIs computed by bootstrapping across trials (n=36 trials) over 1000 iterations. Tuning was assessed by linear regression analysis (see Methods). **b)** Four example tuned channels with firing rates averaged across catch trials, by condition. For visualization only, firing rates were smoothed using a first order Savitzky-Golay filter. Asterisks indicate the 250ms bins in which the channels were tuned relative to baseline, color-coded by condition. Shaded area corresponds to SEM (n=36 trials per condition). **c)** Venn diagram depicting the overlap in channels tuned to abstract and realistic conditions. Percentages are based on the total number of channels tuned overall (15 channels; 15.6% of all S1 channels). **d)** Representational dissimilarity matrix (RDM) of multi-unit neural activity across all channels. Heatmap indicates distances between neural activity patterns associated with each condition and task phase (e.g.. realistic ITI in top left), which are computed as the cross-validated Mahalanobis distance with multivariate noise correction; a distance of 0 indicated conditions are statistically indistinguishable. Each phase represents 0.5s of averaged firing rates; the ITI is based on the 0.5s immediately prior to "down" phase of visual stimulus. **e)** Multi-dimensional scaling (MDS) plot of the RDM in **(d)**. Axes are arbitrary. Grey lines between icons are "rubber bands" whose thickness is based on the goodness of fit of the scaling (Pearson's r=0.92; $p=2.6x10^{-10}$). Thinner, more "stretched" bands indicate that the icons are closer together in the original high-dimensional space than they are shown to be.

### *5.3.3 S1 neural responses to visual stimuli*

Neural activity was recorded in the S1 microelectrode arrays during catch trials, when no ICMS was delivered, and multi-unit channel firing rates were computed. The tuning of channels relative to baseline while visual stimuli were delivered was assessed using a linear regression analysis (**Figure 5.4a, b**). Both abstract and realistic conditions had a peak of tuned channels in the 0 to 0.25s bin immediately following the "visual touch" phase onset. In this bin, 13.5% (95% CI = [6.3, 19.8]) of channels (n=96) were tuned to the abstract condition and 13.5% [10.4, 21.9] were tuned to the realistic condition. In the realistic condition, 6.3% [5.2, 14.6] of channels were also tuned in the -0.25 to 0s bin prior to visual touch, during the "motion down" phase. The timecourse of four example tuned channels are shown in **Figure 5.4b**. The overlap in channels tuned to realistic and abstract conditions during the 0 to 0.25s bin was quantified (**Figure 5.4c**). 73% of tuned channels (n=11) were tuned to both conditions, while 13% (n=2) were tuned only to realistic and a further 13% (n=2) were tuned only to abstract.

To understand the population response in S1 to the visual stimuli, Representational Similarity Analysis (RSA) was employed on the firing rates of all 96 channels (**Figure 5.4d**) (Kriegeskorte, 2008), using cross-validated Mahalanobis distance with multivariate noise correction (Walther et al., 2016). Multi-dimensional scaling (MDS) was used to visualize the computed distances between condition phases (**Figure 5.4e**) (Nili et al., 2014). The data were grouped more tightly by task phase (ITI, down, touch, up) than by condition (abstract, realistic), as assessed by an unpaired t-test on distances within phases/across conditions vs distances within conditions/across phases ($p=0.044$). Qualitatively, this is apparent in the MDS where icons are grouped by phase, but the conditions are intermixed together (**Figure 5.4e**).

## 5.4 Discussion

Behavioral and neural data from a tetraplegic participant receiving ICMS in S1 (**Figure 5.1a**) while observing visual abstract or realistic touch cues (**Figure 5.1b,c**) were examined. Visual cues were delivered at varying temporal offsets relative to ICMS and the participant reported the perceived order of these cues as well as descriptive information about the ICMS-elicited tactile sensation. Across the 9 experimental sessions, there was no change in the participant's ability to accurately assess stimulus order, and the task was also controlled for difficulty across visual conditions (**Figure 5.1d**) and current amplitudes (**Supplemental Figure 5.1**). ICMS only elicited sensations in the participant's arm through all conditions tested, corroborating the idea that the arrays are implanted in the arm region of S1 area 1 (Armenta Salas et al., 2018; Rosenthal et al., 2023).

This experiment yielded three main findings: 1) the perception of ICMS-elicited sensations is influenced by visual information and ICMS current amplitude; 2) the temporal binding window between ICMS and vision varies based on the biological relevance of the visual stimuli; 3) S1 represents visual information relevant to ICMS in a context-independent fashion.

### *5.4.1 ICMS-elicited sensations are affected by visual information and ICMS current amplitude*

This work replicates the previously known result that higher ICMS current amplitudes tend to elicit sensations more frequently, and the sensations tend to be of higher intensity (**Figure 5.2a,c**) (Armenta Salas et al., 2018; Flesher et al., 2016; Hughes et al., 2021a). However, we also find an interaction between current amplitude and vision. During 60µA trials, the percentage of trials which elicited a sensation through ICMS were significantly higher in the baseline than in either of the visual conditions (**Figure 5.2a**). Since 60µA ICMS is typically perceived to be lower intensity than 100µA ICMS (**Figure 5.2c**), it is closer to the perceptual detection threshold. The added cognitive load of

attending to a visual stimulus as well as attending to ICMS may be responsible for lower rates of reported sensations.

The effect of vision on rates of reported sensations was not uniform across all temporal offsets presented (**Figure 5.2b**). While the nature of the interaction between ICMS and the timing of visual cues will need further investigation, it is possible that the very low reported rates of sensation in the realistic 60µA -150ms offset bin is due to a forward masking effect. In other words, it may be that the movement of the visual stimulus in the "down" phase occupied sufficient attentional resources to mask the majority of ICMS percepts that would otherwise have been elicited.

We also demonstrate an effect of ICMS current on the qualia of sensations: "touch" was used as a descriptor more often at 60µA than at 100µA (**Figure 5.2e**). This may be because, within the participant's subjective framework, the word "touch" could represent a tactile stimulus that is inherently of a lower intensity than other descriptors like "squeeze" or "grab."

Furthermore, the qualitative nature of ICMS-elicited sensations was affected by visual content. The participant was more likely to use the word "touch" to describe sensations in the realistic condition than in the baseline (**Figure 5.2d**). Of the words the participant used to describe sensations, which were freely chosen by him, "touch" appears to be the one which most closely matches the visual touch depicted in the realistic condition. This effect is the first evidence to our knowledge that visual information can bias the qualitative experience of ICMS sensations, although previous work has shown that visual information can bias the perceived location of peripheral intraneural stimulation (Christie et al., 2019a). When ICMS is employed on the same electrode, with the same parameters, in the same participant, widely varying qualia often result (**Figure 5.2d**, baseline) (Armenta Salas et al., 2018; Flesher et al., 2016). A viable neural prosthetic would ideally be able to elicit naturalistic sensations of specific qualia as needed (Tabot et al., 2015). If visual information can stabilize ICMS

percepts to some extent, this has the potential to be highly important to the development of a such tactile neural prosthetic.

In addition to the significantly increased rate of "touch" descriptions between baseline and realistic trials, there was also a smaller increase between baseline and abstract. Although this increase failed to reach statistical significance, it may be present due to a priming effect. Realistic and abstract conditions were tested in the same experimental session, consecutively with one another, so the participant may have noticed the similarities between the two and extended tactile associations from the realistic condition to the abstract one, whether consciously or unconsciously.

### *5.4.2 The biological relevance of visual stimuli influences the temporal binding window*

Visual stimuli were presented at five different temporal offsets relative to ICMS (**Figure 5.3**). In both the realistic and abstract condition, the PSS occurred when ICMS preceded the visual cue, with a lag of approximately 50-120ms (**Figure 5.3b**). This result supplements work which has showed that reaction times are slower for ICMS than for visual or tactile stimuli (Christie et al., 2022; Godlove et al., 2014). ECoG stimulation has also been shown to be slower than tactile stimuli (Caldwell et al., 2019).

The slower processing time for ICMS relative to vision may seem counterintuitive because ICMS directly interfaces with S1 while the visual information must travel through the photoreceptors in the eyes and the thalamus before reaching the primary visual cortex. However, ICMS is a highly unnatural input, and typically during a tactile stimulus an entire network of brain regions is activated, rather than just S1. The larger reaction times may be due to the processing time needed to make sense of this irregular activation pattern (Godlove et al., 2014). Regardless, the perceptual lag between vision and ICMS indicates that the parameters used here, which are standard in the field, do not allow ICMS to be perfectly integrated into a temporally well-aligned multisensory experience.

Although the PSS was offset in both visual conditions tested, the temporal binding window varied in shape between these conditions (**Figure 5.3b**). Both the area under the curve of "simultaneous" answers and the JND were larger in realistic trials compared to abstract trials, indicating the temporal binding window between ICMS and vision is larger in the realistic condition. In other words, the participant was more likely to perceive ICMS and vision as occurring synchronously in the realistic condition, and more likely to assign an order to the stimuli in the abstract condition. This difference was not symmetric: the "simultaneous" curves were highly similar across conditions on the left side (vision preceding ICMS) but on the right (ICMS preceding vision) the realistic curve extended past the abstract curve. These changes remained relatively constant across ICMS current amplitudes (**Figure 5.3c**).

These results indicate that a biologically relevant touch input allows the brain to more easily link visual and ICMS inputs together causally, and view them as happening as part of the same event, while in an abstract context, visual and ICMS inputs are interpreted as more likely to be part of separate events. Since a somatosensory neural prosthetic using ICMS would be deployed in a real world environment, this result is encouraging because it supports the idea that the brain is able to combine multisensory realistic inputs with artificial stimulation to generate visually plausible sensations (Christie et al., 2019a).

### *5.4.3 S1 represents ICMS-relevant visual content in a context-independent fashion*

Examining catch trials which contained only visual stimuli without ICMS, we find that a significant percentage of channels are tuned to visual touches relative to baseline activity (**Figure 5.4a**). In particular, S1 activity peaks during the first 250ms of the visual touch during both abstract and realistic trials. Given that up to 12.5% of channels in S1 were tuned to the realistic condition, it is clear that S1 reflects some component of the visual stimulus even when there is no ICMS or physical

tactile event. Realistic trials also elicited tuned activity 250ms before visual touch, during the "motion down" period, indicating possible preparatory or predictive activity (Kimura, 2021).

Furthermore, there was overlap between S1 responses to abstract and realistic trials. Many of the channels tuned to the realistic condition were also tuned to the abstract condition (**Figure 5.4c**). In a population-level analysis, RSA demonstrated that neural activity was relatively similar between abstract and realistic trials, but separated out by task phase (**Figure 5.4d, e**). These results indicate that S1 represents information within the visual stimulus, and furthermore that this information generalizes across abstract and realistic conditions to some degree. Given that abstract and realistic stimuli are very visually distinct (**Figure 5.1c, Supplemental Video 5.1**, **Supplemental Video 5.2**), this means that it is unlikely S1 is representing the actual visual inputs themselves. Rather, S1 is representing some aspect of the visual information that is relevant to the tactile aspect of the task and which generalizes across the two visual contexts in order to differentiate baseline and visual touch activity.

Prior work with the same participant tested in this study showed that S1 did not respond to visually depicted touches without a physical tactile stimulus accompanying them (Rosenthal et al., 2023). In contrast, this study shows that S1 does reflect information in visual stimuli without any tactile stimuli or ICMS. This difference in results supports a hypothesis which suggests that task design has a large effect on whether S1 represents visual information related to touch (Dionne et al., 2013; Rosenthal et al., 2023). The first study used a passive design, in which the participant merely observed tactile stimuli, whereas this study implemented a more active task in which the participant was required to describe perceived tactile sensations and report the order of ICMS and visual stimuli. This effect of task design on S1 modulation by visual stimuli can also be seen in the neuroimaging literature. Experiments with an active task tend to find that S1 responds to observed touches (Blakemore et al.,

2005; Bufalari et al., 2007; Ebisch et al., 2008; Kuehn et al., 2018, 2013; Longo et al., 2011; Schaefer et al., 2009), while experiments with a passive task, or a task that is not touch-related, tend to find the opposite (Chan and Baker, 2015; Keysers et al., 2004; Morrison et al., 2004). Visual information not related to the tactile stimulation also does not modulate somatosensory cortex (Espenhahn et al., 2020).

Given that S1 can reflect visual stimuli based on task relevance, it is likely that attention plays some role in what S1 represents in a given context (Chapman and Meftah, 2005; Dionne et al., 2013; Popovich and Staines, 2014). Such attentional modulation may also underlie the visual enhancement of touch, a phenomenon in which tactile perception is improved when the body part being touched is visible, even if the visual input is non-informative about the touch (Colino et al., 2017; Haggard et al., 2007; Kennett et al., 2001; Press et al., 2004; Tipper et al., 2001). It may also play a role in S1's ability to reflect top-down concepts like affective significance, motor planning, and imagined touches (Ariani et al., 2022, 2022; Bashford et al., 2021; Gale et al., 2021; Yoo et al., 2003). This attentional effect is likely implemented by higher order brain areas which represent the task requirements and compute a relevance threshold for different sensory inputs which can then be implemented in modality specific early processing areas like S1.

Finally, the fact that the results in this work are consistent with other characterizations of S1 in tactile studies indicates that S1 processes visual stimuli related to ICMS in some similar ways to visual stimuli related to real physical touches. This suggests that ICMS is can be a valid substitute for physical touches in tactile tasks, not only in terms of behavioral performance (Berg et al., 2013; Klaes et al., 2014; Tabot et al., 2015), but also in terms of how the stimulation is processed within the somatosensory system.

### *5.4.4 Conclusion*

In order to understand the behavioral and neural relationship between ICMS and vision, we examined responses to paired visual and ICMS stimuli at varying temporal offsets in a tetraplegic patient. This dataset yielded two behavioral findings. The first is that the interpretation of ICMS-elicited sensations is affected by ICMS current amplitude, as well as by visual content. The second is that the temporal binding window between ICMS and vision peaks when ICMS is delivered shortly before the onset of the visual stimulus, and that the size of the temporal binding window is affected by the biological relevance of the visual stimulus. Studies of ICMS frequently examine elicited sensations without including any other type of sensory context (Armenta Salas et al., 2018; Flesher et al., 2016; Hughes et al., 2022, 2021a). While these studies represent important foundational work, it will be important to fully understand how ICMS interacts with a richly complex sensory environment, both for the purpose of stabilizing touch percepts and creating temporally aligned, unified multisensory experiences.

By examining the neural encoding of catch trials in which visual touches were present without ICMS, this work also adds to our understanding of how S1 represents visual information related to tactile sensations. We find that in an active task, S1 firing rates change during a visual touch relative to baseline, in a relatively constant way across visual contexts. This finding supports the idea that high level task-related variables in visual stimuli are represented in S1 and modulated by higher order cognitive brain areas based on attention.

Further experiments should aim to investigate these findings in a larger population of patients, to better understand individual differences. Additionally, it will be important to explore in more depth how ICMS is integrated with other sensory systems and with different environmental contexts, as well as how S1 processes these inputs. By understanding multisensory ICMS integration both

behaviorally and neurally, we can better use ICMS to design stable, naturalistic artificial tactile sensations.

### *5.4.5 Limitations of the study*

While this experiment adds to our understanding of how vision is integrated with ICMS, it is limited in scope. A limited set of ICMS parameters was examined, in only one participant, so it is possible results will be different to some extent using other parameters and in other individuals. Additionally, only five temporal offsets were examined, leading to a relatively coarse resolution of the temporal binding window. Examining a larger set of time points could refine the results and allow for a more complex modeling of the temporal binding window beyond using Gaussian curves. Finally, it is possible that demand characteristics of the task influenced the participant's description of sensation qualia, although we note that the participant never reported a sensation in a catch trial, and reported significantly fewer sensations at lower current amplitudes, despite never being informed of the current amplitude being delivered on any given trial.

## 5.5 Supplemental figure

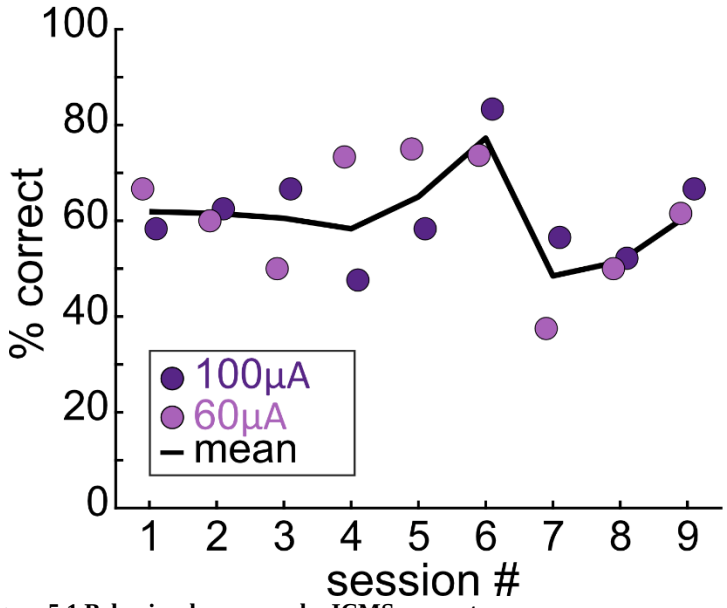


**Supplemental Figure 5.1 Behavioral accuracy by ICMS current**
Accuracy averaged across visual conditions across experimental sessions, quantified as the percentage of the trials where the participant reported a sensation, in which the participant's reported order of stimuli (either vision first, ICMS first, or simultaneous) matched the presented stimulus order. The average number of trials felt per session was 11.6 (std=0.86) for 100µA and 7.1 (std=2.3) for 60µA trials. Black line = mean across all trials per session.

## 5.6 Supplemental video legends

**Supplemental Video 5.1 Sample abstract visual stimulus**
Related to **Figure 5.1c**. Stimulus was presented using a virtual reality headset. The virtual reality environment was constructed to mimic the room in which the experiment was performed.

**Supplemental Video 5.2 Sample realistic visual stimulus**
Related to **Figure 5.1c**. Stimulus was presented using a virtual reality headset. The virtual reality environment was constructed to mimic the room in which the experiment was performed, and the human arm was chosen to be visually similar to the participant's own arm.

# *Chapter 6*

# CONCLUSION

In this thesis, we explore how the somatosensory system constructs tactile sensations based on a variety of bottom-up and top-down variables, using human behavioral and electrophysiological data. Imagined (**Chapter 3**), real (**Chapter 4**), and artificial (**Chapter 5**) tactile sensations are all considered, each with two goals in mind: building a better understanding of the neuroscientific underpinnings of tactile experiences, and applying this knowledge to implementing somatosensory neural prosthetics.

In particular, S1 is a region of interest in neural prosthetics, as it is a brain region that can both represent real tactile sensations and be used to elicit artificial tactile sensations through ICMS (Armenta Salas et al., 2018; Delhaye et al., 2018; Flesher et al., 2016; Hernandez et al., 2000). All experiments presented in this thesis are conducted with the same microelectrode arrays in the same human tetraplegic participant, allowing for an unprecedented level of detail and nuance to be extracted from a specific sub-region of area 1 of S1.

Building on prior work showing activity in S1 during tactile imagery (Yoo et al., 2003), in **Chapter 3**, we find that imagined sensations can be decoded from one another in S1, SMG, and PMv, which are all part of the sensorimotor loop. These sensations are generated by cueing the participant via a written word, and then after a delay giving a generic "go" signal to begin the tactile imagery. Thus, tactile representations here are the result of top-down modulation, and are shown to be encoded distinctly in both firing rate and LFP data. This result is shown to be stable across data collected 11 months apart, indicating that tactile representations remain highly stereotyped over time.

In **Chapter 4**, real touches that vary in their location and multisensory context are examined, yielding several findings. S1 arm area is shown to encode touches in the arm, as well as finger touches in a more generalized manner. This result adds complexity to the classical notion of the cortical homunculus (Ejaz et al., 2015; Penfield and Boldrey, 1937), supporting the hypothesis that the topographic delineation is not as rigid as previously thought (Muret et al., 2022; Wesselink et al., 2022). Additionally, we find that during a passive task, visual information paired with a physical touch modulates S1 in comparison to a blind touch, but visual information on its own does not trigger any detectable S1 activity. Based on this finding, we advance a hypothesis based on task design that provides a way to reconcile literature which has found varying findings on the ability of S1 to represent visual information (Blakemore et al., 2005; Chan and Baker, 2015; Kuehn et al., 2018, 2013; Sharma et al., 2018).

In **Chapter 5**, we build upon our work using real touches to examine artificial tactile sensations. Most research in ICMS considers it in isolation from other stimuli (Armenta Salas et al., 2018; Flesher et al., 2016; Hughes et al., 2022, 2021a). Our research supplements this literature by examining artificial tactile sensations in a multisensory context. The qualitative interpretation of ICMS is found to be affected by both visual context and the current amplitude of stimulation. Additionally, the temporal binding window between ICMS and vision becomes larger when visual stimuli are more biologically relevant, allowing for more ICMS-elicited sensations to be perceived as temporally synchronous with visual stimuli. Finally, S1 is also shown to reflect the moment of a visual "touch" during catch trials in which ICMS is not delivered, suggesting that in an active touch-relevant task, S1 does represent visual information even in the absence of a physical touch. This encoding of visual information corroborates the task design hypothesis advanced in **Chapter 4**, and appears to be context-independent: S1 activity is highly similar across a realistic and an abstract visual condition.

These results contribute to the neuroscientific literature on how experiences of touch are neurally constructed, especially in the early cortical tactile processing area of S1. We see that S1 encodes many modes of touch, including imagined touches, real physical touches, and visual information relating to touches, all in a small sub-region of area 1. The extent to which S1 represents visual stimuli depends on if the task at hand is active or passive, suggesting a role of attention, and is abstract enough to generalize across conditions which have the same underlying task structure but highly different presented visual stimuli. Furthermore, different locations of touch are present in this area, and the strength and specificity of their encoding vary according to the established S1 topography. Taken together, S1 is shown to be a location with complex representations of tactile information which are modulated by multisensory inputs and top-down cognitive factors such as imagination and attention (Blakemore et al., 2005; Dionne et al., 2013; Fiorio and Haggard, 2005; Kennett et al., 2001; Kimura, 2021; Morrison et al., 2004). Additionally, the visual information that S1 does reflect is abstracted across visual contexts. The influence of these conceptual, top-down variables suggests recurrent connections between S1 and higher order cognitive processing areas capable of multisensory integration, such as PPC or the frontal cortex. In other words, S1 processes tactile information for upstream cortical areas, but is likely receiving feedback from these areas about how to interpret this information as well.

Future neuroscientific experiments should interrogate neural representations in the somatosensory system before and after ICMS is delivered in order to understand which brain areas are capable of representing sensation qualia, or even if a sensation is perceived at all, and the time course of these representations. Additionally, examining the results described above in a larger set of participants, including those with varying levels of somatosensory impairment, will be important to distinguish individual differences from population trends.

These findings also provide information as to how ICMS could be used to implement a viable somatosensory BMI with reliable, naturalistic tactile sensations. Given that imagined sensations are represented in SMG and PMv as well as S1, it is possible that novel sensations could be decoded or elicited from these areas as well. While current human studies demonstrate the potential of electrophysiology and ICMS, novel methods currently being tested exclusively in animal models, such as optogenetics, may be able to provide more nuanced feedback in the distant future (Sahel et al., 2021). More concretely, we also see that visual information and attention modulate S1, and visual context affects the interpretation of ICMS when delivered through S1. Given that visual stimuli can bias ICMS-elicited sensations towards a specific type of percept, it is possible that visual information can be harnessed to better stabilize ICMS percepts more generally. Overall, these results indicate strongly that a multisensory, biomimetic environment must be considered when testing how to elicit specific types of ICMS sensations (Risso and Valle, 2022). If a somatosensory prosthetic is to be implemented in the rich, complex, real world environment, then the effects of different sensory modalities and of attention must be understood in order to generate sensations that feel temporally and qualitatively natural.

To validate these theories, it will be necessary to further explore the relationship between ICMS parameters, perceived sensations, and multisensory environments. The results discussed here examine only a narrow subset of ICMS parameters and only use one channel for stimulation. Examining a larger set of channels, as well as multichannel stimulation, will be necessary to map the full range of potential sensations and their interactions with the environment (Kim et al., 2015b; Sombeck and Miller, 2020). It is possible that a different pattern of stimulation will also yield a different temporal binding window between ICMS and vision. It would also be instructive to try to implement the rubber hand illusion (Botvinick and Cohen, 1998; Tsakiris and Haggard, 2005) using

ICMS, since this illusion traditionally combines vision and touch to manipulate the sense of embodiment. Prior work has shown that artificial embodiment of a prosthetic can be elicited in epilepsy subjects implanted with ECoG grids using the rubber hand illusion (Collins et al., 2017). If ICMS can similarly be used to trigger the illusion in SCI patients, this will mean that it can be used to aid embodiment of a prosthetic device (Maimon-Mor and Makin, 2020; Marasco et al., 2011). An embodied neural prosthetic may have more accurate motor decoding and higher naturalness of use, providing a substantive improvement in quality-of-life for patients (Marasco et al., 2021; Preatoni et al., 2021).

In summary, this thesis explores varying types of tactile sensations across different contexts in order to better understand how sensations of touch are constructed. This work contributes to the neuroscientific literature on the somatosensory system, suggesting that early tactile processing is affected by complex, multisensory, contextual factors. These findings also have clinical applications towards generating artificial sensations in a BMI with naturalistic properties, which would be an invaluable step in providing restorative care for individuals with impaired somatosensation (Anderson, 2004).

# BIBLIOGRAPHY


Aflalo, T., Kellis, S., Klaes, C., Lee, B., Shi, Y., Pejsa, K., Shanfield, K., Hayes-Jackson, S., Aisen, M., Heck, C., Liu, C., Andersen, R.A., 2015. Decoding motor imagery from the posterior parietal cortex of a tetraplegic human. Science 348, 906–910.

Alchalabi, B., Faubert, J., Labbe, D.R., 2019. EEG can be used to measure embodiment when controlling a walking self-avatar. Presented at the 2019 IEEE Conference on Virtual Reality and 3D User Interfaces (VR), IEEE, Osaka, Japan, pp. 776–783. https://doi.org/10.1109/VR.2019.8798263

Andersen, R.A., Buneo, C.A., 2002. Intentional maps in posterior parietal cortex. Annu Rev Neurosci 25, 189–220. https://doi.org/10.1146/annurev.neuro.25.112701.142922

Anderson, K.D., 2004. Targeting recovery: Priorities of the spinal cord-injured population. Journal of Neurotrauma 21, 1371–1383. https://doi.org/10.1089/neu.2004.21.1371

Arbuckle, S.A., Pruszynski, J.A., Diedrichsen, J., 2022. Mapping the integration of sensory information across fingers in human sensorimotor cortex. J. Neurosci. 42, 5173–5185. https://doi.org/10.1523/JNEUROSCI.2152-21.2022

Ariani, G., Pruszynski, J.A., Diedrichsen, J., 2022. Motor planning brings human primary somatosensory cortex into action-specific preparatory states. eLife 11, e69517. https://doi.org/10.7554/eLife.69517

Armenta Salas, M., Bashford, L., Kellis, S., Jafari, M., Jo, H., Kramer, D., Shanfield, K., Pejsa, K., Lee, B., Liu, C.Y., Andersen, R.A., 2018. Proprioceptive and cutaneous sensations in humans elicited by intracortical microstimulation. eLife 7. https://doi.org/10.7554/eLife.32904

Augurelle, A.-S., Smith, A.M., Lejeune, T., Thonnard, J.-L., 2003. Importance of cutaneous feedback in maintaining a secure grip during manipulation of hand-held objects. Journal of Neurophysiology 89, 665–671. https://doi.org/10.1152/jn.00249.2002

Azañón, E., Longo, M.R., Soto-Faraco, S., Haggard, P., 2010. The posterior parietal cortex remaps touch into external space. Current Biology 20, 1304–1309. https://doi.org/10.1016/j.cub.2010.05.063

Baldwin, M.K.L., Cooke, D.F., Goldring, A.B., Krubitzer, L., 2018. Representations of fine digit movements in posterior and anterior parietal cortex revealed using long-train intracortical microstimulation in macaque monkeys. Cerebral Cortex 28, 4244–4263. https://doi.org/10.1093/cercor/bhx279

Baldwin, M.K.L., Cooke, D.F., Krubitzer, L., 2017. Intracortical microstimulation maps of motor, somatosensory, and posterior parietal cortex in tree shrews (tupaia belangeri) reveal complex movement representations. Cereb Cortex 27, 1439–1456. https://doi.org/10.1093/cercor/bhv329

Balslev, D., Cole, J., Miall, R.C., 2007. Proprioception contributes to the sense of agency during visual observation of hand movements: evidence from temporal judgments of action. J Cogn Neurosci 19, 1535–1541. https://doi.org/10.1162/jocn.2007.19.9.1535

Banakou, D., Groten, R., Slater, M., 2013. Illusory ownership of a virtual child body causes overestimation of object sizes and implicit attitude changes. Proceedings of the National Academy of Sciences 110, 12846–12851. https://doi.org/10.1073/pnas.1306779110

Bashford, L., Rosenthal, I., Kellis, S., Pejsa, K., Kramer, D., Lee, B., Liu, C., Andersen, R.A., 2021. The neurophysiological representation of imagined somatosensory percepts in human cortex. J. Neurosci. 41, 2177–2185. https://doi.org/10.1523/JNEUROSCI.2460-20.2021

Baumann, M.A., Fluet, M.-C., Scherberger, H., 2009. Context-specific grasp movement representation in the macaque anterior intraparietal area. J Neurosci 29, 6436–6448. https://doi.org/10.1523/JNEUROSCI.5479-08.2009

Beckerle, P., Kõiva, R., Kirchner, E.A., Bekrater-Bodmann, R., Dosen, S., Christ, O., Abbink, D.A., Castellini, C., Lenggenhager, B., 2018. Feel-good robotics: Requirements on touch for embodiment in assistive robotics. Front. Neurorobot. 12, 84. https://doi.org/10.3389/fnbot.2018.00084

Bekrater-Bodmann, R., Foell, J., Diers, M., Kamping, S., Rance, M., Kirsch, P., Trojan, J., Fuchs, X., Bach, F., Çakmak, H.K., Maaß, H., Flor, H., 2014. The importance of synchrony and temporal order of visual

and tactile input for illusory limb ownership experiences – an fMRI study applying virtual reality. PLoS One 9. https://doi.org/10.1371/journal.pone.0087013

Bensmaia, S.J., Miller, L.E., 2014. Restoring sensorimotor function through intracortical interfaces: Progress and looming challenges. Nat Rev Neurosci 15, 313–325. https://doi.org/10.1038/nrn3724

Berg, J.A., Dammann, III, J.F., Tenore, F.V., Tabot, G.A., Boback, J.L., Manfredi, L.R., Peterson, M.L., Katyal, K.D., Johannes, M.S., Makhlin, A., Wilcox, R., Franklin, R.K., Vogelstein, R.J., Hatsopoulos, N.G., Bensmaia, S.J., 2013. Behavioral demonstration of a somatosensory neuroprosthesis. IEEE Trans. Neural Syst. Rehabil. Eng. 21, 500–507. https://doi.org/10.1109/TNSRE.2013.2244616

Bjånes, D.A., Moritz, C.T., 2019. A robust encoding scheme for delivering artificial sensory information via direct brain stimulation. IEEE Transactions on Neural Systems and Rehabilitation Engineering. https://doi.org/10.1109/TNSRE.2019.2936739

Blakemore, S.-J., Bristow, D., Bird, G., Frith, C., Ward, J., 2005. Somatosensory activations during the observation of touch and a case of vision–touch synaesthesia. Brain 128, 1571–1583. https://doi.org/10.1093/brain/awh500

Blakemore, S.-J., Frith, C.D., Wolpert, D.M., 1999. Spatio-temporal prediction modulates the perception of self-produced stimuli. Journal of Cognitive Neuroscience 11, 551–559. https://doi.org/10.1162/089892999563607

Blakemore, S.-J., Oakley, D.A., Frith, C.D., 2003. Delusions of alien control in the normal brain. Neuropsychologia 41, 1058–1067. https://doi.org/10.1016/S0028-3932(02)00313-5

Blakemore, S.-J., Wolpert, D.M., Frith, C.D., 1998. Central cancellation of self-produced tickle sensation. Nat Neurosci 1, 635–640. https://doi.org/10.1038/2870

Bogen, J.E., Bogen, G.M., 1976. Wernicke's region? Where is it? Ann NY Acad Sci 280, 834–843. https://doi.org/10.1111/j.1749-6632.1976.tb25546.x

Bolognini, N., Maravita, A., 2007. Proprioceptive alignment of visual and somatosensory maps in the posterior parietal cortex. Current Biology 17, 1890–1895. https://doi.org/10.1016/j.cub.2007.09.057

Bolognini, N., Rossetti, A., Maravita, A., Miniussi, C., 2011. Seeing touch in the somatosensory cortex: A TMS study of the visual perception of touch. Hum. Brain Mapp. 32, 2104–2114. https://doi.org/10.1002/hbm.21172

Botvinick, M., Cohen, J., 1998. Rubber hands 'feel' touch that eyes see. Nature 391, 756. https://doi.org/10.1038/35784

Bufalari, I., Aprile, T., Avenanti, A., Di Russo, F., Aglioti, S.M., 2007. Empathy for pain and touch in the human somatosensory cortex. Cerebral Cortex 17, 2553–2561. https://doi.org/10.1093/cercor/bhl161

Caldwell, D.J., Cronin, J.A., Wu, J., Weaver, K.E., Ko, A.L., Rao, R.P.N., Ojemann, J.G., 2019. Direct stimulation of somatosensory cortex results in slower reaction times compared to peripheral touch in humans. Sci Rep 9. https://doi.org/10.1038/s41598-019-38619-2

Callier, T., Brantly, N.W., Caravelli, A., Bensmaia, S.J., 2020. The frequency of cortical microstimulation shapes artificial touch. Proc Natl Acad Sci U S A 117, 1191–1200. https://doi.org/10.1073/pnas.1916453117

Canolty, R.T., Edwards, E., Dalal, S.S., Soltani, M., Nagarajan, S.S., Kirsch, H.E., Berger, M.S., Barbaro, N.M., Knight, R.T., 2006. High gamma power is phase-locked to theta oscillations in human neocortex. Science 313, 1626–1628. https://doi.org/10.1126/science.1128115

Cardini, F., Longo, M.R., Driver, J., Haggard, P., 2012. Rapid enhancement of touch from non-informative vision of the hand. Neuropsychologia 50, 1954–1960. https://doi.org/10.1016/j.neuropsychologia.2012.04.020

Cardini, F., Longo, M.R., Haggard, P., 2011. Vision of the body modulates somatosensory intracortical inhibition. Cereb Cortex 21, 2014–2022. https://doi.org/10.1093/cercor/bhq267

Chan, A.W.-Y., Baker, C.I., 2015. Seeing is not feeling: Posterior parietal but not somatosensory cortex engagement during touch observation. Journal of Neuroscience 35, 1468–1480. https://doi.org/10.1523/JNEUROSCI.3621-14.2015

Chan, A.W.-Y., Bilger, E., Griffin, S., Elkis, V., Weeks, S., Hussey-Anderson, L., Pasquina, P.F., Tsao, J.W., Baker, C.I., 2019. Visual responsiveness in sensorimotor cortex is increased following amputation and reduced after mirror therapy. Neuroimage Clin 23, 101882. https://doi.org/10.1016/j.nicl.2019.101882

Chapman, C.E., Meftah, E.-M., 2005. Independent controls of attentional influences in primary and secondary somatosensory cortex. Journal of Neurophysiology 94, 4094–4107. https://doi.org/10.1152/jn.00303.2005

Chivukula, S., Jafari, M., Aflalo, T., Yong, N.A., Pouratian, N., 2019. Cognition in sensorimotor control: Interfacing with the posterior parietal cortex. Front. Neurosci. 13. https://doi.org/10.3389/fnins.2019.00140

Chivukula, S., Zhang, C.Y., Aflalo, T., Jafari, M., Pejsa, K., Pouratian, N., Andersen, R.A., 2021. Neural encoding of actual and imagined touch within human posterior parietal cortex. eLife 28. https://doi.org/10.7554/eLife.61646

Christie, B.P., Charkhkar, H., Shell, C.E., Marasco, P.D., Tyler, D.J., Triolo, R.J., 2019a. Visual inputs and postural manipulations affect the location of somatosensory percepts elicited by electrical stimulation. Sci Rep 9, 11699. https://doi.org/10.1038/s41598-019-47867-1

Christie, B.P., Graczyk, E.L., Charkhkar, H., Tyler, D.J., Triolo, R.J., 2019b. Visuotactile synchrony of stimulation-induced sensation and natural somatosensation. J. Neural Eng. 16, 036025. https://doi.org/10.1088/1741-2552/ab154c

Christie, B.P., Osborn, L.E., McMullen, D.P., Pawar, A.S., Thomas, T.M., Bensmaia, S.J., Celnik, P.A., Fifer, M.S., Tenore, F.V., 2022. Perceived timing of cutaneous vibration and intracortical microstimulation of human somatosensory cortex. Brain Stimulation 15, 881–888. https://doi.org/10.1016/j.brs.2022.05.015

Christie, B.P., Tat, D.M., Irwin, Z.T., Gilja, V., Nuyujukian, P., Foster, J.D., Ryu, S.I., Shenoy, K.V., Thompson, D.E., Chestek, C.A., 2015. Comparison of spike sorting and thresholding of voltage waveforms for intracortical brain-machine interface performance. J Neural Eng 12, 016009. https://doi.org/10.1088/1741-2560/12/1/016009

Colino, F.L., Lee, J.-H., Binsted, G., 2017. Availability of vision and tactile gating: vision enhances tactile sensitivity. Exp Brain Res 235, 341–348. https://doi.org/10.1007/s00221-016-4785-3

Collinger, J.L., Wodlinger, B., Downey, J.E., Wang, W., Tyler-Kabara, E.C., Weber, D.J., McMorland, A.J., Velliste, M., Boninger, M.L., Schwartz, A.B., 2013. High-performance neuroprosthetic control by an individual with tetraplegia. The Lancet 381, 557–564. https://doi.org/10.1016/S0140-6736(12)61816-9

Collins, K.L., Guterstam, A., Cronin, J., Olson, J.D., Ehrsson, H.H., Ojemann, J.G., 2017. Ownership of an artificial limb induced by electrical brain stimulation. Proc Natl Acad Sci USA 114, 166–171. https://doi.org/10.1073/pnas.1616305114

Costantini, M., Robinson, J., Migliorati, D., Donno, B., Ferri, F., Northoff, G., 2016. Temporal limits on rubber hand illusion reflect individuals' temporal resolution in multisensory perception. Cognition 157, 39–48. https://doi.org/10.1016/j.cognition.2016.08.010

Cunningham, D.A., Machado, A., Yue, G.H., Carey, J.R., Plow, E.B., 2013. Functional somatotopy revealed across multiple cortical regions using a model of complex motor task. Brain Res 1531, 25–36. https://doi.org/10.1016/j.brainres.2013.07.050

Dadarlat, M.C., O'Doherty, J.E., Sabes, P.N., 2015. A learning-based approach to artificial sensory feedback leads to optimal integration. Nat Neurosci 18, 138–144. https://doi.org/10.1038/nn.3883

Dai, J., Zhang, P., Sun, H., Qiao, X., Zhao, Y., Ma, J., Li, S., Zhou, J., Wang, C., 2019. Reliability of motor and sensory neural decoding by threshold crossings for intracortical brain–machine interface. J. Neural Eng. 16, 036011. https://doi.org/10.1088/1741-2552/ab0bfb

Daprati, E., Franck, N., Georgieff, N., Proust, J., Pacherie, E., Dalery, J., Jeannerod, M., 1997. Looking for the agent: an investigation into consciousness of action and self-consciousness in schizophrenic patients. Cognition 65, 71–86. https://doi.org/10.1016/S0010-0277(97)00039-5

Davis, K.C., Meschede-Krasa, B., Cajigas, I., Prins, N.W., Alver, C., Gallo, S., Bhatia, S., Abel, J.H., Naeem, J.A., Fisher, L., Raza, F., Rifai, W.R., Morrison, M., Ivan, M.E., Brown, E.N., Jagid, J.R., Prasad, A.,

2022. Design-development of an at-home modular brain–computer interface (BCI) platform in a case study of cervical spinal cord injury. J Neuroeng Rehabil 19, 53. https://doi.org/10.1186/s12984-022-01026-2

de Haan, E.H.F., Dijkerman, H.C., 2020. Somatosensation in the brain: A theoretical re-evaluation and a new model. Trends in Cognitive Sciences S1364661320301054. https://doi.org/10.1016/j.tics.2020.04.003

de Lafuente, V., Romo, R., 2006. Neural correlate of subjective sensory experience gradually builds up across cortical areas. PNAS 103, 14266–14271. https://doi.org/10.1073/pnas.0605826103

de Lafuente, V., Romo, R., 2005. Neuronal correlates of subjective sensory experience. Nat Neurosci 8, 1698–1703. https://doi.org/10.1038/nn1587

Dekleva, B.M., Weiss, J.M., Boninger, M.L., Collinger, J.L., 2021. Generalizable cursor click decoding using grasp-related neural transients. J Neural Eng 18, 10.1088/1741-2552/ac16b2. https://doi.org/10.1088/1741-2552/ac16b2

Delhaye, B.P., Long, K.H., Bensmaia, S.J., 2018. Neural basis of touch and proprioception in primate cortex. Comprehensive Physiology 8, 1575–1602. https://doi.org/10.1002/cphy.c170033

Deschrijver, E., Wiersema, J.R., Brass, M., 2016. The interaction between felt touch and tactile consequences of observed actions: an action-based somatosensory congruency paradigm. Soc Cogn Affect Neurosci 11, 1162–1172. https://doi.org/10.1093/scan/nsv081

Desmurget, M., Richard, N., Beuriat, P.-A., Szathmari, A., Mottolese, C., Duhamel, J.-R., Sirigu, A., 2018. Selective inhibition of volitional hand movements after stimulation of the dorsoposterior parietal cortex in humans. Current Biology 28, 3303–3309. https://doi.org/10.1016/j.cub.2018.08.027

Diedrichsen, J., Berlot, E., Mur, M., Schütt, H.H., Shahbazi, M., Kriegeskorte, N., 2021. Comparing representational geometries using whitened unbiased-distance-matrix similarity. arXiv:2007.02789 [stat].

Dionne, J.K., Legon, W., Staines, W.R., 2013. Crossmodal influences on early somatosensory processing: interaction of vision, touch, and task-relevance. Exp Brain Res 226, 503–512. https://doi.org/10.1007/s00221-013-3462-z

Dionne, J.K., Meehan, S.K., Legon, W., Staines, W.R., 2010. Crossmodal influences in somatosensory cortex: Interaction of vision and touch. Hum Brain Mapp 31, 14–25. https://doi.org/10.1002/hbm.20841

Dong, W.K., Chudler, E.H., Sugiyama, K., Roberts, V.J., Hayashi, T., 1994. Somatosensory, multisensory, and task-related neurons in cortical area 7b (PF) of unanesthetized monkeys. J Neurophysiol 72, 542–564. https://doi.org/10.1152/jn.1994.72.2.542

Dummer, T., Picot-Annand, A., Neal, T., Moore, C., 2009. Movement and the rubber hand illusion. Perception 38, 271–280. https://doi.org/10.1068/p5921

Ebisch, S.J.H., Perrucci, M.G., Ferretti, A., Del Gratta, C., Romani, G.L., Gallese, V., 2008. The sense of touch: Embodied simulation in a visuotactile mirroring mechanism for observed animate or inanimate touch. Journal of Cognitive Neuroscience 20, 1611–1623. https://doi.org/10.1162/jocn.2008.20111

Eck, J., Kaas, A.L., Goebel, R., 2013. Crossmodal interactions of haptic and visual texture information in early sensory cortex. NeuroImage 75, 123–135. https://doi.org/10.1016/j.neuroimage.2013.02.075

Ehrsson, H.H., 2020. Multisensory processes in body ownership, in: Multisensory Perception. Elsevier, pp. 179–200. https://doi.org/10.1016/B978-0-12-812492-5.00008-5

Ehrsson, H.H., Spence, C., Passingham, R.E., 2004. That's my hand! Activity in premotor cortex reflects feeling of ownership of a limb. Science 305, 875–877. https://doi.org/10.1126/science.1097011

Ejaz, N., Hamada, M., Diedrichsen, J., 2015. Hand use predicts the structure of representations in sensorimotor cortex. Nat Neurosci 18, 1034–1040. https://doi.org/10.1038/nn.4038

Ekman, G., 1959. Weber's Law and related functions. The Journal of Psychology 47, 343–352. https://doi.org/10.1080/00223980.1959.9916336

Enander, J.M.D., Jörntell, H., 2019. Somatosensory cortical neurons decode tactile input patterns and location from both dominant and non-dominant digits. Cell Reports 26, 3551-3560.e4. https://doi.org/10.1016/j.celrep.2019.02.099

Ernst, M.O., Banks, M.S., 2002. Humans integrate visual and haptic information in a statistically optimal fashion. Nature 415, 429–433. https://doi.org/10.1038/415429a

Espenhahn, S., Yan, T., Beltrano, W., Kaur, S., Godfrey, K., Cortese, F., Bray, S., Harris, A.D., 2020. The effect of movie-watching on electroencephalographic responses to tactile stimulation. NeuroImage 220, 117130. https://doi.org/10.1016/j.neuroimage.2020.117130

Fagg, A.H., Hatsopoulos, N.G., de Lafuente, V., Moxon, K.A., Nemati, S., Rebesco, J.M., Romo, R., Solla, S.A., Reimer, J., Tkach, D., Pohlmeyer, E.A., Miller, L.E., 2007. Biomimetic brain machine interfaces for the control of movement. Journal of Neuroscience 27, 11842–11846. https://doi.org/10.1523/JNEUROSCI.3516-07.2007

Feinberg, T.E., Venneri, A., Simone, A.M., Fan, Y., Northoff, G., 2010. The neuroanatomy of asomatognosia and somatoparaphrenia. Journal of Neurology, Neurosurgery & Psychiatry 81, 276–281. https://doi.org/10.1136/jnnp.2009.188946

Felleman, D.J., Van Essen, D.C., 1991. Distributed hierarchical processing in the primate cerebral cortex. Cerebral Cortex 1, 1–47. https://doi.org/10.1093/cercor/1.1.1

Fiorio, M., Haggard, P., 2005. Viewing the body prepares the brain for touch: effects of TMS over somatosensory cortex. European Journal of Neuroscience 22, 773–777. https://doi.org/10.1111/j.1460-9568.2005.04267.x

Fitzgibbon, B.M., Enticott, P.G., Rich, A.N., Giummarra, M.J., Georgiou-Karistianis, N., Bradshaw, J.L., 2012. Mirror-sensory synaesthesia: Exploring 'shared' sensory experiences as synaesthesia. Neuroscience & Biobehavioral Reviews 36, 645–657. https://doi.org/10.1016/j.neubiorev.2011.09.006

Flesher, S.N., Collinger, J.L., Foldes, S.T., Weiss, J.M., Downey, J.E., Tyler-Kabara, E.C., Bensmaia, S.J., Schwartz, A.B., Boninger, M.L., Gaunt, R.A., 2016. Intracortical microstimulation of human somatosensory cortex. Science Translational Medicine 8, 361ra141. https://doi.org/10.1126/scitranslmed.aaf8083

Flesher, S.N., Downey, J.E., Weiss, J.M., Hughes, C.L., Herrera, A.J., Tyler-Kabara, E.C., Boninger, M.L., Collinger, J.L., Gaunt, R.A., 2021. A brain-computer interface that evokes tactile sensations improves robotic arm control. Science 372, 831–836. https://doi.org/10.1126/science.abd0380

Fogassi, L., Gallese, V., Fadiga, L., Luppino, G., Matelli, M., Rizzolatti, G., 1996. Coding of peripersonal space in inferior premotor cortex (area F4). Journal of Neurophysiology 76, 141–157. https://doi.org/10.1152/jn.1996.76.1.141

Fornia, L., Puglisi, G., Leonetti, A., Bello, L., Berti, A., Cerri, G., Garbarini, F., 2020. Direct electrical stimulation of the premotor cortex shuts down awareness of voluntary actions. Nat Commun 11, 705. https://doi.org/10.1038/s41467-020-14517-4

French, B., Chiaro, N.V.D., Holmes, N.P., 2022. Hand posture, but not vision of the hand, affects tactile spatial resolution in the grating orientation discrimination task. Exp Brain Res. https://doi.org/10.1007/s00221-022-06450-3

Gale, D.J., Flanagan, J.R., Gallivan, J.P., 2021. Human somatosensory cortex is modulated during motor planning. J. Neurosci. JN-RM-0342-21. https://doi.org/10.1523/JNEUROSCI.0342-21.2021

Gallivan, J.P., Chapman, C.S., Wolpert, D.M., Flanagan, J.R., 2018. Decision-making in sensorimotor control. Nat Rev Neurosci 19, 519–534. https://doi.org/10.1038/s41583-018-0045-9

Gazzola, V., Spezio, M.L., Etzel, J.A., Castelli, F., Adolphs, R., Keysers, C., 2012. Primary somatosensory cortex discriminates affective significance in social touch. PNAS 109, E1657–E1666. https://doi.org/10.1073/pnas.1113211109

Gentile, G., Björnsdotter, M., Petkova, V.I., Abdulkarim, Z., Ehrsson, H.H., 2015. Patterns of neural activity in the human ventral premotor cortex reflect a whole-body multisensory percept. NeuroImage 109, 328–340. https://doi.org/10.1016/j.neuroimage.2015.01.008

Gentilucci, M., Toni, I., Daprati, E., Gangitano, M., 1997. Tactile input of the hand and the control of reaching to grasp movements. Exp Brain Res 114, 130–137. https://doi.org/10.1007/PL00005612

Georgopoulos, A., Kalaska, J., Caminiti, R., Massey, J., 1982. On the relations between the direction of two-dimensional arm movements and cell discharge in primate motor cortex. J. Neurosci. 2, 1527–1537. https://doi.org/10.1523/JNEUROSCI.02-11-01527.1982

Ghazanfar, A., Schroeder, C., 2006. Is neocortex essentially multisensory? Trends in Cognitive Sciences 10, 278–285. https://doi.org/10.1016/j.tics.2006.04.008

Ghez, C., Gordon, J., Ghilardi, M.F., 1995. Impairments of reaching movements in patients without proprioception. II. Effects of visual information on accuracy. Journal of Neurophysiology 73, 361–372. https://doi.org/10.1152/jn.1995.73.1.361

Giummarra, M.J., Gibson, S.J., Georgiou-Karistianis, N., Bradshaw, J.L., 2008. Mechanisms underlying embodiment, disembodiment and loss of embodiment. Neuroscience & Biobehavioral Reviews 32, 143–160. https://doi.org/10.1016/j.neubiorev.2007.07.001

Godlove, J.M., Whaite, E.O., Batista, A.P., 2014. Comparing temporal aspects of visual, tactile, and microstimulation feedback for motor control. J. Neural Eng. 11, 046025. https://doi.org/10.1088/1741-2560/11/4/046025

Gonzalez-Franco, M., Ofek, E., Pan, Y., Antley, A., Steed, A., Spanlang, B., Maselli, A., Banakou, D., Pelechano, N., Orts-Escolano, S., Orvalho, V., Trutoiu, L., Wojcik, M., Sanchez-Vives, M.V., Bailenson, J., Slater, M., Lanier, J., 2020. The Rocketbox library and the utility of freely available rigged avatars. Front. Virtual Real. 1, 561558. https://doi.org/10.3389/frvir.2020.561558

Goodman, J.M., Tabot, G.A., Lee, A.S., Suresh, A.K., Rajan, A.T., Hatsopoulos, N.G., Bensmaia, S., 2019. Postural representations of the hand in the primate sensorimotor cortex. Neuron 104, 1000-1009.e7. https://doi.org/10.1016/j.neuron.2019.09.004

Graziano, M.S., 1999. Where is my arm? The relative role of vision and proprioception in the neuronal representation of limb position. Proc Natl Acad Sci U S A 96, 10418–10421. https://doi.org/10.1073/pnas.96.18.10418

Graziano, M.S., Hu, X.T., Gross, C.G., 1997. Visuospatial properties of ventral premotor cortex. J Neurophysiol 77, 2268–2292. https://doi.org/10.1152/jn.1997.77.5.2268

Graziano, M.S.A., Aflalo, T.N., 2007. Mapping behavioral repertoire onto the cortex. Neuron 56, 239–251. https://doi.org/10.1016/j.neuron.2007.09.013

Gregoriou, G.G., Borra, E., Matelli, M., Luppino, G., 2006. Architectonic organization of the inferior parietal convexity of the macaque monkey. J Comp Neurol 496, 422–451. https://doi.org/10.1002/cne.20933

Guan, C., Aflalo, T., Zhang, C.Y., Amoruso, E., Rosario, E.R., Andersen, R.A., 2022. Stability of motor representations after paralysis. eLife 63. https://doi.org/10.7554/eLife.74478

Hadjidimitrakis, K., Bakola, S., Wong, Y.T., Hagan, M.A., 2019. Mixed spatial and movement representations in the primate posterior parietal cortex. Front. Neural Circuits 13, 15. https://doi.org/10.3389/fncir.2019.00015

Haggard, P., Christakou, A., Serino, A., 2007. Viewing the body modulates tactile receptive fields. Exp Brain Res 180, 187–193. https://doi.org/10.1007/s00221-007-0971-7

Hanks, T.D., Ditterich, J., Shadlen, M.N., 2006. Microstimulation of macaque area LIP affects decision-making in a motion discrimination task. Nat Neurosci 9, 682–689. https://doi.org/10.1038/nn1683

Hardwick, R.M., Caspers, S., Eickhoff, S.B., Swinnen, S.P., 2018. Neural correlates of action: Comparing meta-analyses of imagery, observation, and execution. Neurosci Biobehav Rev 94, 31–44. https://doi.org/10.1016/j.neubiorev.2018.08.003

Harpaz, Y., Levkovitz, Y., Lavidor, M., 2009. Lexical ambiguity resolution in Wernicke's area and its right homologue. Cortex 45, 1097–1103. https://doi.org/10.1016/j.cortex.2009.01.002

Heller, M.A., 1982. Visual and tactual texture perception: Intersensory cooperation. Perception & Psychophysics 31, 339–344. https://doi.org/10.3758/BF03202657

Hernandez, A., Zainos, A., Romo, R., 2000. Neuronal correlates of sensory discrimination in the somatosensory cortex. Proceedings of the National Academy of Sciences 97, 6191–6196. https://doi.org/10.1073/pnas.120018597

Hodge, C., Dubroff, J., Huckins, S., Szeverenyi, N., 1996. Somatosensory imagery activates primary sensory cortex in human: A functional MRI study. NeuroImage 3, S209. https://doi.org/10.1016/S1053-8119(96)80211-4

Hughes, C.L., Flesher, S.N., Gaunt, R.A., 2022. Effects of stimulus pulse rate on somatosensory adaptation in the human cortex. Brain Stimulation 15, 987–995. https://doi.org/10.1016/j.brs.2022.05.021

Hughes, C.L., Flesher, S.N., Weiss, J.M., Boninger, M.L., Collinger, J., Gaunt, R., 2021a. Perception of microstimulation frequency in human somatosensory cortex. eLife 10, e65128. https://doi.org/10.7554/eLife.65128

Hughes, C.L., Flesher, S.N., Weiss, J.M., Downey, J.E., Boninger, M., Collinger, J.L., Gaunt, R.A., 2021b. Neural stimulation and recording performance in human sensorimotor cortex over 1500 days. J Neural Eng 18, 10.1088/1741-2552/ac18ad. https://doi.org/10.1088/1741-2552/ac18ad

Hyvärinen, J., Poranen, A., 1978. Receptive field integration and submodality convergence in the hand area of the post-central gyrus of the alert monkey. J Physiol 283, 539–556. https://doi.org/10.1113/jphysiol.1978.sp012518

Iwamura, Y., 1998. Hierarchical somatosensory processing. Current Opinion in Neurobiology 8, 522–528. https://doi.org/10.1016/S0959-4388(98)80041-X

Iwamura, Y., Tanaka, M., Sakamoto, M., Hikosaka, O., 1993. Rostrocaudal gradients in the neuronal receptive field complexity in the finger region of the alert monkey's postcentral gyrus. Exp Brain Res 92, 360–368. https://doi.org/10.1007/BF00229023

Jeannerod, M., 2003. The mechanism of self-recognition in humans. Behavioural Brain Research 142, 1–15. https://doi.org/10.1016/S0166-4328(02)00384-4

Jeannerod, M., 1994. The representing brain: Neural correlates of motor intention and imagery. Behav Brain Sci 17, 187–202. https://doi.org/10.1017/S0140525X00034026

Johansson, R.S., Vallbo, A.B., 1979. Tactile sensibility in the human hand: Relative and absolute densities of four types of mechanoreceptive units in glabrous skin. The Journal of Physiology 286, 283–300. https://doi.org/10.1113/jphysiol.1979.sp012619

Johnson, R.M., Burton, P.C., Ro, T., 2006. Visually induced feelings of touch. Brain Research 1073–1074, 398–406. https://doi.org/10.1016/j.brainres.2005.12.025

Kaas, A., Goebel, R., Valente, G., Sorger, B., 2019. Topographic somatosensory imagery for real-time fMRI brain-computer interfacing. Front Hum Neurosci 13. https://doi.org/10.3389/fnhum.2019.00427

Kaas, J.H., 1983. What, if anything, is SI? Organization of first somatosensory area of cortex. Physiological Reviews 63, 206–231. https://doi.org/10.1152/physrev.1983.63.1.206

Kaas, J.H., Nelson, R.J., Sur, M., Lin, C.-S., Merzenich, M.M., 1979. Multiple representations of the body within the primary somatosensory cortex of primates. Science, New Series 204, 521–523.

Kandula, M., Hofman, D., Dijkerman, H.C., 2015. Visuo-tactile interactions are dependent on the predictive value of the visual stimulus. Neuropsychologia 70, 358–366. https://doi.org/10.1016/j.neuropsychologia.2014.12.008

Kaufman, M.T., Churchland, M.M., Ryu, S.I., Shenoy, K.V., 2014. Cortical activity in the null space: permitting preparation without movement. Nat Neurosci 17, 440–448. https://doi.org/10.1038/nn.3643

Kennett, S., Taylor-Clarke, M., Haggard, P., 2001. Noninformative vision improves the spatial resolution of touch in humans. Current Biology 11, 1188–1191. https://doi.org/10.1016/S0960-9822(01)00327-X

Keshtkaran, M.R., Sedler, A.R., Chowdhury, R.H., Tandon, R., Basrai, D., Nguyen, S.L., Sohn, H., Jazayeri, M., Miller, L.E., Pandarinath, C., 2022. A large-scale neural network training framework for generalized estimation of single-trial population dynamics. Nat Methods 19, 1572–1577. https://doi.org/10.1038/s41592-022-01675-0

Keysers, C., Kaas, J.H., Gazzola, V., 2010. Somatosensation in social perception. Nat Rev Neurosci 11, 417–428. https://doi.org/10.1038/nrn2833

Keysers, C., Wicker, B., Gazzola, V., Anton, J.-L., Fogassi, L., Gallese, V., 2004. A touching sight: SII/PV activation during the observation and experience of touch. Neuron 42, 335–346. https://doi.org/10.1016/S0896-6273(04)00156-4

Kieliba, P., Clode, D., Maimon-Mor, R.O., Makin, T.R., 2021. Robotic hand augmentation drives changes in neural body representation. Sci. Robot. 6, eabd7935. https://doi.org/10.1126/scirobotics.abd7935

Kikkert, S., Pfyffer, D., Verling, M., Freund, P., Wenderoth, N., 2021. Finger somatotopy is preserved after tetraplegia but deteriorates over time. eLife 10, e67713. https://doi.org/10.7554/eLife.67713

Kilteni, K., Ehrsson, H.H., 2017. Body ownership determines the attenuation of self-generated tactile sensations. Proc Natl Acad Sci U S A 114, 8426–8431. https://doi.org/10.1073/pnas.1703347114

Kilteni, K., Groten, R., Slater, M., 2012a. The sense of embodiment in virtual reality. Presence: Teleoperators and Virtual Environments 21, 373–387. https://doi.org/10.1162/PRES_a_00124

Kilteni, K., Normand, J.-M., Sanchez-Vives, M.V., Slater, M., 2012b. Extending body space in immersive virtual reality: A very long arm illusion. PLoS ONE 7, e40867. https://doi.org/10.1371/journal.pone.0040867

Kim, S., Callier, T., Tabot, G.A., Gaunt, R.A., Tenore, F.V., Bensmaia, S.J., 2015a. Behavioral assessment of sensitivity to intracortical microstimulation of primate somatosensory cortex. Proc Natl Acad Sci USA 112, 15202–15207. https://doi.org/10.1073/pnas.1509265112

Kim, S., Callier, T., Tabot, Gregg A., Tenore, F.V., Bensmaia, S.J., 2015b. Sensitivity to microstimulation of somatosensory cortex distributed over multiple electrodes. Front Syst Neurosci 9. https://doi.org/10.3389/fnsys.2015.00047

Kimura, T., 2021. Approach of visual stimuli facilitates the prediction of tactile events and suppresses beta band oscillations around the primary somatosensory area. Neuroreport 32, 631–635. https://doi.org/10.1097/WNR.0000000000001643

Klaes, C., Shi, Y., Kellis, S., Minxha, J., Revechkis, B., Andersen, R.A., 2014. A cognitive neuroprosthetic that uses cortical stimulation for somatosensory feedback. J. Neural Eng. 11. https://doi.org/10.1088/1741-2560/11/5/056024

Kolasinski, J., Makin, T.R., Jbabdi, S., Clare, S., Stagg, C.J., Johansen-Berg, H., 2016. Investigating the stability of fine-grain digit somatotopy in individual human participants. J. Neurosci. 36, 1113–1127. https://doi.org/10.1523/JNEUROSCI.1742-15.2016

Körding, K.P., Wolpert, D.M., 2004. Bayesian integration in sensorimotor learning. Nature 427, 244–247. https://doi.org/10.1038/nature02169

Kriegeskorte, N., 2008. Representational similarity analysis – connecting the branches of systems neuroscience. Front. Sys. Neurosci. 2. https://doi.org/10.3389/neuro.06.004.2008

Krubitzer, L., Huffman, K.J., Disbrow, E., Recanzone, G., 2004. Organization of area 3a in macaque monkeys: Contributions to the cortical phenotype. J. Comp. Neurol. 471, 97–111. https://doi.org/10.1002/cne.20025

Kuehn, E., Haggard, P., Villringer, A., Pleger, B., Sereno, M.I., 2018. Visually-driven maps in Area 3b. J Neurosci 38, 1295–1310. https://doi.org/10.1523/JNEUROSCI.0491-17.2017

Kuehn, E., Trampel, R., Mueller, K., Turner, R., Schütz-Bosbach, S., 2013. Judging roughness by sight-A 7-tesla fMRI study on responsivity of the primary somatosensory cortex during observed touch of self and others. Hum. Brain Mapp. 34, 1882–1895. https://doi.org/10.1002/hbm.22031

Kumaravelu, K., Sombeck, J., Miller, L.E., Bensmaia, S.J., Grill, W.M., 2022. Stoney vs. Histed: Quantifying the spatial effects of intracortical microstimulation. Brain Stimulation 15, 141–151. https://doi.org/10.1016/j.brs.2021.11.015

Lang, C.E., Schieber, M.H., 2003. Differential impairment of individuated finger movements in humans after damage to the motor cortex or the corticospinal tract. Journal of Neurophysiology 90, 1160–1170. https://doi.org/10.1152/jn.00130.2003

Leinonen, L., Hyvärinen, J., Nyman, G., Linnankoski, I., 1979. I. Functional properties of neurons in lateral part of associative area 7 in awake monkeys. Exp Brain Res 34, 299–320. https://doi.org/10.1007/BF00235675

Lenggenhager, B., Scivoletto, G., Molinari, M., Pazzaglia, M., 2013. Restoring tactile awareness through the rubber hand illusion in cervical spinal cord injury. Neurorehabilitation and Neural Repair 5.

Lenggenhager, B., Tadi, T., Metzinger, T., Blanke, O., 2007. Video Ergo Sum: Manipulating bodily self-consciousness. Science 317, 1096–1099. https://doi.org/10.1126/science.1143439

Limanowski, J., Blankenburg, F., 2016. Integration of visual and proprioceptive limb position information in human posterior parietal, premotor, and extrastriate cortex. J Neurosci 36, 2582–2589. https://doi.org/10.1523/JNEUROSCI.3987-15.2016

London, B.M., Jordan, L.R., Jackson, C.R., Miller, L.E., 2008. Electrical stimulation of the proprioceptive cortex (Area 3a) used to instruct a behaving monkey. IEEE Trans. Neural Syst. Rehabil. Eng. 16, 32–36. https://doi.org/10.1109/TNSRE.2007.907544

Long, K.H., Lieber, J.D., Bensmaia, S.J., 2022. Texture is encoded in precise temporal spiking patterns in primate somatosensory cortex. Nat Commun 13, 1311. https://doi.org/10.1038/s41467-022-28873-w

Longo, M.R., Pernigo, S., Haggard, P., 2011. Vision of the body modulates processing in primary somatosensory cortex. Neuroscience Letters 489, 159–163. https://doi.org/10.1016/j.neulet.2010.12.007

Longo, M.R., Schüür, F., Kammers, M.P.M., Tsakiris, M., Haggard, P., 2008. What is embodiment? A psychometric approach. Cognition 107, 978–998. https://doi.org/10.1016/j.cognition.2007.12.004

Maimon-Mor, R.O., Makin, T.R., 2020. Is an artificial limb embodied as a hand? Brain decoding in prosthetic limb users. PLoS Biol 18, e3000729. https://doi.org/10.1371/journal.pbio.3000729

Makin, T.R., Bensmaia, S.J., 2017. Stability of sensory topographies in adult cortex. Trends in Cognitive Sciences 21, 195–204. https://doi.org/10.1016/j.tics.2017.01.002

Marasco, P.D., Hebert, J.S., Sensinger, J.W., Beckler, D.T., Thumser, Z.C., Shehata, A.W., Williams, H.E., Wilson, K.R., 2021. Neurorobotic fusion of prosthetic touch, kinesthesia, and movement in bionic upper limbs promotes intrinsic brain behaviors. Sci. Robot. 6, eabf3368. https://doi.org/10.1126/scirobotics.abf3368

Marasco, P.D., Kim, K., Colgate, J.E., Peshkin, M.A., Kuiken, T.A., 2011. Robotic touch shifts perception of embodiment to a prosthesis in targeted reinnervation amputees. Brain 134, 747–758. https://doi.org/10.1093/brain/awq361

Marshall, W.H., Woolsey, C.N., Bard, P., 1937. Cortical representation of tactile sensibility as indicated by cortical potentials. Science 85, 388–390. https://doi.org/10.1126/science.85.2207.388

Maselli, A., Kilteni, K., López-Moliner, J., Slater, M., 2016. The sense of body ownership relaxes temporal constraints for multisensory integration. Sci Rep 6, 30628. https://doi.org/10.1038/srep30628

McDowell, T., Holmes, N.P., Sunderland, A., Schürmann, M., 2018. TMS over the supramarginal gyrus delays selection of appropriate grasp orientation during reaching and grasping tools for use. Cortex 103, 117–129. https://doi.org/10.1016/j.cortex.2018.03.002

Meftah, E.-M., Shenasa, J., Chapman, C.E., 2002. Effects of a cross-modal manipulation of attention on somatosensory cortical neuronal responses to tactile stimuli in the monkey. Journal of Neurophysiology 88, 3133–3149. https://doi.org/10.1152/jn.00121.2002

Metzger, S.L., Liu, J.R., Moses, D.A., Dougherty, M.E., Seaton, M.P., Littlejohn, K.T., Chartier, J., Anumanchipalli, G.K., Tu-Chan, A., Ganguly, K., Chang, E.F., 2022. Generalizable spelling using a speech neuroprosthesis in an individual with severe limb and vocal paralysis. Nat Commun 13, 6510. https://doi.org/10.1038/s41467-022-33611-3

Meyer, K., Kaplan, J.T., Essex, R., Damasio, H., Damasio, A., 2011. Seeing touch is correlated with content-specific activity in primary somatosensory cortex. Cerebral Cortex 21, 2113–2121. https://doi.org/10.1093/cercor/bhq289

Miall, R.C., Afanasyeva, D., Cole, J.D., Mason, P., 2021. The role of somatosensation in automatic visuo-motor control: a comparison of congenital and acquired sensory loss. Exp Brain Res 239, 2043–2061. https://doi.org/10.1007/s00221-021-06110-y

Miall, R.C., Rosenthal, O., Ørstavik, K., Cole, J.D., Sarlegna, F.R., 2019. Loss of haptic feedback impairs control of hand posture: a study in chronically deafferented individuals when grasping and lifting objects. Exp Brain Res 237, 2167–2184. https://doi.org/10.1007/s00221-019-05583-2

Michelson, N.J., Eles, J.R., Vazquez, A.L., Ludwig, K.A., Kozai, T.D.Y., 2019. Calcium activation of cortical neurons by continuous electrical stimulation: Frequency dependence, temporal fidelity, and activation density. J Neurosci Res 97, 620–638. https://doi.org/10.1002/jnr.24370

Miller, L.E., Fabio, C., Ravenda, V., Bahmad, S., Koun, E., Salemme, R., Luauté, J., Bolognini, N., Hayward, V., Farnè, A., 2019. Somatosensory cortex efficiently processes touch located beyond the body. Current Biology S0960982219313831. https://doi.org/10.1016/j.cub.2019.10.043

Miller, L.E., Montroni, L., Koun, E., Salemme, R., Hayward, V., Farnè, A., 2018. Sensing with tools extends somatosensory processing beyond the body. Nature 561, 239–242. https://doi.org/10.1038/s41586-018-0460-0

Mirpour, K., Ong, W.S., Bisley, J.W., 2010. Microstimulation of posterior parietal cortex biases the selection of eye movement goals during search. J Neurophysiol 104, 3021–3028. https://doi.org/10.1152/jn.00397.2010

Morrison, I., Lloyd, D., Di Pellegrino, G., Roberts, N., 2004. Vicarious responses to pain in anterior cingulate cortex: Is empathy a multisensory issue? Cognitive, Affective, & Behavioral Neuroscience 4, 270–278. https://doi.org/10.3758/CABN.4.2.270

Moses, D.A., Metzger, S.L., Liu, J.R., Anumanchipalli, G.K., Makin, J.G., Sun, P.F., Chartier, J., Dougherty, M.E., Liu, P.M., Abrams, G.M., Tu-Chan, A., Ganguly, K., Chang, E.F., 2021. Neuroprosthesis for decoding speech in a paralyzed person with anarthria. N Engl J Med 385, 217–227. https://doi.org/10.1056/NEJMoa2027540

Murata, A., Gallese, V., Luppino, G., Kaseda, M., Sakata, H., 2000. Selectivity for the shape, size, and orientation of objects for grasping in neurons of monkey parietal area AIP. Journal of Neurophysiology 83, 2580–2601. https://doi.org/10.1152/jn.2000.83.5.2580

Murata, Y., Higo, N., Oishi, T., Yamashita, A., Matsuda, K., Hayashi, M., Yamane, S., 2008. Effects of motor training on the recovery of manual dexterity after primary motor cortex lesion in macaque monkeys. Journal of Neurophysiology 99, 773–786. https://doi.org/10.1152/jn.01001.2007

Muret, D., Root, V., Kieliba, P., Clode, D., Makin, T.R., 2022. Beyond body maps: Information content of specific body parts is distributed across the somatosensory homunculus. Cell Reports 38, 110523. https://doi.org/10.1016/j.celrep.2022.110523

Neal, J.W., Pearson, R.C., Powell, T.P., 1990. The ipsilateral cortico-cortical connections of area 7b, PF, in the parietal and temporal lobes of the monkey. Brain Res 524, 119–132. https://doi.org/10.1016/0006-8993(90)90500-b

Nili, H., Wingfield, C., Walther, A., Su, L., Marslen-Wilson, W., Kriegeskorte, N., 2014. A toolbox for representational similarity analysis. PLoS Comput Biol 10, e1003553. https://doi.org/10.1371/journal.pcbi.1003553

Oby, E.R., Perel, S., Sadtler, P.T., Ruff, D.A., Mischel, J.L., Montez, D.F., Cohen, M.R., Batista, A.P., Chase, S.M., 2016. Extracellular voltage threshold settings can be tuned for optimal encoding of movement and stimulus parameters. J Neural Eng 13, 036009. https://doi.org/10.1088/1741-2560/13/3/036009

O'Doherty, J.E., Lebedev, M.A., Ifft, P.J., Zhuang, K.Z., Shokur, S., Bleuler, H., Nicolelis, M.A.L., 2011. Active tactile exploration using a brain–machine–brain interface. Nature 479, 228–231. https://doi.org/10.1038/nature10489

O'Doherty, J.E., Shokur, S., Medina, L.E., Lebedev, M.A., Nicolelis, M.A.L., 2019. Creating a neuroprosthesis for active tactile exploration of textures. Proc Natl Acad Sci USA 201908008. https://doi.org/10.1073/pnas.1908008116

Orban, G.A., Caruana, F., 2014. The neural basis of human tool use. Front. Psychol. 5. https://doi.org/10.3389/fpsyg.2014.00310

Osborn, L.E., Christie, B.P., McMullen, D.P., Nickl, R.W., Thompson, M.C., Pawar, A.S., Thomas, T.M., Alejandro Anaya, M., Crone, N.E., Wester, B.A., Bensmaia, S.J., Celnik, P.A., Cantarero, G.L., Tenore, F.V., Fifer, M.S., 2021. Intracortical microstimulation of somatosensory cortex enables object identification through perceived sensations. Presented at the 2021 43rd Annual International Conference of the IEEE Engineering in Medicine Biology Society (EMBC), pp. 6259–6262. https://doi.org/10.1109/EMBC46164.2021.9630450

Page, D.M., George, J.A., Kluger, D.T., Duncan, C., Wendelken, S., Davis, T., Hutchinson, D.T., Clark, G.A., 2018. Motor control and sensory feedback enhance prosthesis embodiment and reduce phantom pain after long-term hand amputation. Front. Hum. Neurosci. 12, 352. https://doi.org/10.3389/fnhum.2018.00352

Pandarinath, C., Bensmaia, S.J., 2022. The science and engineering behind sensitized brain-controlled bionic hands. Physiological Reviews 102, 551–604. https://doi.org/10.1152/physrev.00034.2020

Pandarinath, C., O'Shea, D.J., Collins, J., Jozefowicz, R., Stavisky, S.D., Kao, J.C., Trautmann, E.M., Kaufman, M.T., Ryu, S.I., Hochberg, L.R., Henderson, J.M., Shenoy, K.V., Abbott, L.F., Sussillo, D., 2018.

Inferring single-trial neural population dynamics using sequential auto-encoders. Nat Methods 15, 805–815. https://doi.org/10.1038/s41592-018-0109-9

Peeters, R., Simone, L., Nelissen, K., Fabbri-Destro, M., Vanduffel, W., Rizzolatti, G., Orban, G.A., 2009. The representation of tool use in humans and monkeys: Common and uniquely human features. J. Neurosci. 29, 11523–11539. https://doi.org/10.1523/JNEUROSCI.2040-09.2009

Pei, Y.-C., Denchev, P.V., Hsiao, S.S., Craig, J.C., Bensmaia, S.J., 2009. Convergence of submodality-specific input onto neurons in primary somatosensory cortex. Journal of Neurophysiology 102, 1843–1853. https://doi.org/10.1152/jn.00235.2009

Penfield, W., Boldrey, E., 1937. Somatic motor and sensory representation in the cerebral cortex of man as studied by electrical stimulation. Brain 60, 389–443. https://doi.org/10.1093/brain/60.4.389

Petkova, V.I., Björnsdotter, M., Gentile, G., Jonsson, T., Li, T.-Q., Ehrsson, H.H., 2011. From part- to whole-body ownership in the multisensory brain. Current Biology 21, 1118–1122. https://doi.org/10.1016/j.cub.2011.05.022

Petkova, V.I., Ehrsson, H.H., 2008. If I were you: Perceptual illusion of body swapping. PLoS ONE 3, e3832. https://doi.org/10.1371/journal.pone.0003832

Pihko, E., Nangini, C., Jousmäki, V., Hari, R., 2010. Observing touch activates human primary somatosensory cortex. European Journal of Neuroscience 31, 1836–1843. https://doi.org/10.1111/j.1460-9568.2010.07192.x

Pons, T.P., Garraghty, P.E., Ommaya, A.K., Kaas, J.H., Taub, E., Mishkin, M., 1991. Massive cortical reorganization after sensory deafferentation in adult macaques. Science 252, 1857–1860. https://doi.org/10.1126/science.1843843

Popovich, C., Staines, W.R., 2014. The attentional-relevance and temporal dynamics of visual-tactile crossmodal interactions differentially influence early stages of somatosensory processing. Brain Behav 4, 247–260. https://doi.org/10.1002/brb3.210

Pozeg, P., Palluel, E., Ronchi, R., Solcà, M., Al-Khodairy, A.-W., Jordan, X., Kassouha, A., Blanke, O., 2017. Virtual reality improves embodiment and neuropathic pain caused by spinal cord injury. Neurology 89, 1894–1903. https://doi.org/10.1212/WNL.0000000000004585

Preatoni, G., Valle, G., Petrini, F.M., Raspopovic, S., 2021. Lightening the perceived prosthesis weight with neural embodiment promoted by sensory feedback. Current Biology 31, 1065-1071.e4. https://doi.org/10.1016/j.cub.2020.11.069

Press, C., Taylor-Clarke, M., Kennett, S., Haggard, P., 2004. Visual enhancement of touch in spatial body representation. Experimental Brain Research 154, 238–245. https://doi.org/10.1007/s00221-003-1651-x

Qi, H.-X., Kaas, J.H., 2004. Myelin stains reveal an anatomical framework for the representation of the digits in somatosensory area 3b of macaque monkeys. Journal of Comparative Neurology 477, 172–187. https://doi.org/10.1002/cne.20247

Qi, H.-X., Reed, J.L., Franca, J.G., Jain, N., Kajikawa, Y., Kaas, J.H., 2016. Chronic recordings reveal tactile stimuli can suppress spontaneous activity of neurons in somatosensory cortex of awake and anesthetized primates. Journal of Neurophysiology 115, 2105–2123. https://doi.org/10.1152/jn.00634.2015

Ramachandran, V.S., Rogers-Ramachandran, D., 1996. Synaesthesia in phantom limbs induced with mirrors 10.

Ramachandran, V.S., Rogers-Ramachandran, D., Stewart, M., 1992. Perceptual correlates of massive cortical reorganization. Science 258, 1159–1160. https://doi.org/10.1126/science.1439826

Risso, G., Valle, G., 2022. Multisensory integration in bionics: Relevance and perspectives. Curr Phys Med Rehabil Rep. https://doi.org/10.1007/s40141-022-00350-x

Risso, G., Valle, G., Iberite, F., Strauss, I., Stieglitz, T., Controzzi, M., Clemente, F., Granata, G., Rossini, P.M., Micera, S., Baud-Bovy, G., 2019. Optimal integration of intraneural somatosensory feedback with visual information: A single-case study. Sci Rep 9, 7916. https://doi.org/10.1038/s41598-019-43815-1

Robles-De-La-Torre, G., 2006. The importance of the sense of touch in virtual and real environments. IEEE MultiMedia 13, 24–30. https://doi.org/10.1109/MMUL.2006.69

Romo, R., de Lafuente, V., 2013. Conversion of sensory signals into perceptual decisions. Prog Neurobiol 103, 41–75. https://doi.org/10.1016/j.pneurobio.2012.03.007

Romo, R., Hernández, A., Zainos, A., Salinas, E., 1998. Somatosensory discrimination based on cortical microstimulation. Nature 392, 387–390. https://doi.org/10.1038/32891

Root, V., Muret, D., Arribas, M., Amoruso, E., Thornton, J., Tarall-Jozwiak, A., Tracey, I., Makin, T.R., 2022. Complex pattern of facial remapping in somatosensory cortex following congenital but not acquired hand loss. eLife 11, e76158. https://doi.org/10.7554/eLife.76158

Rosén, G., Hugdahl, K., Ersland, L., Lundervold, A., Smievoll, A.I., Barndon, R., Sundberg, H., Thomsen, T., Roscher, B.E., Tjølsen, A., Engelsen, B., 2001. Different brain areas activated during imagery of painful and non-painful 'finger movements' in a subject with an amputated arm. Neurocase 7, 255–260. https://doi.org/10.1093/neucas/7.3.255

Rosenthal, I.A., Bashford, L., Kellis, S., Pejsa, K., Lee, B., Liu, C., Andersen, R.A., 2023. S1 represents multisensory contexts and somatotopic locations within and outside the bounds of the cortical homunculus. Cell Reports 42, 112312. https://doi.org/10.1016/j.celrep.2023.112312

Rossetti, A., Miniussi, C., Maravita, A., Bolognini, N., 2012. Visual perception of bodily interactions in the primary somatosensory cortex: Touch observation in primary somatosensory cortex. European Journal of Neuroscience 36, 2317–2323. https://doi.org/10.1111/j.1460-9568.2012.08137.x

Rouiller, E.M., Yu, X.H., Moret, V., Tempini, A., Wiesendanger, M., Liang, F., 1998. Dexterity in adult monkeys following early lesion of the motor cortical hand area: the role of cortex adjacent to the lesion. European Journal of Neuroscience 10, 729–740. https://doi.org/10.1046/j.1460-9568.1998.00075.x

Saal, H.P., Bensmaia, S.J., 2015. Biomimetic approaches to bionic touch through a peripheral nerve interface. Neuropsychologia 79, 344–353. https://doi.org/10.1016/j.neuropsychologia.2015.06.010

Saal, H.P., Harvey, M.A., Bensmaia, S.J., 2015. Rate and timing of cortical responses driven by separate sensory channels. eLife 4, e10450. https://doi.org/10.7554/eLife.10450

Sagar, S., Rick, J., Chandra, A., Yagnik, G., Aghi, M.K., 2019. Functional brain mapping: overview of techniques and their application to neurosurgery. Neurosurg Rev 42, 639–647. https://doi.org/10.1007/s10143-018-1007-4

Sahel, J.-A., Boulanger-Scemama, E., Pagot, C., Arleo, A., Galluppi, F., Martel, J.N., Esposti, S.D., Delaux, A., De Saint Aubert, J.-B., De Montleau, C., Gutman, E., Audo, I., Duebel, J., Picaud, S., Dalkara, D., Blouin, L., Taiel, M., Roska, B., 2021. Partial recovery of visual function in a blind patient after optogenetic therapy. Nat Med 27, 1223–1229. https://doi.org/10.1038/s41591-021-01351-4

Sainburg, R.L., Ghilardi, M.F., Poizner, H., Ghez, C., 1995. Control of limb dynamics in normal subjects and patients without proprioception. Journal of Neurophysiology 73, 820–835. https://doi.org/10.1152/jn.1995.73.2.820

Sakata, H., Taira, M., Murata, A., Mine, S., 1995. Neural mechanisms of visual guidance of hand action in the parietal cortex of the monkey. Cereb Cortex 5, 429–438. https://doi.org/10.1093/cercor/5.5.429

Sakellaridi, S., Christopoulos, V.N., Aflalo, T., Pejsa, K.W., Rosario, E.R., Ouellette, D., Pouratian, N., Andersen, R.A., 2019. Intrinsic variable learning for brain-machine interface control by human anterior intraparietal cortex. Neuron 102, 1–12. https://doi.org/10.1016/j.neuron.2019.02.012

Sanchez-Panchuelo, R.M., Francis, S., Bowtell, R., Schluppeck, D., 2010. Mapping human somatosensory cortex in individual subjects with 7T functional MRI. Journal of Neurophysiology 103, 2544–2556. https://doi.org/10.1152/jn.01017.2009

Sanders, Z.-B., Wesselink, D.B., Dempsey-Jones, H., Makin, T.R., 2019. Similar somatotopy for active and passive digit representation in primary somatosensory cortex (preprint). Neuroscience. https://doi.org/10.1101/754648

Sanes, J.N., Donoghue, J.P., Thangaraj, V., Edelman, R.R., Warach, S., 1995. Shared neural substrates controlling hand movements in human motor cortex. Science 268, 1775–1777. https://doi.org/10.1126/science.7792606

Santhanam, G., Ryu, S.I., Yu, B.M., Afshar, A., Shenoy, K.V., 2006. A high-performance brain–computer interface. Nature 442, 195–198. https://doi.org/10.1038/nature04968

Saxe, R., Kanwisher, N., 2003. People thinking about thinking people: The role of the temporo-parietal junction in "theory of mind." NeuroImage 19, 1835–1842. https://doi.org/10.1016/S1053-8119(03)00230-1

Scandola, M., Tidoni, E., Avesani, R., Brunelli, G., Aglioti, S.M., Moro, V., 2014. Rubber hand illusion induced by touching the face ipsilaterally to a deprived hand: evidence for plastic "somatotopic" remapping in tetraplegics. Front Hum Neurosci 8. https://doi.org/10.3389/fnhum.2014.00404

Schaefer, M., Flor, H., Heinze, H.-J., Rotte, M., 2006. Dynamic modulation of the primary somatosensory cortex during seeing and feeling a touched hand. NeuroImage 29, 587–592. https://doi.org/10.1016/j.neuroimage.2005.07.016

Schaefer, M., Heinze, H.-J., Rotte, M., 2008. Observing the touched body magnified alters somatosensory homunculus 19, 901–905. https://doi.org/10.1097/WNR.0b013e328301a629

Schaefer, M., Rothemund, Y., Heinze, H.-J., Rotte, M., 2004. Short-term plasticity of the primary somatosensory cortex during tool use. NeuroReport 15, 1293–1297. https://doi.org/10.1097/01.wnr.0000129573.36301.db

Schaefer, M., Xu, B., Flor, H., Cohen, L.G., 2009. Effects of different viewing perspectives on somatosensory activations during observation of touch. Hum Brain Mapp 30, 2722–2730. https://doi.org/10.1002/hbm.20701

Schaffelhofer, S., Agudelo-Toro, A., Scherberger, H., 2015. Decoding a wide range of hand configurations from macaque motor, premotor, and parietal cortices. J. Neurosci. 35, 1068–1081. https://doi.org/10.1523/JNEUROSCI.3594-14.2015

Schaffelhofer, S., Scherberger, H., 2016. Object vision to hand action in macaque parietal, premotor, and motor cortices. eLife 5, e15278. https://doi.org/10.7554/eLife.15278

Schettler, A., Raja, V., Anderson, M.L., 2019. The embodiment of objects: Review, analysis, and future directions. Front. Neurosci. 13, 1332. https://doi.org/10.3389/fnins.2019.01332

Seelke, A.M.H., Padberg, J.J., Disbrow, E., Purnell, S.M., Recanzone, G., Krubitzer, L., 2012. Topographic maps within Brodmann's Area 5 of macaque monkeys. Cerebral Cortex 22, 1834–1850. https://doi.org/10.1093/cercor/bhr257

Sharma, S., Fiave, P.A., Nelissen, K., 2018. Functional MRI responses to passive, active, and observed touch in somatosensory and insular cortices of the macaque monkey. J Neurosci 38, 3689–3707. https://doi.org/10.1523/JNEUROSCI.1587-17.2018

Shimada, S., Suzuki, T., Yoda, N., Hayashi, T., 2014. Relationship between sensitivity to visuotactile temporal discrepancy and the rubber hand illusion. Neuroscience Research 85, 33–38. https://doi.org/10.1016/j.neures.2014.04.009

Simeral, J.D., Hosman, T., Saab, J., Flesher, S.N., Vilela, M., Franco, B., Kelemen, J., Brandman, D.M., Ciancibello, J.G., Rezaii, P.G., Eskandar, E.N., Rosler, D.M., Shenoy, K.V., Henderson, J.M., Nurmikko, A.V., Hochberg, L.R., 2021. Home use of a percutaneous wireless intracortical brain-computer interface by individuals with tetraplegia. IEEE Transactions on Biomedical Engineering 1–1. https://doi.org/10.1109/TBME.2021.3069119

Skedung, L., Arvidsson, M., Chung, J.Y., Stafford, C.M., Berglund, B., Rutland, M.W., 2013. Feeling small: Exploring the tactile perception limits. Sci Rep 3, 2617. https://doi.org/10.1038/srep02617

Slater, M., Spanlang, B., Sanchez-Vives, M.V., Blanke, O., 2010. First person experience of body transfer in virtual reality. PLoS ONE 5, e10564. https://doi.org/10.1371/journal.pone.0010564

Sliwinska, M.W., Khadilkar, M., Campbell-Ratcliffe, J., Quevenco, F., Devlin, J.T., 2012. Early and sustained supramarginal gyrus contributions to phonological processing. Front Psychol 3, 161. https://doi.org/10.3389/fpsyg.2012.00161

Smit, S., Rich, A.N., Zopf, R., 2019. Visual body form and orientation cues do not modulate visuo-tactile temporal integration. PLoS One 14, e0224174. https://doi.org/10.1371/journal.pone.0224174

Snyder, L.H., Batista, A.P., Andersen, R.A., 1997. Coding of intention in the posterior parietal cortex. Nature 386, 167–170. https://doi.org/10.1038/386167a0

Sobinov, A.R., Bensmaia, S.J., 2021. The neural mechanisms of manual dexterity. Nat Rev Neurosci. https://doi.org/10.1038/s41583-021-00528-7

Sombeck, J.T., Miller, L.E., 2020. Short reaction times in response to multi-electrode intracortical microstimulation may provide a basis for rapid movement-related feedback. J. Neural Eng. 17, 016013. https://doi.org/10.1088/1741-2552/ab5cf3

Staines, W.R., Popovich, C., Legon, J.K., Adams, M.S., 2014. Early modality-specific somatosensory cortical regions are modulated by attended visual stimuli: interaction of vision, touch and behavioral intent. Front Psychol 5, 351. https://doi.org/10.3389/fpsyg.2014.00351

Stavisky, S.D., Willett, F.R., Wilson, G.H., Murphy, B.A., Rezaii, P., Avansino, D.T., Memberg, W.D., Miller, J.P., Kirsch, R.F., Hochberg, L.R., Ajiboye, A.B., Druckmann, S., Shenoy, K.V., Henderson, J.M., 2019. Neural ensemble dynamics in dorsal motor cortex during speech in people with paralysis. eLife 8, e46015. https://doi.org/10.7554/eLife.46015

Tabot, G.A., Kim, S.S., Winberry, J.E., Bensmaia, S.J., 2015. Restoring tactile and proprioceptive sensation through a brain interface. Neurobiology of Disease 83, 191–198. https://doi.org/10.1016/j.nbd.2014.08.029

Taoka, M., Toda, T., Iriki, A., Tanaka, M., Iwamura, Y., 2000. Bilateral receptive field neurons in the hindlimb region of the postcentral somatosensory cortex in awake macaque monkeys. Exp Brain Res 134, 139–146. https://doi.org/10.1007/s002210000464

Taylor-Clarke, M., Kennett, S., Haggard, P., 2002. Vision modulates somatosensory cortical processing. Current Biology 12, 233–236. https://doi.org/10.1016/S0960-9822(01)00681-9

Thakur, P.H., Fitzgerald, P.J., Hsiao, S.S., 2012. Second-order receptive fields reveal multidigit interactions in area 3b of the macaque monkey. Journal of Neurophysiology 108, 243–262. https://doi.org/10.1152/jn.01022.2010

Theys, T., Pani, P., van Loon, J., Goffin, J., Janssen, P., 2013. Three-dimensional shape coding in grasping circuits: A comparison between the anterior intraparietal area and ventral premotor area F5a. Journal of Cognitive Neuroscience 25, 352–364. https://doi.org/10.1162/jocn_a_00332

Tidoni, E., Grisoni, L., Liuzza, M.T., Aglioti, S.M., 2014. Rubber hand illusion highlights massive visual capture and sensorimotor face-hand remapping in a tetraplegic man. Restorative Neurology and Neuroscience 611–622. https://doi.org/10.3233/RNN-130385

Tipper, S., Phillips, N., Dancer, C., Lloyd, D., Howard, L., McGlone, F., 2001. Vision influences tactile perception at body sites that cannot be viewed directly. Experimental Brain Research 139, 160–167. https://doi.org/10.1007/s002210100743

Tsakiris, M., Carpenter, L., James, D., Fotopoulou, A., 2010. Hands only illusion: multisensory integration elicits sense of ownership for body parts but not for non-corporeal objects. Exp Brain Res 204, 343–352. https://doi.org/10.1007/s00221-009-2039-3

Tsakiris, M., Costantini, M., Haggard, P., 2008. The role of the right temporo-parietal junction in maintaining a coherent sense of one's body. Neuropsychologia 46, 3014–3018. https://doi.org/10.1016/j.neuropsychologia.2008.06.004

Tsakiris, M., Haggard, P., 2005. The rubber hand illusion revisited: Visuotactile integration and self-attribution. Journal of Experimental Psychology: Human Perception and Performance 31, 80–91. https://doi.org/10.1037/0096-1523.31.1.80

Umilta, M.A., Brochier, T., Spinks, R.L., Lemon, R.N., 2007. Simultaneous recording of macaque premotor and primary motor cortex neuronal populations reveals different functional contributions to visuomotor grasp. Journal of Neurophysiology 98, 488–501. https://doi.org/10.1152/jn.01094.2006

Valle, G., Mazzoni, A., Iberite, F., D'Anna, E., Strauss, I., Granata, G., Controzzi, M., Clemente, F., Rognini, G., Cipriani, C., Stieglitz, T., Petrini, F.M., Rossini, P.M., Micera, S., 2018. Biomimetic intraneural sensory feedback enhances sensation naturalness, tactile sensitivity, and manual dexterity in a bidirectional prosthesis. Neuron 100, 37-45.e7. https://doi.org/10.1016/j.neuron.2018.08.033

Walther, A., Nili, H., Ejaz, N., Alink, A., Kriegeskorte, N., Diedrichsen, J., 2016. Reliability of dissimilarity measures for multi-voxel pattern analysis. NeuroImage 137, 188–200. https://doi.org/10.1016/j.neuroimage.2015.12.012

Wandelt, S.K., Kellis, S., Bjånes, D.A., Pejsa, K., Lee, B., Liu, C., Andersen, R.A., 2022. Decoding grasp and speech signals from the cortical grasp circuit in a tetraplegic human. Neuron S0896627322002458. https://doi.org/10.1016/j.neuron.2022.03.009

Wesselink, D.B., Sanders, Z.-B., Edmondson, L., Dempsey-Jones, H., Kieliba, P., Kikkert, S., Themistocleous, A., Emir, U., Diedrichsen, J., Saal, H.P., Makin, T.R., 2022. Malleability of the cortical hand map following a finger nerve block. SCIENCE ADVANCES 8. https://doi.org/10.1126/sciadv.abk2393

Willett, F.R., Deo, D.R., Avansino, D.T., Rezaii, P., Hochberg, L.R., Henderson, J.M., Shenoy, K.V., 2020. Hand knob area of premotor cortex represents the whole body in a compositional way. Cell S0092867420302208. https://doi.org/10.1016/j.cell.2020.02.043

Willsey, M.S., Nason-Tomaszewski, S.R., Ensel, S.R., Temmar, H., Mender, M.J., Costello, J.T., Patil, P.G., Chestek, C.A., 2022. Real-time brain-machine interface in non-human primates achieves high-velocity prosthetic finger movements using a shallow feedforward neural network decoder. Nat Commun 13, 6899. https://doi.org/10.1038/s41467-022-34452-w

Woeppel, K., Hughes, C., Herrera, A.J., Eles, J.R., Tyler-Kabara, E.C., Gaunt, R.A., Collinger, J.L., Cui, X.T., 2021. Explant analysis of Utah electrode arrays implanted in human cortex for brain-computer-interfaces. Front Bioeng Biotechnol 9, 759711. https://doi.org/10.3389/fbioe.2021.759711

Woolsey, C.N., Erickson, T.C., Gilson, W.E., 1979. Localization in somatic sensory and motor areas of human cerebral cortex as determined by direct recording of evoked potentials and electrical stimulation. Journal of Neurosurgery 51, 476–506. https://doi.org/10.3171/jns.1979.51.4.0476

Yamamoto, S., Kitazawa, S., 2001. Sensation at the tips of invisible tools. Nat Neurosci 4, 979–980. https://doi.org/10.1038/nn721

Yamamoto, S., Moizumi, S., Kitazawa, S., 2005. Referral of tactile sensation to the tips of L-shaped sticks. Journal of Neurophysiology 93, 2856–2863. https://doi.org/10.1152/jn.01015.2004

Yoo, S.-S., Freeman, D.K., McCarthy, J.J., Jolesz, F.A., 2003. Neural substrates of tactile imagery: a functional MRI study. NeuroReport 14, 581–585. https://doi.org/10.1097/00001756-200303240-00011

Young, L., Cushman, F., Hauser, M., Saxe, R., 2007. The neural basis of the interaction between theory of mind and moral judgment. Proc. Natl. Acad. Sci. U.S.A. 104, 8235–8240. https://doi.org/10.1073/pnas.0701408104

Zhang, C.Y., Aflalo, T., Revechkis, B., Rosario, E.R., Ouellette, D., Pouratian, N., Andersen, R.A., 2017. Partially mixed selectivity in human posterior parietal association cortex. Neuron 95, 697–708. https://doi.org/10.1016/j.neuron.2017.06.040

Zhou, Y.-D., Fuster, J.M., 2000. Visuo-tactile cross-modal associations in cortical somatosensory cells. Proceedings of the National Academy of Sciences 97, 9777–9782. https://doi.org/10.1073/pnas.97.17.9777